TIDAL EFFECTS AND GALAXY EVOLUTION IN CLUSTERS OF GALAXIES

Oleg Y. Gnedin

A DISSERTATION
PRESENTED TO THE FACULTY
OF PRINCETON UNIVERSITY
IN CANDIDACY FOR THE DEGREE
OF DOCTOR OF PHILOSOPHY

RECOMMENDED FOR ACCEPTANCE
BY THE DEPARTMENT OF
ASTROPHYSICAL SCIENCES

January, 1999

I certify that I have read this thesis and that in my opinion it is fully adequate, in scope and in quality, as a dissertation for the degree of Doctor of Philosophy.

Jeremiah P. Ostriker
(Principal Adviser)

I certify that I have read this thesis and that in my opinion it is fully adequate, in scope and in quality, as a dissertation for the degree of Doctor of Philosophy.

David N. Spergel

I certify that I have read this thesis and that in my opinion it is fully adequate, in scope and in quality, as a dissertation for the degree of Doctor of Philosophy.

Jeremy Goodman

Approved for the Princeton University Graduate School:

Dean of the Graduate School

To my family,

whose support has always been invaluable

Acknowledgments

This thesis is the result of the invaluable help and support from my colleagues, friends, and family. To all of them, I offer my sincere gratitude.

First and foremost, I wish to thank my advisor, Jerry Ostriker, who guided me through the puzzles and mysteries of astronomy and the astronomical world, who provided a wealth of ideas and encouragement at all stages of this thesis, who despite the busiest schedule always had time to help me overcome the obstacles, and most importantly, who taught me to search for the truthful and complete understanding of any scientific problem.

The faculty at Princeton have set a wonderful example of openness and unselfishness in science and real life, donating their time during the daily teas, coffees, and the otherwise working hours. Jeremy Goodman and David Spergel provided not only the healthy criticism of this thesis, but the continuous help over these four years when I had the privilege to ask them numerous questions. I am grateful to Neta Bahcall for many discussions and for serving on the FPO committee, and to Jim Gunn and Scott Tremaine for valuable advice and encouragement.

Semester projects have been one of the most useful and enlightening experiences at Princeton. I had the good fortune to work with Jeremy Goodman on my first quasi-observational project. John Bahcall has generously instructed me in collecting data from the people I did not know and has taught me how to deal with referees. Jerry Ostriker has launched my successful collaborations with Hyung Mok Lee and Lars Hernquist. I am particularly indebted to Lars Hernquist and Renyue Cen for letting me use their N-body codes, all of which have been used in this thesis.

Princeton has granted me the opportunity to teach and be taught. Bohdan Paczyński, Bruce Draine, Russell Kulsrud, Jeremy Goodman, and Jim Gunn have all greatly expanded my knowledge in astronomy. Ed Turner and Robert Lupton, with their shot-gun seminar, have made me appreciate that statistics should always be done correctly. The student seminar has been a great school of giving clear, concise, and understandable talks. I am grateful to Michael Strauss and Neta Bahcall for showing me how to teach in our Astro 203 and Astro 204 undergraduate courses. I cannot understate how much I have taken from that experience.

Peyton Hall has been a wonderful source of inspiration. Rich Gott and Neil Tyson, in often long but always exciting conversations, have helped to appreciate the many sides of life. Jill Knapp and Jim Gunn have provided both astronomical and gastronomical support. I was also fortunate to know Lyman Spitzer and to enjoy many pleasant discussions with him, ranging from the emission lines to the fate of the Palmer Stadium. His paper with Walter Baade in 1951 pioneered the general topic of my thesis. I regret that he did not see this work completed.

I wish to thank my friends and colleagues at Peyton Hall and the Institute for Advanced Study for numerous discussions and valuable assistance, in particular Greg Bryan, Kathryn Johnston, and Daniel Eisenstein. I am grateful to David Hogg for sharing his wisdom with me. Mike Blanton has made available his excellent Points software. I also wish to thank our system managers, Bill Sproule and Michael Way, for supporting Hecate and letting my work finish.

The beginning of my astronomical career was shaped at the Ioffe Institute of Physics and Technology in Saint Petersburg. I owe a great debt to my colleagues and mentors for painstakingly teaching me to do science and write papers, for granting me a lion share of the scare computational resources, and for tolerating my frequent mistakes. My undergraduate advisor, Dmitrii Georgievich Yakovlev, guided me through my first research and first publications. He laid the foundation for everything I have done since.

The life as a graduate student at Peyton Hall is not only about tedious integrations and nightless programming, but is also about the ping-pong tournament, open houses for public observations, going out, round, and about Princeton, and simply chatting at night in the computer room illuminated by a smooth light of the disco balls. I owe the happy and well-rounded life in these four years to my fellow graduate students, Ue-Li Pen, Tomislav Kundić, Gouhong Xu, Vika Dorman, Ben Chandran, James Rhoads, Krzysztof Stanek, Wes Colley, Antonio Peimbert, Andrew Ulmer, Jeremy Kepner, Erick Lee, Mike Blanton, Peng Oh, Rita Kim, Xiaohui Fan, Arielle Phillips, Przemek Wozniak, David Goldberg, and Leonid Malyshkin. Special thanks go to Wes for touring with me all around Princeton, from Charlottesville to Toronto.

My friends outside Princeton have frequently kept in touch and made sure I am not occupied with the science only. For the many sincere conversations and exciting adventures I have had with Gera Mikhailov, Pasha Anashkin, Serezha Iskoz, and Xenia Bonch-Bruevich, thank you. In Princeton, I have spent many pleasant hours with Mary Ann and Dick Hansler and Jordi Miralda-Escude, whose hospitality and friendship I will always hold dear. Finally, I am grateful to Wes and Xenia for generously checking my English on countless occasions.

For the privilege of knowing all of you, thank you.

My family has always been the main source of support for me. My parents, Irina and Yuri Gnedin, raised me to be everything that I am. My brother, Nickolay Gnedin, has always been the one I was looking up to. He, Marianna and Nina, have helped me in everything since I came to the U.S., and to them all I owe an infinite amount of gratitude. Kolya's expertise in cosmology has been a great deal of help in the final weeks. And each and every moment I spent on this thesis, I have missed Irka and Alenka.

Abstract

This dissertation focuses on the problem of tidal effects on the evolution of galaxies in clusters. The topic is motivated by the wealth of observational evidence, collected using both the Hubble Space Telescope and ground-based telescopes, that a strong morphological evolution of galaxies has occurred in clusters between redshift 0.5 and now. A possible theoretical explanation involves tidal interactions between galaxies and the evolving potential of the cluster, including the interactions between galaxies themselves. Large particle-mesh simulations are performed to generate cosmologically viable clusters of galaxies in three different models of structure formation. The tidal field from these clusters is used to model the dynamics of individual galaxies using a high resolution N-body code. The results demonstrate that large spiral galaxies retain their stellar disks but in a significantly thickened form. A large fraction of the gas may be lost due to interaction with the intracluster media or in interpenetrating collisions with other galaxies. As the disks become gravitationally stable, the remaining gas is unlikely to form new stars. Dark matter halos are stripped at a radius of about 30 kpc, regardless of their initial size. The effect of the tidal interactions is to transform a spiral galaxy into an S0, but not elliptical galaxy. Dwarf spheroidal galaxies are completely torn apart due to their low central density. Their unbound stars contribute to the diffuse cluster light. With a degree of uncertainty, several lines of reasoning favor the low density cosmological models as fitting observations better.

Preface

This Thesis consists of three chapters that all deal with the tidal effects in clusters of galaxies. Chapter 1 presents an introduction to the problem and covers relevant observational evidence and previous theoretical work. Chapter 2 describes the cosmological simulations of three clusters of galaxies and investigates galaxy trajectories and the tidal field around them. Chapter 3 presents high-resolution simulations of the dynamics of disk galaxies under the influence of the external tidal field.

Chapter 1 introduces the reader to the questions poised by recent observations by the Hubble Space Telescope. The HST reveals numerous blue spiral galaxies in the clusters at redshift $z \sim 0.5$, which are almost absent from the nearby clusters. A new technique of image reconstruction of gravitational lensing shows for the first time large concentrations of dark matter, not associated with the luminous galaxies in a $z = 0.39$ cluster. Of several theoretical scenarios aimed at explaining these puzzles, tidal interactions among the galaxies and between the galaxies and the cluster potential seem the most promising. The two subsequent chapters investigate in detail the tidally-driven evolution of galaxies.

Chapter 2 describes the self-consistent cosmological simulations of a representative cluster of galaxies in each of the three currently popular cosmological models. Using these simulations, I identify galaxy trajectories and the tidal forces along them. The tidal forces are comprised of individual tidal shocks from the time-varying cluster potential and the substructure in it. The simulations cannot resolve very close encounters between galaxies, but their contribution to the total tidal force is calculated and found to be modest.

Chapter 3 builds upon these results and constructs a fully self-consistent dynamical evolution of galaxies in clusters. Assuming that all galaxies were formed as spirals, the simulations demonstrate that the dark matter halos are stripped to a radius of 30 kpc, regardless of their initial size. The galactic disks thicken significantly, by a factor of 2 or larger, thereby preventing gravitational instability that might have lead to new star formation. Moreover, a large fraction of gas is expected to be removed from the galaxies in close collisions with their neighbors. Thus, the resulting galaxy would look as an S0, but not as an elliptical galaxy. Limiting the dynamical evolution to the spiral$\rightarrow$S0 transformation implies that ellipticals must have formed earlier than the cluster. These claims should be resolved by the upcoming Sloan Digital Sky Survey and the continuing work of the Hubble Space Telescope.

Chapters 2 and 3 are each the basis of the single-author papers which will be submitted to journals as listed below:

Ch.2 "Tidal Effects in Clusters of Galaxies" Gnedin, O. Y. 1998, Astrophysical Journal, to be submitted

Ch.3 "Evolution of Galaxies in Clusters" Gnedin, O. Y. 1998, Astrophysical Journal, to be submitted

Contents

Chapter 1

Motivation

1.1 Abstract

Recent observations of high redshift clusters show an abundance of blue spiral galaxies, often distorted. Since nearby clusters are populated mostly by elliptical and S0 galaxies, a strong morphological evolution of galaxies has occurred between redshift 0.5 and now. A discovery of massive dark objects in the $z = 0.39$ cluster further indicates that dark matter halos are stripped from the galaxies. Of the possible theoretical explanations, tidal interactions with the time-variable cluster potential and between the galaxies seem to be the most promising.

1.2 Observational Discoveries

This thesis is motivated by the wealth of recent observational discoveries of the strong morphological, chemical, and dynamical evolution of galaxies in clusters. In addition, the discovery of massive dark objects separate from the luminous galaxies and the evolution of cluster substructure further intensify the need of theoretical understanding. Several different phenomena have been proposed in the past as the “likely” explanation. While all of them take place in some form or the other, it has eluded our understanding which process is primarily responsible for the evolution. In this Chapter, I review the present observational status of galaxies in clusters at various redshifts and the current theoretical mechanisms to connect the pieces of the puzzle. I argue that tidal interactions between galaxies and the cluster potential, as well as between galaxies themselves, are the favored scenario. Subsequent Chapters provide the numerical realization of this idea.

1.2.1 “Spirals versus Ellipticals” or “Spirals versus S0s”?

The Hubble Space Telescope has been instrumental in shaping our current understanding of high redshift clusters of galaxies. The unique resolving power of the HST brings us exquisite details of the distorted profiles of the otherwise normal spiral galaxies. Strongly depleted in the nearby clusters, spirals make up to 50% of the galaxies in clusters at redshift $z \sim 0.5$ (Dressler et al. 1997; Oemler et al. 1997; Ellis et al. 1997; Smail et al. 1997). These results are in agreement with the Butcher-Oemler (1978) effect, an abundance of blue irregular galaxies at an intermediate redshift. Spectroscopic evidence (Dressler et al. 1997) suggests bursts of recent, or even current, star formation. This picture is drastically different from the present day clusters, populated mostly by featureless elliptical or S0 galaxies (the local morphology-density relation; Dressler 1980). It is now well established that a strong chemical and morphological evolution took place in clusters of galaxies.

What are the options? Did the $z = 0.5$ spirals become $z = 0$ ellipticals? On the contrary, the HST data shows that the fraction of elliptical galaxies *increases* with redshift, although not as strongly as that of spirals. Both of these effects occur at the expense of the S0s. Their population is depleted by about a factor of two at $z \sim 0.5$ (Dressler et al. 1997). Observations suggest that star formation has ceased in the ellipticals by an epoch $z \sim 0.6$, but continued in the S0s until at least $z \sim 0.3$ (van Dokkum et al. 1998). The ellipticals must have formed and exhausted their supply of fresh gas at some early redshift. The early formation epoch of ellipticals is also suggested by their very high central densities (Kormendy 1989).

At low redshift, the situation is also far from being smooth (Conselice & Gallagher 1998). New ground-based imaging of the Coma and five other nearby clusters reveals a variety of distorted, tailed, "line", and dwarf galaxies. These are indicators of ongoing dynamical evolution. Many galaxies are distorted and some show blue colors. Also, individual groups of dwarf galaxies have been found in Coma. These results have not been expected for such smooth and regular clusters.

1.2.2 Isolated Dark Matter Halos

A new observational puzzle has been presented by the discovery of massive dark objects in the cluster CL 0024+1654, through the technique of image reconstruction of strong gravitational lensing (Tyson, Kochanski & Dell'Antonio 1998; Kochanski, Dell'Antonio & Tyson 1998). The dark objects are not associated with any of the luminous galaxies in the cluster and may contain about $10^{10}\,M_\odot$ of mass. One of the possible explanations is that these objects are just "failed" galaxies, in which gaseous dissipation was insufficient to form stars. Another explanation involves an abundance of stripped dark matter halos. Analytical arguments and previous studies (§1.3.2) suggest that the extended galactic halos may be effectively swept away in close encounters with other large galaxies or with the cluster center. However, it has not yet been possible to investigate the distribution of matter in such halos.

1.3 Scenarios of Galactic Evolution

The idea that the environment plays a role in the evolution of galaxies has been recognized long ago and has a rich history. Spitzer & Baade (1951) suggested that collisions between spiral galaxies might be responsible for transforming spirals into gas-free S0s. Toomre (1977) advocated a merger of two spirals to produce an elliptical. Richstone (1976) argued for the truncation of dark matter halos of galaxies by the tidal field of the cluster. Gunn & Gott (1972) proposed gas stripping of spirals by the ram pressure of the intracluster medium. Finally, Merritt (1983) and most recently Moore et al. (1996), considered tidal interactions between the galaxies and the dense cluster core and between the galaxies themselves. I now mention briefly the pros and cons of each of these scenarios.

1.3.1 Mergers of Galaxies

Collisions of galaxies are enhanced in the dense environment of the cluster. However, in a virialized cluster, galaxies move with relative velocities of the order 1000 km s^{-1} and even in a head-on trajectory will pass through each other without doing much harm to the stellar disks. Gas can be shocked and stripped away in such a collision (Spitzer & Baade 1951), which would leave two gas-free S0 galaxies. But a simple analytical estimate argues that such close collisions must be very infrequent.

Consider a virialized cluster of galaxies with the three-dimensional velocity dispersion $\sigma_{cl} \approx 1000$ km s^{-1} and the virial radius[1] $R_{cl} \approx 1$ Mpc. Assuming that the cluster contains 1000 galaxies inside this radius, the number of close encounters a given galaxy of size R_g will experience in a Hubble time ($t_H = 10^{10}$ yr) is

$$N_{enc,1} \approx \frac{N_g}{\frac{4\pi}{3}R_{cl}^3}\,\pi R_g^2\, 2^{1/2}\sigma_{cl}\, t_H \tag{1-1}$$

$$\approx 1\left(\frac{N_g}{1000}\right)\left(\frac{R_g}{10\text{ kpc}}\right)^2\left(\frac{\sigma_{cl}}{1000\text{ km s}^{-1}}\right). \tag{1-2}$$

Here I have neglected gravitational focusing of the two galaxies and assumed their relative velocity to be of the order $2^{1/2}\sigma_{cl}$. The galaxy is expected to encounter one other galaxy over the course of its evolution. However, the probability of a merger between the two galaxies is much smaller:

$$P_{mer} \approx N_{enc,1}\left(\frac{V_c}{\sigma_{cl}}\right)^4 \tag{1-3}$$

$$\approx 10^{-3}\left(\frac{N_g}{1000}\right)\left(\frac{R_g}{10\text{ kpc}}\right)^2\left(\frac{V_c}{200\text{ km s}^{-1}}\right)^4\left(\frac{\sigma_{cl}}{1000\text{ km s}^{-1}}\right)^{-3}. \tag{1-4}$$

Here three powers of the ratio of the circular speed of the galaxy, V_c, to the cluster velocity dispersion come from the phase space density and another power of V_c/σ_{cl} comes from the limitation of the velocity that leads to a merger (Binney & Tremaine 1987).

Also, ellipticals usually have much higher central densities than spiral galaxies. So if two spirals merge, it seems hard to close the gap in density without strong dissipation (Carlberg 1986). As Jim Gunn once said (Gunn 1987), "I do not think you can make rocks by merging clouds."

Thus, the merger scenario appears unlikely to dominate dynamics of the galaxies, although mergers are important for the formation of the giant cD galaxy (Ostriker & Hausman 1977; Merritt 1985; Lauer 1988).

1.3.2 Truncation of Dark Matter Halos

Richstone (1976), White (1976), and Merritt (1983), among others, have investigated the effect of the cutoff imposed on the distribution of the galactic dark matter by the tidal field

[1]The virial radius of the cluster is defined in §2.4.

of the cluster. In the simplest case of a perfectly smooth cluster, where both the cluster and the galaxy have singular isothermal distributions of dark matter with the velocity dispersions σ_{cl} and σ_g, respectively, the tidal radius is

$$R_t = \frac{\sigma_g}{\sigma_{cl}} R_p, \tag{1-5}$$

where R_p is the distance of the closest approach to the center of the cluster.

Real clusters are not completely smooth. Any substructure within clusters, such as the remnants of the former groups of galaxies merged during the hierarchical formation of the cluster, will amplify the truncation effect. Thus, this effect is expected to control the amount of dark matter, and therefore, the mass of the galaxies.

On the other hand, tidal truncation should not significantly affect the dynamics of the galactic disks which are much more compact. Morphological evolution of galaxies must be due to something else.

1.3.3 Ram-Pressure Stripping of Gas

Gunn & Gott (1972) argued that the ram pressure of the intracluster medium (ICM) might have swept away gas from the galactic disks. X-ray observations indicate the presence of a significant amount of hot gas at the virial temperature, contributing as much as 10% of the cluster mass. While stars move freely through this media, the gas in the disks is subject to the ram pressure $P_{ram} \approx \rho_{\rm ICM} v^2$, where $\rho_{\rm ICM}$ is the density of the ICM and v is the velocity of the galaxy. In order to strip the gas, the ram pressure should exceed the vertical force per unit area of the disk:

$$\rho_{\rm ICM} v^2 > 2\pi G\, \Sigma_s\, \Sigma_g, \tag{1-6}$$

where Σ_s is the surface density of the stars, and Σ_g is the surface density of the gas. Assuming the gas of an average density 1 cm^{-3} distributed over a scale height 100 pc, and a stellar surface density typical of the solar neighborhood, $\Sigma_s \approx 75\ M_\odot\ \mathrm{pc}^{-2}$, the ICM needs to be as dense as

$$n_{\rm ICM} > 4 \times 10^{-4} \left(\frac{v}{1000\ \mathrm{km\ s}^{-1}}\right)^{-2}\ \mathrm{cm}^{-3}. \tag{1-7}$$

Such densities of the intracluster gas are reachable in centers of rich clusters. Kundić et al. (1993) have conducted numerical experiments and found that for $n_{\rm ICM} > 10^{-3}\ \mathrm{cm}^{-3}$ and $v > 1500\ \mathrm{km\ s}^{-1}$, a typical spiral loses all of its atomic gas.

Spiral galaxies in clusters have long been known to be deficient of atomic hydrogen (Haynes, Giovanelli & Chincarini 1984). These "anemic" galaxies (van den Bergh 1991) have normal molecular hydrogen abundances but lack the atomic component in the outer parts of their disks. Since the H_2 gas resides in dense molecular clouds, it is able to withstand the external pressure; on the other hand, the H I gas is usually distributed much more smoothly at lower densities and is susceptible to the ram pressure stripping.

Recently, an interesting feature has been noted in three rich Abell clusters and the Virgo cluster: the H I deficiency is stronger for larger galaxies (Valluri & Jog 1991). Bigger spirals (excluding the LSBs) usually have higher surface density and therefore should be able to protect their gaseous component better. The statistical trend is opposite to what is expected from the ram pressure stripping. Having considered several possible mechanisms able to remove the gas, Valluri and Jog conclude that the H I deficiency can only be explained by tidal interactions.

The effects of the ram pressure stripping are also affected by the hierarchical formation of the cluster. When individual substructures, such as groups of galaxies, merge into the cluster, a bow shock may form slightly ahead of the group's motion. A bow shock forms when the ram pressure exceeds the thermal pressure of the infalling gas and when the ram pressure increases faster than a pressure wave can propagate across the substructure (Fabian & Daines 1991). Numerical simulations (Roettiger, Loken & Burns 1997) indicate that bow shocks do form for substructures falling in at supersonic speeds, up to 2000 km s^{-1}. Such shocks complicate the dynamics of the gas until it heats to the virial temperature. New X-ray observations of the Coma cluster by *ASCA* (Hank Donnelly et al. 1998) find a cold and a hot spot in the temperature distribution in the central region of the cluster. Such variations can be naturally explained by the bow shock associated with the group around the bright galaxy NGC 4869.

To summarize, ram pressure stripping is an important mechanism of gas removal from the galaxies. It should certainly operate in the central parts of clusters. However, it is inefficient in the outer regions and may not account for the morphology of galaxies in the recently infalling groups. The discrepancy is more pronounced in the weakly virialized clusters with a lot of substructure, arising in the $\Omega_0 = 1$ cosmological model. Therefore, the only dynamical process that operates at all times without regard to gas shocks is tidal interactions.

1.3.4 Tidal Interactions

Tides *are* a critical factor of the galactic environment. Tidal effects depend on the relative sizes of the system and of the perturber. Consider stellar systems from the smallest to the largest scales: stars are 10^8 times smaller than star clusters and experience almost no tidal effects (except in close binaries). Star clusters are 10^4 times smaller than galaxies and experience significant tidal effects, which however operate on a long time scale (Gnedin & Ostriker 1997). In contrast, galaxies are just 30 to 100 times smaller than clusters of galaxies. Here the tidal effects ought to be important!

Semi-analytic models of galactic encounters (Merritt 1983) predict segregation of galaxies by mass and the formation of a large cD galaxy at the cluster center. The giant cD grows by swallowing the next massive galaxies in a process that widens the gap between the first and the second ranking galaxies (Ostriker & Hausman 1977). Mass segregation in clusters is supported by numerical simulations as well (Frenk et al. 1996). Most recently, Dubinski (1998) confirmed that the central galaxy, rising by mergers of its neighbors, follows a de Vaucouleurs profile and would be classified as a giant elliptical.

Restricted numerical simulations of Byrd & Valtonen (1990) and Valluri (1993) show that the tidal compression by the cluster potential produces spiral arms and tidal tails in some of the representative models of disk galaxies.

Most recently, Moore et al. (1996) simulated the dynamics of galaxies in a cluster with a fixed, isothermal potential. They found that fast close encounters with the central massive galaxies tend to destroy many dwarf galaxies. Even large galaxies lose most of their mass along with the thin disks. These authors find that spiral galaxies essentially transform into ellipticals or dwarf spheroidals. The primary mechanism responsible for such destruction is gravitational tidal shocks. However, those simulations may bear a significant degree of uncertainty in assessing the effects of the shocks. The potential of a real cluster is not fixed in time but varies along the entire course of evolution. In fact, in the $\Omega_0 = 1$ cosmological model, the cluster is still in the process of formation at the present epoch. This time-varying potential gives rise to large-scale perturbations in the tidal field and causes tidal shocks comparable to those from the individual massive galaxies. On the other hand, assuming a large Coma-size cluster at the time of galaxy formation severely overestimates the effect of "harassment" between the galaxies. Which of these two competing effects dominates has not yet been understood.

1.4 Discussion

Despite some large uncertainties, it seems that tidal effects are primarily responsible for the morphological, chemical, and dynamical evolution of galaxies in clusters. Tides operate even before the cluster dynamically relaxes and affect both the stars and gas in the galaxies.

Tidal effects add enough random motion to thin galactic disks to form kinematically hot thick-disk configurations. Relaxation of stellar energies enhances the rate of radial infall of stars in the central regions of galaxies, perhaps leading to the growth of massive bulges.

Tidal truncation of dark matter halos controls the amount of mass left in the galaxies. In the simulations reported in Chapter 3, we find that large galaxies lose a significant fraction of their mass due to this effect.

The relative importance of tides depends on the cosmological context. In an $\Omega_0 = 1$ universe, gravitational structures assemble late and the tidal effects are only starting to play a role in shaping the galaxies, whereas in an open universe, $\Omega_0 \sim 0.4$, galaxies have formed early and experienced a substantial metamorphosis by the tides. A flat universe with $\Omega_0 = 0.4$ and a cosmological constant provides an intermediate case. In Chapter 2, I present the simulations of the self-consistent evolution of clusters in each of these cosmological models. In Chapter 3, I apply the resulting tidal field to investigate the dynamics of galaxies.

REFERENCES

Binney, J., & Tremaine, S. 1987, Galactic Dynamics (Princeton: Princeton Univ. Press), p. 454

Butcher, H., & Oemler, A. 1978, ApJ, 219, 18

Byrd, G., & Valtonen, M. 1990, ApJ, 350, 89

Carlberg, R. G. 1986, ApJ, 310, 593

Conselice, C. J., & Gallagher, J. S. III 1998, AJ, submitted; `astro-ph/9809390`

Dressler, A. 1980, ApJ, 236, 351

Dressler, A., Oemler, A., Couch, W. J., Smail, I., Ellis, R. S., Barger, A., Butcher, H., Poggianti, B. M., & Sharples, R. M. 1997, ApJ, 490, 577

Dubinski, J. 1998, ApJ, 502, 141

Ellis, R. S., Smail, I., Dressler, A., Couch, W. J., Oemler, A., Butcher, H., & Sharples, R. 1997, ApJ, 483, 582

Fabian, A. C., & Daines, S. J. 1991, MNRAS, 252, 17P

Frenk, C. S., Evrard, A. E., White, S. D. M., & Summers, F. J. 1996, ApJ, 472, 460

Gnedin, O. Y., & Ostriker, J. P. 1997, ApJ, 474, 223

Gunn, J. E. 1987, in Nearly Normal Galaxies: From the Planck Time to the Present, ed. S. M. Faber (New York: Springer), p. 455

Gunn, J. E., & Gott, J. R. III 1972, ApJ, 176, 1

Hank Donnelly, R., Markevitch, M., Forman, W., Jones, C., Churazov, E., & Gilfanov, M. 1998, ApJ, in press; `astro-ph/9809380`

Haynes, M. P., Giovanelli, R., & Chincarini, G. L. 1984, ARA&A, 22, 445

Kochanski, G. P., Dell'Antonio, I. P., & Tyson, J. A. 1998, BAAS, 191, #83.12

Kormendy, J. 1989, ApJ, 342, L63

Kundić, T., Hernquist, L., & Spergel, D. N. 1993, unpublished

Lauer, T. R. 1988, ApJ, 325, 49

Merritt, D. 1983, ApJ, 264, 24

Merritt, D. 1985, ApJ, 289, 18

Moore, B., Katz, N., & Lake, G. 1996, ApJ, 457, 455

Moore, B., Katz, N., Lake, G., Dressler, A., & Oemler, A. 1996, Nature, 379, 613

Oemler, A., Dressler, A., & Butcher, H. 1997, ApJ, 474, 561

Ostriker, J. P., & Hausman, M. A. 1977, ApJ, 217, L125

Richstone, D. O. 1976, ApJ, 204, 642

Roettiger, K., Loken, C., & Burns, J. O. 1997, ApJS, 109, 307

Smail, I., Dressler, A., Couch, W. J., Ellis, R. S., Oemler, A., Butcher, H., & Sharples, R. 1997, ApJS, 110, 213

Spitzer, L. Jr., & Baade, W. 1951, ApJ, 113, 413

Toomre, A. 1977, in The Evolution of Galaxies and Stellar Populations, ed. B. M. Tinsley & R. B. Larson (New Haven: Yale Univ. Observatory), p. 401

Tyson, J. A., Kochanski, G. P., & Dell'Antonio, I. P. 1998, ApJ, 498, L107

Valluri, M. 1993, ApJ, 408, 57

Valluri, M., & Jog, C. J. 1991, ApJ, 374, 103

van den Bergh, S. 1991, PASP, 103, 390

van Dokkum, P. G., Franx, M., Kelson, D. D., Illingworth, G. D., Fisher, D., & Fabricant, D. 1998, ApJ, 500, 714

White, S. D. M. 1976, MNRAS, 177, 717

Chapter 2

Tidal Effects in Clusters of Galaxies

2.1 Abstract

A representative cluster of galaxies is formed using the Particle-Mesh numerical simulations in each of the three cosmologies: a critical density model $\Omega_0 = 1$, an open model $\Omega_0 = 0.4$, and a flat model $\Omega_0 = 0.4$ with a cosmological constant. All three clusters have similar velocity dispersions and density profiles. The tidal field along the trajectories of the identified galaxies is carefully extracted, correcting for the effects of self-interaction. The maxima of the tidal force do not always correlate with the closest approach to the cluster center. They are produced to a large extent by the local density structures, such as massive galaxies and the unvirialized remnants of groups of galaxies. Close encounters between the galaxies are significantly intensified by the substructure, with about 4 encounters per galaxy within 10 kpc in the Hubble time. These very close encounters contribute an important amount of tidal heating of galaxies.

2.2 Introduction

In this Chapter, I present the results of numerical simulations of the evolution of a medium-size cluster of galaxies in the three cosmological models. At some early redshift, $z_g = 5$, groups of dark matter particles are identified as possible galactic halos. Their trajectories are followed using two independent methods: in one, the galactic centers of mass are assumed to be test particles following the overall cluster potential; in the other, the center of mass is calculated using the densest subset of particles constituting the actual galaxy.

Along the galactic trajectories, I calculate the components of the tidal shear tensor of the cluster potential. Because of particle noise, it is necessary to apply a smoothing filter extending over a range of few grid cells. Also, large halos contribute significantly to the tidal field around their centers. Since we are interested only in the external tidal force on the galaxy, this self-contribution needs to be removed. Special care is taken to evaluate the contribution of the galactic particles and subtract it from the total tidal tensor.

The simulations are performed using the Particle-Mesh code on a rectangular grid of

512^3 cells with a fixed comoving box size of 32 h^{-1} Mpc. The chosen size of the simulation box is a compromise between the desire to reach high resolution in the cluster center and the need to have enough computational volume to assemble a cosmologically viable cluster of galaxies. The mass of all particles in the box is $9.1 \times 10^{15}\,\Omega_0 h^{-1}\ M_\odot$, which gives $1.4 \times 10^{16}\ M_\odot$ in the $\Omega_0 = 1$ simulation, and $5.6 \times 10^{15}\ M_\odot$ in the lower density cases. In comparison, the virial mass of the simulated clusters in the latter models is about $4 \times 10^{14}\ M_\odot$, or 7% of the total mass. The actual amount of mass bound to the cluster may be a factor of 2-3 higher, up to 20% of the total mass.

Tests with different amplitudes of the initial density perturbations show that the relevant modes are present in the low density simulations for the mass fluctuations $\sigma_8 \lesssim 1$. Higher initial perturbations would try to bring to the center more particles than is available in the whole box. As a result, the cluster would "underform". This effect is clearly indicated by the saturation of the velocity dispersion in the limit of very strong initial perturbations. The choice of $\sigma_8 = 1$ for the $\Omega_0 = 0.4$ models avoids this problem and fits nicely in the current set of favorable cosmological parameters.

The comparison of the N-body simulations of large scale structure formation with the all-sky survey of X-ray clusters yields a certain relation between the normalization of the power spectrum, σ_8, and the mean density of matter, Ω_0. Two different methods converge to a remarkably similar result. Eke, Cole & Frenk (1996), using the Adaptive P^{3}M code and the Press-Schechter formalism, give

$$\sigma_8\ \Omega_0^p = 0.52 \pm 0.04, \tag{2-1}$$

where

$$\begin{aligned} p &= 0.46 - 0.10\,\Omega_0 \quad \text{for } \Omega_\Lambda = 0, && \text{(2-2)}\\ p &= 0.52 - 0.13\,\Omega_0 \quad \text{for } \Omega_0 + \Omega_\Lambda = 1. && \text{(2-3)} \end{aligned}$$

Pen (1998), using the Moving Mesh code, gives

$$\sigma_8\ \Omega_0^p = 0.53 \pm 0.05, \tag{2-4}$$

where

$$\begin{aligned} p &= 0.45 \quad \text{for } \Omega_\Lambda = 0, && \text{(2-5)}\\ p &= 0.53 \quad \text{for } \Omega_0 + \Omega_\Lambda = 1. && \text{(2-6)} \end{aligned}$$

I have chosen to model the clusters roughly consistent with this cosmological constraint. For the $\Omega_0 = 1$ model, I take $\sigma_8 = 0.5$, and for the the lower density models, $\sigma_8 = 1$.

All simulations presented in this Thesis were done using the 64-processor SGI Origin 2000 supercomputer at the Princeton University Observatory.

2.3 Method

2.3.1 Initial Conditions

The cluster simulations use the constrained Gaussian random initial conditions, generated using the method of Hoffman & Ribak (1991). The actual realization was taken from the cluster comparison project of Frenk et al. (1998). The density perturbations were chosen to produce a 3σ peak with a Gaussian filter of radius 5 h^{-1} Mpc. Retaining only the random phases from the original realization of Frenk et al. (1998), I have renormalized the perturbations according to the power spectrum of the chosen cosmological models.

The parameters of the cosmological models are summarized in Table 1. The Hubble constant is assumed to be $H_0 = 65$ km s^{-1} Mpc^{-1}, following the recent measurement of the time delay in a gravitational lens system 0957+561 (Kundić et al. 1997), and other independent methods.

The power spectrum of the initial density fluctuations includes the effects of baryons using the fitting expressions by Bardeen et al. (1986) and Hu & Sugiyama (1996) (their eqs. [D-28] and [E-12]) in the limit when baryonic oscillations are small:

$$P(k) \propto k\,T^2(k), \tag{2-7}$$

where $T(k)$ is the transfer function, accounting for the causality effects in the linear perturbation theory:

$$T(k) = \frac{\ln(1+2.34q)}{2.34q}\left[1 + 3.89q + (16.1q)^2 + (5.46q)^3 + (6.71q)^4\right]^{-1/4}. \tag{2-8}$$

Here

$$q = \frac{k}{h\ \mathrm{Mpc}^{-1}}\,(\Omega_0 h)^{-1}\,(1-\Omega_B/\Omega_0)^{1/2}\,\alpha^{-1/2}\,\Theta_{2.7}^2, \tag{2-9}$$

$$\alpha = a_1^{-\Omega_B/\Omega_0}\,a_2^{-(\Omega_B/\Omega_0)^3}, \tag{2-10}$$

$$a_1 = (46.9\Omega_0 h^2)^{0.670}\,[1 + (32.1\Omega_0 h^2)^{-0.532}], \tag{2-11}$$

$$a_2 = (12.0\Omega_0 h^2)^{0.424}\,[1 + (45.0\Omega_0 h^2)^{-0.582}], \tag{2-12}$$

where the cosmic microwave background radiation temperature is expressed as $T_{\rm CMB} \equiv 2.7\Theta_{2.7}$ K, and the *COBE* FIRAS observations give 2.728 ± 0.004 K (Fixsen et al. 1996; 95% confidence level).

The growth factor for various cosmological models is given by the following approximation (Lahav et al. 1991; Carroll, Press & Turner 1992; Eisenstein & Hu 1998)

$$D_1(z) = (1+z)^{-1}\,\frac{5\,\Omega(z)}{2}\left[\Omega(z)^{4/7} - \Omega_\Lambda(z) + \left(1+\frac{\Omega(z)}{2}\right)\left(1+\frac{\Omega_\Lambda(z)}{70}\right)\right]^{-1}, \tag{2-13}$$

where $\Omega(z)$ and $\Omega_\Lambda(z)$ are the density parameters as seen by an observer at redshift z:

$$\Omega(z) \equiv \frac{\Omega_0(1+z)^3}{\Omega_0(1+z)^3 + \Omega_R(1+z)^2 + \Omega_\Lambda}, \tag{2-14}$$

$$\Omega_\Lambda(z) \equiv \frac{\Omega_\Lambda}{\Omega_0(1+z)^3 + \Omega_R(1+z)^2 + \Omega_\Lambda}. \tag{2-15}$$

The initial conditions for each of the cosmological models are generated using the same initial phases as in the Frenk et al. (1998) work. The initial displacements are transformed into the Fourier space and the amplitudes are renormalized to agree with the new power spectrum:

$$d_k^{new} = d_k^{old}\left(\frac{P(k)_{new}}{P(k)_{old}}\right)^{1/2}. \tag{2-16}$$

The power spectrum at the initial redshift z_i is normalized as

$$\sigma_8^2(z) = \frac{1}{2\pi^2} \int_0^\infty dk\, k^2\, P(k)\, W^2(kR), \tag{2-17}$$

where $W(x) = 3(\sin x - x\cos x)/x^3$ is the top-hat window function; $R = 8\ h^{-1}$ Mpc. At redshift z_i, the normalization parameter is $\sigma_8(z) = \sigma_8(0) \times D_1(z_i)/D_1(0)$. The perturbation field is then transformed back to real space to yield the initial displacements for the dark matter particles. On the cluster and sub-cluster scales, the power spectrum follows approximately a power law $P(k) \propto k^{-2.5}$.

The internal independent variable of the PM code is the expansion parameter, a. To link the cosmological and galactic simulations, we need a correspondence to the real cosmic time. For all of the three models, the look-back time as a function of redshift (Peebles 1993) can be calculated analytically.

$$H_0\ t(z) = \int_z^\infty \frac{dz}{(1+z)\,[\Omega_0(1+z)^3 + \Omega_R(1+z)^2 + \Omega_\Lambda]^{1/2}}. \tag{2-18}$$

For $\Omega_0 = 1$, the result is

$$H_0\ t(z) = \frac{2}{3}\,(1+z)^{-3/2}. \tag{2-19}$$

For $\Omega_\Lambda = 0$,

$$H_0\ t(z) = \frac{(1+\Omega_0 z)^{1/2}}{(1-\Omega_0)(1+z)} + \frac{\Omega_0}{2(1-\Omega_0)^{3/2}}\ \ln\frac{f^{1/2}-1}{f^{1/2}+1}, \qquad f \equiv \frac{1+\Omega_0 z}{1-\Omega_0}. \tag{2-20}$$

For $\Omega_0 + \Omega_\Lambda = 1$,

$$H_0\ t(z) = \frac{2}{3(1-\Omega_0)^{1/2}}\ \ln\frac{1+(1+f)^{1/2}}{f^{1/2}}, \qquad f \equiv \frac{\Omega_0}{1-\Omega_0}\,(1+z)^3. \tag{2-21}$$

2.3.2 Particle-Mesh code

The main code I used for cluster simulations is the Particle-Mesh code (Cen 1992), kindly provided by Renyue Cen. The code solves Poisson's equation using FFT on a rectangular grid and calculates the density field using the Cloud-in-Cell (CIC) method. The code runs fast in parallel, allowing a large simulation on a 512^3 grid or larger. Particles are assigned initially one per two cells cubed, so that the 512^3 grid simulation has 256^3 particles. The simulations start at redshift $z_i = 20$.

The time step is determined by the requirement that no particle crosses more than half a grid cell, $0.5\ \Delta$. Also, it limits the expansion parameter a to grow by no more than 0.05 $(1+z_i)^{-1}$. I have checked that reducing the time step by a factor of two does not change noticeably the structure of the resulting cluster.

On 16 processors of the SGI Origin 2000, the full simulation with a 512^3 grid runs for about 36 hours. Here, a large part of the time is spent on the calculation of the tidal field due to and around the identified galaxies.

Some of the PM results were checked with the Adaptive Mesh Refinement code of Greg Bryan (Bryan et al. 1995). Specifically, I checked the calculation and normalization of the tidal force, and the galaxy trajectories.

2.4 The Structure of the Clusters

The calculated parameters of the clusters are given in Table 2. The virial values are calculated in a sphere, originating from the cluster center, with a mean overdensity $\delta = 200$. The mean mass of the clusters is $4 \times 10^{14}\ M_\odot$, and the one-dimensional velocity dispersion is 660 km s^{-1}.

Figure 2.1 shows the projected surface density of the three clusters at the present epoch. While the lower density clusters look more spherical and well relaxed, the $\Omega_0 = 1$ cluster is in the continuing process of formation. Note a large group of galaxies to the upper right from the cluster on the enlarged panel. This group will merge with the cluster in a few billion years.

Figures 2.2–2.4 show the evolution with redshift of each of the three clusters. As expected, the $\Omega_0 = 1$ cluster does not exist at early redshift and is very weak even at $z = 1$. In contrast, both of the lower density clusters are essentially formed at $z = 1$. Note that the two latter clusters have very similar appearance at all times; the cosmological constant does not seem to affect the cluster properties.

Figure 2.5 shows that the density profiles of the three clusters are very similar, with the slight excursion of the $\Omega_0 = 1$ cluster at $r \approx 2h^{-1}$ Mpc due to the infalling group. This group is clearly visible on the velocity dispersion plot, Figure 2.6.

The decrease of the velocity dispersion at small distances from the center is partly real and partly numerical. The highest resolution dark matter simulations in Frenk et al. (1998) show a similar decrease; our models should exhibit a similar trend. On the other hand, the present simulations lose resolution in the cluster core and cannot be trusted at small radii. To illustrate the resolution effects, I have repeated the simulations of Cluster III ($\Omega_0 = 0.4$, $\Omega_\Lambda = 0.6$) on the smaller grids, 256^3 and 128^3 cells. Table 3 gives the virial parameters, while Figure 2.7 shows the density and velocity profiles of the additional models. The density structure is reproduced well to the resolution limit of each of the simulations, but the velocity dispersion starts to decline much earlier for the lower resolution runs. Nevertheless, the difference between the 512^3 and the 256^3 runs is small and confirms the accuracy of the larger simulation.

The simulated clusters should be representative of the observed ones. The virial masses and radii are quite common, as follows from the survey of the nearby optical and X-ray clusters by Girardi et al. (1998). In terms of the galaxy population, the clusters are relatively poor. They could be assigned an Abell richness of 0 to 1, if found at low redshift.

Of the local sample, the simulated clusters are similar to the Virgo cluster. Huchra (1985) reports the line-of-sight velocity dispersion for all galaxies of 721 ± 27 km s^{-1}. However, this estimate may be affected by the spiral galaxies on the outskirts of the cluster, which may not yet have virialized. If only the ellipticals in the cluster core are included, the velocity dispersion drops to 581 ± 33 km s^{-1}. The ROSAT results (Böhringer 1994) indicate the X-ray size of the Virgo cluster $R_X = 1.8$ Mpc and the total mass $M = (1.5 - 5.5) \times 10^{14}\ M_\odot$. Often cited in theoretical work, the Coma cluster is much larger, with the mean velocity dispersion about 1000 km s^{-1} (Merritt & Gebhardt 1994). The ROSAT values are $R_X = 4$ Mpc and $M = (1.1 - 2.8) \times 10^{15}\ M_\odot$ (Böhringer 1994). However, that cluster is unusually rich. Our models, therefore, represent modest but more common clusters of galaxies.

2.5 Galaxies in the Simulation

2.5.1 Group Finding Algorithm

Dark matter halos are identified in the simulations using the recent algorithm HOP by Eisenstein & Hut (1998). The new algorithm is similar in spirit to DENMAX (Gelb & Bertschinger 1994) but uses densities at the particle positions instead of those on a regular grid. The method is coordinate free and is very fast.

I have extended the original HOP algorithm by including the procedure for removing the particles which are not gravitationally bound to the group. The procedure is similar in spirit to the existing SKID algorithm (Weinberg, Hernquist & Katz 1997). I now briefly outline this unbinding procedure.

The gravitational energy of the particles in a group is calculated by direct summation of the Plummer potential with a smoothing length corresponding to one grid size of the cluster simulation. The kinetic energy includes the Hubble expansion term. The total energy per unit mass is

$$E_i = \frac{1}{2}\left[\mathbf{v}_i - \mathbf{v}_{\rm com} + H(\mathbf{r}_i - \mathbf{r}_{\rm com})\right]^2 - \sum_j \frac{G\,m_p}{((\mathbf{r}_i - \mathbf{r}_j)^2 + \epsilon^2)^{1/2}}, \tag{2-22}$$

where m_p is the particle mass, $\mathbf{r}_i$ is the physical coordinate, and $\mathbf{v}_i$ is the particle velocity in km s^{-1}. Here H is the Hubble constant at the given epoch (Peebles 1993):

$$H(z) = H_0\,\left[\Omega_0(1+z)^3 + \Omega_R(1+z)^2 + \Omega_\Lambda\right]^{1/2}, \tag{2-23}$$

where Ω_R is the curvature contribution; $\Omega_R \equiv 1 - \Omega_0 - \Omega_\Lambda$.

The particles are unbound as follows. I find the particle m with the maximum energy and discard it, if $E_m > 0$. I recalculate the center of mass of the group using the remaining particles and update the potential energy. Then, I find the new highest energy particle and repeat the procedure. In the end, all remaining particles are bound or else the group is dispersed.

A straightforward implementation of the unbinding procedure works well, although somewhat slowly for groups containing more than 10000 particles. Also, the algorithm is intrinsically serial. In the longest case, the unbinding algorithm took about 40 minutes on a single SGI R10000 processor.

The second part of the HOP algorithm, REGROUP, allows three different density parameters to be used to define the outer boundary of the group (δ_{outer}), the saddle point for merging two groups together (δ_{saddle}), and the minimum density of a viable group (δ_{peak}). Here δ is the relative local overdensity. After some experimenting, I have taken the following parameters to produce reasonable size halos: $[\delta_{outer}, \delta_{saddle}, \delta_{peak}] = [15,45,50]$ for the $\Omega_0 = 1$ model, and [20,55,60] for the low density models. The different sets of parameters for the two values of Ω_0 are necessary because of the different masses of the particles.

Figures 2.8–2.10 show the particles in the identified galaxies for the three clusters. Because of the difference in masses, the $\Omega_0 = 1$ galaxies contain significantly fewer particles than their lower Ω_0 counterparts.

2.5.2 Galaxy Mass Function

The mass function of the identified galaxies can be compared with the prediction of the Press-Schechter theory (Press & Schechter 1974). The number density of galaxies at the given epoch, z_g, is calculated using equations (A4-A9) of Mo, Mao & White (1998).

Figure 2.11 shows the mass functions of the halos in the three clusters. Note the relative depletion of the low mass halos in the simulations. This is due to the truncation of the input power spectrum at the Nyquist frequency, which effectively prevents the formation of small-scale objects. For comparison, the lower right panel shows the mass function obtained in the lower resolution, 256^3 simulation of Cluster III. As expected, the lower mass halos are depleted more strongly than the larger halos.

2.6 Galaxy Trajectories

The definition of a galaxy in the cluster simulation is not obvious. While at high redshift the dark matter halos are significantly denser than the surrounding environment, at low redshift the density contrast effectively disappears. This effect is known as overmerging of halos (e.g., Moore, Katz & Lake 1996) due to insufficient mass resolution. Therefore, it is difficult and, to some extent, uncertain to try to identify the galaxy halos from the particle distribution at all times. Instead, I have implemented the following simple procedure, which can be extended to a higher degree of sophistication.

I identify the dark matter halos at early enough redshift when the density contrast is large, but late enough when galaxies are known to exist. A fiducial epoch at which the central parts of most of the large galaxies are assumed to have formed is taken to be $z_g = 5$. This is also an epoch at which I start the N-body galactic simulations reported in Chapter 3. To obtain a statistically significant sample, I follow the $N_g = 100$ most massive galaxies.

As the output, the HOP algorithm produces the masses of the N_g dark matter halos and the coordinates and velocities of their centers of mass. Then, the N_g massless particles are added to the PM simulation with the calculated initial conditions. These new "galactic" particles do not affect either the density or the potential calculation but rather act as test particles. I follow the motion of these galactic particles and output the tidal field of the cluster along their trajectories.

By not using the real particles to calculate the center of mass of the galaxies, we effectively avoid the overmerging problem: the test particles will not merge even if they come very close to each other. The drawback is that we ignore the effect of the galaxy of interest on other galaxies; the galactic center of mass simply moves in the potential of other galaxies and the cluster itself. It is possible that, due to strong perturbations, the test center of mass may depart from the bulk of the particles in the galaxy. To guard against this effect, I have implemented another scheme for calculating the galactic trajectories.

The second scheme involves a subset of real particles constituting the galaxy. The density at each particle's position is calculated using the CIC kernel, which is also used in the main PM calculation. Then the densest subset of the particles, 1/8 of the total, is used to calculate the center of mass directly. These dense particles presumably lie deep in the potential well of the galaxy and should serve as robust indicators of the galactic center. In case of the two galaxies merging, their centers defined this way would clearly indicate it. However, I do not attempt to study the internal structure of galaxies in the cluster simulations and only use them to trace the centers of mass.

In general, I found a very good agreement between the trajectories calculated in the two ways, especially for the less massive galaxies. For the very massive halos, the "test particle" center of mass occasionally tends to oscillate around the trajectory determined by the second method. I have therefore decided to use the latter as the more reliable trajectories.

Figures 2.12–2.14 show the trajectories of the two selected galaxies in each of the clusters. One of these galaxies is very massive, taken from the top of the list, the other is taken from the bottom. These galaxies are used for the galactic simulations in Chapter 3, representing large spiral and dwarf galaxies, respectively. The large galaxies rank #4 in each of the clusters, while the dwarf galaxies rank #93 in Clusters I and II, and #87 in Cluster III. The galaxies are chosen to be within the virial radius of their respective cluster at the end of the simulation.

The galactic trajectories are quite irregular. In the $\Omega_0 = 1$ case, the galaxies are just getting into the cluster at the present epoch, although not on a free-fall path. These trajectories are similar to those shown in Frenk et al. (1996). In the low density cases, the galaxies have enough time to orbit around the cluster center several times, more in the open model. These differences will have major effects on the dynamical evolution of the galaxies.

2.6.1 Merger History

Mergers of galaxies may play an important role, especially if the galaxies collide at relatively low velocities (see §2.8). However, the cluster simulations do not provide enough resolution to study the mergers of individual galaxies. Therefore, I have adopted a simple prescription for identifying a merger, similar to that in Binney & Tremaine (1987); S. Tremaine (private communication).

First, I select all close encounters with the impact parameter 20 kpc or less. Assuming that at such short distances the effect of all other galaxies can be ignored, the encounter can be considered as a two-body problem. The relative distance is $\mathbf{R} = \mathbf{r}_1 - \mathbf{r}_2$, the relative velocity is $\mathbf{V}_{rel} = \mathbf{v}_1 - \mathbf{v}_2$, where indeces 1 and 2 refer to the two galaxies, and I assume that galaxy 1 is more massive; $m_1 \geq m_2$.

The galaxies will merge if both the orbital energy and the angular momentum of the reduced particle satisfy their respective criteria. Using the reduced mass, $\mu = m_1 m_2/(m_1 + m_2)$, the energy criterion is

$$\frac{1}{2}\mu V_{rel}^2 - \frac{G\,m_1\,m_2}{R} \lesssim \mu\,\frac{m_2}{m_1}\,\frac{\sigma_1^4}{\sigma_1^2 + V_{rel}^2}, \tag{2-24}$$

where σ_1 is the velocity dispersion of the larger galaxy. The right hand side comes from the consideration that even if the smaller galaxy is not gravitationally bound to the larger galaxy, the former may merge due to dynamical friction with the larger halo. The mass ratio, m_2/m_1, emphasizes the rate of spiraling in due to dynamical friction, while the V_{rel}^2 term in the denominator provides the correct limiting behavior for $V_{rel} \gg \sigma_1$.

The second criterion involves the orbital angular momentum, $J = |\mathbf{r} \times \mathbf{v}|$. The galaxies will merge within the Hubble time (Binney & Tremaine 1987) if

$$J < J_{max} \approx 3\, R_h\, \sigma_1, \tag{2-25}$$

where R_h is the half-mass radius of the larger galaxy. This condition selects more radial orbits with respect to the center of mass of the two galaxies. The second criterion is not very restrictive and is usually satisfied if the first criterion is satisfied.

The distribution of close encounters and possible mergers of galaxies are discussed in detail in §2.8.

2.7 Calculating the Tidal Field

The tidal field of the cluster is calculated along the trajectories of the identified galaxies. The tidal force $F_{tid,\alpha}$ and the shear tensor $F_{\alpha,\beta}$ are

$$F_{tid,\alpha} = -\left(\frac{d\Phi}{dr_\alpha dr_\beta}\right)_0 r_\beta \tag{2-26}$$

$$= F_{\alpha,\beta}\, r_\beta, \tag{2-27}$$

where Φ is the external potential and $\mathbf{r}$ is the radius vector in the galactic reference frame. By definition, the tidal force is zero at the center of mass of the galaxy.

The second derivative of the potential is calculated using finite differences. The value of Φ is obtained by tri-linear interpolation from the 8 nearest mesh points enclosing the current position of the galaxy. At each of the mesh points, the tidal components are calculated using Savitzky-Golay smoothing filters of the 4th order (Press et al. 1992, §14.8). These filters replace each data value f_i with a linear combination of itself and a few nearby neighbors:

$$f_i^* = \sum_{n=-N_L}^{N_R} c_n^{(0)}\, f_{i+n}, \tag{2-28}$$

where N_L and N_R are the number of points used "to the left" and "to the right" of a data point, respectively. The coefficients are chosen such that the 4th derivative (the smoothing order) of the field is preserved by the smoothing. I take $N_L = N_R = 4$, which corresponds to an effective smoothing of the tidal field, on the scale of $0.25 - 0.5\ h^{-1}$ Mpc for a simulation on the 512^3 grid. The first and second derivatives of the potential field are obtained through the similar expression (2-28) with the different coefficients $c_n^{(1)}$ and $c_n^{(2)}$ (Table 4).

The double derivatives, Φ_{xx}, Φ_{yy}, Φ_{zz}, were calculated at the mesh points (i, j, k) as

$$\Phi_{xx}(i,j,k) = \frac{1}{\Delta^2} \sum_{n=-N_L}^{N_R} c_n^{(2)}\, \Phi(i+n, j, k), \tag{2-29}$$

where Δ is the mesh size. The mixed derivatives, Φ_{xy}, Φ_{xz}, and Φ_{yz}, were calculated using smoothing in both directions:

$$\Phi_{xy}(i,j,k) = \frac{1}{\Delta^2} \sum_{n_1=-N_L}^{N_R} \sum_{n_2=-N_L}^{N_R} c_{n_1}^{(1)} c_{n_2}^{(1)} \Phi(i+n_1, j+n_2, k). \tag{2-30}$$

The accuracy of the above smoothing has been tested against the analytic NFW profile (Navarro, Frenk & White 1997):

$$\rho(r) = \frac{\rho_0}{(r/r_s)(1+r/r_s)^2}, \tag{2-31}$$

where r_s is the scale radius. The exact tidal force is readily calculated using equation (5) of Gnedin, Hernquist & Ostriker (1999). The parameters of the NFW model were chosen to mimic those of the real cluster simulation. Assuming the virial radius of the NFW model, $R_{vir} \approx 1.5\,h^{-1}$ Mpc, and the "concentration" relation $R_{vir} = 10\ r_s$, we find $r_s = 0.15\,h^{-1}$ Mpc. For the 512^3 simulation in the box of 32 h^{-1} Mpc, the grid cell size is $\Delta = 0.063\,h^{-1}$ Mpc. Therefore, the appropriate scaling radius is $r_s \approx 2.5\,\Delta$.

Figure 2.15 shows that our method reproduces well the mixed derivative F_{xy} up to 3 cell sizes from the center, and somewhat worse the double derivative F_{xx}. In all cases, however, the smoothing filter is more accurate than the straightforward two-point finite difference. In the real cluster, the advantage of the smoothing filter is much greater because of the numerical noise of the particle distribution.

2.7.1 Test: The Pancake Simulation

As another test of calculating the tidal field, I have run a test simulation with the one-dimensional Zeldovich's pancake. The initial conditions are set up as described in Bryan et al. 1995. The wavelength of the sine wave perturbation equals the size of the simulation box; the maximum displacement is in the center. The only non-zero component of the tidal tensor, $\Phi_{xx} = 4\pi G \Delta\rho$, from Poisson's equation. Here $\Delta\rho$ is the density perturbation. Simulations start at the redshift $z_i = 20$, while the caustic forms at $z = 0$.

I have run two simulations, with the high (512^3) and low (128^3) resolution. The density in both simulations is reproduced very accurately. However, the tidal force follows the exact solution only in the beginning, when the perturbation is small. At later times, the perturbation grows and the accuracy of the tidal force calculation decreases. The smoothing filter cannot resolve a very narrow caustic. As expected, the higher-resolution simulation departs from the exact solution closer to the time of caustic formation. The effect of the resolution loss in the high density regions will be emphasized again in the next section.

2.7.2 Subtracting the Galaxy Self-Contribution

Large halos may contribute significantly to the value of the tidal field around them. If the halo extends more than a couple of cell sizes, it will contaminate the calculation of the *external* tidal force on the galaxy. It is necessary to subtract the self-contribution.

For this purpose, I have implemented a potential solver for the isolated galaxy. On a rectangular grid of 16^3 cells, the density is assigned using the CIC method and including only the galactic particles. Then the potential is obtained using the FFT method with the isolated boundary conditions. The same procedure for calculating the tidal force is applied here as for the main cluster potential. The resulting self-force due to the galaxy is then subtracted from the previously calculated total value.

The FFT solver for Poisson's equation with the isolated boundary conditions is implemented as described in Hockney & Eastwood (1981). Twice as large a density grid is used padded with zeros in the extra space. Green's function in real space is translated correctly to the new grid quadrants, and then Fourier transformed and stored on the grid for the potential calculation. After that, the method proceeds as usual: Fourier transforming the density field, multiplying by the Green's function $G_{isol}(k)$, and transformed back to real space.

The trick with the extended grid is required to avoid multiple images of the galaxy, which appear in the usual FFT with the periodic boundary conditions. The resulting Green's function differs from the usual dependence, $G(k) = k^{-2}$, cutting the high frequency tail (Figure 2.16).

Several tests have been performed for the isolated FFT procedure. Using the same 16^3 grid, a total of 2^{15} particles have been distributed in the central cell according to the Hernquist (1990) model,

$$\rho(r) = \frac{M}{2\pi}\,\frac{a}{r}\,\frac{1}{(r+a)^3}, \tag{2-32}$$

with the tiny core radius, $a = 0.1\,\Delta$; here M is the total mass of the model. Essentially, it is a point mass represented by particles.

Figure 2.17 shows that the exact potential is reproduced with very high accuracy, all the way to the edge of the simulation box. For comparison, the plot shows the periodic FFT on the same grid: the potential significantly deviates on most of the grid. The force calculation is limited in the center at about $2\,\Delta$, as in any grid-based method, but behaves perfectly at all larger radii. The force calculated with the periodic FFT shows much more noise.

Another test has been applied to make sure the procedure works in the real simulation. Particles constituting a large galaxy in the $\Omega_0 = 1$ simulation and located within a single cell have been taken to calculate the 16^3 density field. The above procedure is repeated for such a distribution, which resembles a point source. Figure 2.18 shows a still good agreement with the exact potential and the force, although with increased scatter. These tests confirm that the isolated FFT method works correctly.

Finally, Figure 2.19 shows the self-contribution of the large galaxy in Cluster III simulation. For the ease of comparison, I plot the sum of the diagonal components of the tidal tensor (the trace $\Phi_{xx} + \Phi_{yy} + \Phi_{zz}$). The trace generally follows the actual density of the galactic particles, as it should according to Poisson's equation. However, because of the smoothing filter used to calculate the tidal force, it misses the very high and low density regions. Otherwise, the amplitude of the tidal force is correct. When subtracted from the total tidal force, it should properly remove the self-contribution of the galactic particles.

Also, Figure 2.19 shows the scaling $(1+z)^3$, which a galaxy with the fixed comoving density would have in physical units. The galactic density follows this scaling quite accurately, indicating that the galaxy expands in real space. This numerical artifact is due to the loss of force resolution within one cell. The galactic particles cannot effectively collapse below 1 Δ because they do not feel each other's force. In comoving coordinates, the galaxy continues to occupy the same volume. This effect also explains why the galactic contribution to the tidal field declines with time. However, the global tidal field of the cluster is largely unaffected by the force resolution because the characteristic scale of the cluster potential is much larger than a single cell.

2.7.3 The Resulting Tidal Field

Figures 2.20–2.22 show the tidal field around the large and dwarf galaxies, chosen in §2.6, for each of the cluster simulations. The time behavior of the tidal force is very irregular. There are many strong peaks, with an amplitude up to 150 Gyr^{-2} and higher. The main peaks are usually narrow, with the characteristic duration about 0.2 Gyr, the smaller peaks are broader and last longer. The occurrence of the large and intermediate peaks is clearly differentiated in time: the former happen early, when the galaxies are distinctly dense relative to the background; the latter happen at the late stages of the evolution, when the dark matter halos merge and the gravitational potential becomes smoother.

The amplitude of the tidal field is the largest in the $\Omega_0 = 0.4$ simulation, although strong perturbations continue for longer time in the Λ model. In the $\Omega_0 = 1$ model, the overall amplitude is smaller but the force shows more temporal structure. The main distinction between the galaxies in the low and high Ω_0 models is the time spent within the cluster. In the latter case, the galaxies are just arriving to the center, when the substructure has been effectively erased. In the low Ω_0 models, the galaxies have arrived sooner and experienced more interaction with the collapsing cluster.

The overall amplitude of the tidal force is determined by the epoch of cluster formation. In the low Ω_0 models the clusters form at earlier redshift, when the mean density of the Universe is high. Thus, the corresponding tidal force is stronger than in the $\Omega_0 = 1$ model. Since the growth of the clusters is balanced by the drop of the mean density, the tidal force is expected to be of the same order of magnitude throughout the evolution.

Note, that the peaks of the tidal force are not always correlated with the closest approach to the cluster center. The galaxies are being tidally "shocked" at 1 Mpc from the center as often as within 400 kpc. Even though the Figures 2.20–2.22 reflect only the final position of the cluster center which has been moving slowly in the simulation box, it is likely that many encounters with large galaxies or groups of galaxies happen at relatively large distances from the center. As the cluster forms, such tidal encounters may occur within a fairly large (comoving) volume.

The amplitude of the tidal force tells us about the effective scale of the perturbations causing it. For a large smooth cluster, the expected tidal force is of the order

$$F_{\alpha,\beta} \sim \frac{GM(r)}{r^3} \sim \frac{\sigma_{cl}^2(r)}{r^2}, \tag{2-33}$$

where $M(r)$ is the enclosed mass at the radius r, and $\sigma_{cl}(r)$ is the cluster velocity dispersion. For the simulated clusters, the three-dimensional dispersion is $\sqrt{3} \times 660$ km s^{-1} ≈ 1100 km s^{-1}. If the characteristic scale, the cluster core radius, is 200 kpc, the resulting tidal perturbation is

$$F_{\alpha,\beta} \sim 32 \left(\frac{\sigma_{cl}}{1100 \text{ km s}^{-1}}\right)^2 \left(\frac{r}{200 \text{ kpc}}\right)^{-2} \text{ Gyr}^{-2}. \quad (2\text{-}34)$$

The actual amplitude of the tidal force (cf. Figures 2.20–2.22) is about 150 Gyr^{-2}. Turning the argument around, such tidal force corresponds to the effective scale of the perturbation

$$r_p = 92 \left(\frac{\sigma_{cl}}{1100 \text{ km s}^{-1}}\right) \left(\frac{F_{\alpha,\beta}}{150 \text{ Gyr}^{-2}}\right)^{-1/2} \text{ kpc}. \quad (2\text{-}35)$$

Smaller than the core radius but larger than individual galaxies, this scale is appropriate for small groups of galaxies. As is discussed in the next section, the groups maintain their identity in many clusters. Even such a relaxed cluster as Coma shows a detectable amount of substructure. The large peaks of the tidal force dominate the total amount of heating (see §3.3). Thus, I conclude that the interaction of galaxies with the remaining substructure in clusters is primarily responsible for the tidal effects.

2.8 Discussion

The rich time structure of the tidal force around galaxies suggests many close encounters with massive objects. In particular, galaxy-galaxy collisions might be assisted by mergers of poor groups of galaxies. The actual galaxy trajectories provide detailed statistics of the close encounters.

Figure 2.23 shows the number of collisions within four different impact parameters for the 100 most massive galaxies in Cluster III. The impact parameter Δr_i is defined as the distance between the centers of mass of the galaxies. In order to detect all close encounters, the galaxy trajectories were linearly interpolated between the successive time steps. The number of encounters within 5 kpc to 15 kpc scales roughly as Δr_i^2, in agreement with the estimate (1-2). However, the total number of encounters is much higher than expected. The effect is mainly due to the non-uniform distribution of galaxies within the cluster, which increases the probability of a collision within a group of galaxies. Equation (1-2) can be rewritten for the total number of encounters in the cluster:

$$N_{enc} = \int n_g^2(r)\, \pi R_g^2\, V_{rel}\, t_H \left(1 + \frac{V_c^2}{4V_{rel}^2}\right) d\mathbf{r}, \quad (2\text{-}36)$$

where the integration extends over the virial volume of the cluster. I have also included here the effect of gravitational focusing (Binney & Tremaine 1987); $V_c \sim 250$ km s^{-1} is the circular speed, V_{rel} is the relative velocity of the galaxies. The mean value of the number density of galaxies squared, $\langle n_g^2 \rangle$, may be substantially higher than the square of the mean density, $\langle n_g \rangle^2$, because of galaxy clustering in groups. The clumping factor,

$$C \equiv \frac{\langle n_g^2 \rangle}{\langle n_g \rangle^2}, \quad (2\text{-}37)$$

can be estimated by representing each galaxy by a smooth Gaussian function in space and integrating $n_g(r)$ and $n_g^2(r)$ over the virial volume of the cluster. Taking the width of the smoothing function to be equal one cell size, Δ, gives $C = 36$ for Cluster III. However, this value may be uncertain due to the small number of galaxies, 65 within the virial radius of the cluster. Taking larger smoothing length reduces the clumping factor. Now, the number of encounters may be written as

$$N_{enc} = 133 \left(\frac{C}{36}\right) \left(\frac{\Theta}{1.08}\right) \left(\frac{N_g}{100}\right)^2 \left(\frac{\Delta r_i}{10 \text{ kpc}}\right)^2 \left(\frac{R_{cl}}{1 \text{ Mpc}}\right)^{-3} \left(\frac{V_{rel}}{450 \text{ km s}^{-1}}\right), \qquad (2\text{-}38)$$

where Θ is a short notation for the gravitational focusing factor. Note that this number is much higher than what follows from the naive estimate (1-2), mainly because of the large clumping factor.

Table 5 shows the total number of encounters for each of the four values of the impact parameter. Given the uncertainty introduced by the evolution of the cluster, the estimate (2-38) agrees with the simulations to within a factor of 2. Also, Figure 2.23 and Table 5 show the number of possible mergers, estimated using the criterion (2-24). Only about 6% of the close encounters might result in a merger, if the impact parameter is larger than 10 kpc. For the very close collisions within 4 kpc, the merger fraction is higher but may be due to a respectively low number of encounters. The fraction of likely mergers agrees roughly with the scaling indicated by equation (1-4). Table 5 also shows the expectation number of close encounters per galaxy, $N_{enc,1}$. Since each encounter involves two galaxies, the number of encounters per galaxy is twice the total number of encounters over the number of galaxies. The probability of a merger per galaxy is obtained as N_{mer}/N_g, since each merger removes only one galaxy.

Note that most collisions take place close to the end of the simulation, when the galaxies assembled inside the cluster. Also, more than half of all encounters occur within the inner 300 kpc from the cluster center. However, there are two distint peaks at about 8 Gyr and 10 Gyr, presumably due to a merger of individual groups of galaxies.

Figure 2.23 shows the relative velocities of the galaxies at the time of collision. The velocities are surprisingly low: the distribution peaks at about 200 km s^{-1}, the median is 330 km s^{-1}, and the mean is 450 km s^{-1}. Since the number of encounters depends linearly on V_{rel}, ignoring the small effect of gravitational focusing, I take the mean value as representative. Even that value is significantly lower than the three-dimensional velocity dispersion of dark matter, roughly by a factor of two. The pairwise velocities of galaxies are clearly biased in the simulation.

A review of the literature reveals that numerical simulations often produce "galaxies" with the velocity dispersion lower than that of dark matter (Summers, Davis & Evrard 1995; Carlberg 1994 and references therein). One possible explanation involves bias in the hierarchical structure formation: galaxies form around high density peaks and those peaks are likely to be clustered. Therefore, one would expect large galaxies to be always around the center of the cluster and do not gain velocity from the gravitational infall. Another explanation involves dynamical friction removing angular momentum of large galaxies as they sink closer to the center.

There is also a numerical cause of the lower galactic velocities. The PM code loses force resolution within the inner two cells, which leads to galaxies not "feeling" each other's gravity. This effect cannot be successfully remedied with the present numerical scheme; a higher resolution code is needed for a careful study of galaxy dynamics near the cluster center.

Also, the individual particles initially bound to a galaxy may depart substantially from the galactic center of mass due to a small difference in the initial conditions. If these particles are scattered throughout the cluster, the estimate of the center-of-mass velocity would be significantly reduced. I have run a test by combining a random set of dark matter particles within the cluster virial radius into groups, according to the galactic mass function (see §2.5.2). The constructed this way "random galaxies" have much lower velocities than the real galaxies in the simulation, below 100 km s^{-1}. Thus, the most bound particles in the galaxies did not dissolve completely and maintain their identity even at the end of the simulation.

The high-resolution simulations reported in the literature indicate somewhat similar results. Tormen, Diaferio & Syer (1998) find the peak of the relative velocity distribution at the time of galaxy collisions to be $V_{rel} \sim 2.5\,\sigma_g$, or about 500 km s^{-1}. This is again much lower than the velocity dispersion of dark matter in that simulation. Also, Ghigna et al. (1998) find very few mergers within the virial radius of their simulated cluster. Thus, it is possible that the criteria (2-24,2-25) overestimate the number of true mergers.

At the present, observations neither confirm nor reject the velocity bias. Carlberg, Yee & Ellingson (1997), in a survey of 1150 galaxies from 14 clusters, find an almost flat projected velocity dispersion up to the virial radius of their ensemble cluster. The line-of-sight projection may, however, wash out a decrease in the true velocity dispersion near the center. Another large survey of 15 rich clusters (Dressler & Shectman 1988) shows a significant amount of substructure in many of the clusters. The pairwise velocities of galaxies in subgroups are lower than the global velocity dispersion. Also, the azimuthally averaged velocity dispersion exhibits a modest decline in the central regions. The magnitude of the effect is of the order 20%. Therefore, the current observational status of the velocity bias is inconclusive.

Table 6 shows the galaxy velocity dispersion as a function of distance from the cluster center. Due to a small number of galaxies within the virial radius, 65 out of the total 100, I have split them in only three radial bins. The velocity gradient is very strong, with the lowest dispersion within the inner one simulation cell.

Dynamical friction with dark matter reduces the angular momentum of large galaxies and moves them closer to the cluster center. In the present simulations, the effect of dynamical friction may be compromised by the loss of force resolution on the galactic scale. As the dark matter halos merge, the density contrast between the galaxies and dark matter reduces and so is the efficiency of mass segregation. In Cluster III, the masses of the galaxies are only slightly anticorrelated with their final distance from the center: Spearman's correlation coefficient is $r_s = -0.08$.

The spatial distribution of galaxies in Cluster III also hints to a modest amount of mass segregation. The number density profile is approximately $n_g(r) \propto r^{-2.7}$, whereas the mass density is steeper, $\rho_g(r) \propto r^{-3.3}$. Note, however, that due to small number statistics these slopes are largely uncertain. For comparison, the dark matter follows approximately an isothermal profile in the inner parts of the cluster, $\rho_{dm} \propto r^{-2}$. Thus, galaxies are distributed more steeply than the dark matter.

Interestingly, a momentum loss due to ram-pressure of the ICM also contributes to the sinking of massive galaxies to the cluster centers. Kundić et al. (1993) find the timescale for this process to be comparable to that of dynamical friction. However, the cluster simulations do not include gas dynamics and, therefore, are insensitive to this effect.

The smoothing filter used to calculate the tidal field (§2.7) automatically removes the effect of close encounters between the galaxies. The additional contribution to the tidal force due to close encounters can be estimated as follows. The number of close encounters per galaxy in the simulation can be approximately fitted as

$$N_{enc,1} \approx 1 \left(\frac{R}{5\,\mathrm{kpc}}\right)^2 \left(\frac{V_{rel}}{450\ \mathrm{km\ s^{-1}}}\right), \tag{2-39}$$

where $R = \Delta r_i$. The amplitude of the tidal force from a galaxy of mass M_g at an impact parameter R is of the order $F_{\alpha,\beta} \sim GM_g/R^3$. The duration of the encounter is approximately R/V_{rel}, so that the contribution to the heating parameter I (see §3.3) of an encounter at a distance R is

$$I_{enc}(R) = \left(\int F_{\alpha,\beta}\, dt\right)^2 \approx \left(\frac{G\, M_g}{R^2\, V_{rel}}\right)^2. \tag{2-40}$$

The total contribution of all encounters is

$$\begin{aligned} I_{enc} &= \int_{R_{min}}^{R_{max}} I_{enc}(R)\, dN_{enc,1}(R) \\ &\approx 1.4 \times 10^4 \left(\frac{M_g}{3 \times 10^{11}\, M_\odot}\right)^2 \left(\frac{V_{rel}}{450\ \mathrm{km\ s^{-1}}}\right)^{-1} \left(\frac{R_{min}}{5\,\mathrm{kpc}}\right)^{-2} \mathrm{Gyr}^{-2}. \end{aligned} \tag{2-41}$$

The integral is dominated by the very close encounters, which allows me to ignore the upper limit of integration. The lower limit is set by the condition $N_{enc,1} > 1$, i.e. that the encounter takes place. Also, the value for the galactic mass, M_g, is the upper limit on the tidally truncated halo (cf. eq. [3-7]). Therefore, equation (2-41) gives the upper limit on the effect of close encounters. Figure 3.1 in Chapter 3 shows that this value of I_{enc} is comparable to I for many galaxies but is smaller by a factor of few than the maximum value. Thus, close encounters contribute an important part, but do not dominate the tidal heating.

2.9 Conclusions

The tidal field around galaxies in the self-consistent cluster simulations shows a lot of temporal structure. The peaks of the tidal force are not always correlated with the closest distance to the cluster center and are likely to be due to surviving groups of galaxies or large individual galaxies. The number of close encounters is enhanced by the remaining substructure, with about 4 encounters per galaxy within 10 kpc in the Hubble time. The probability of a possible merger is also amplified to about 30% per galaxy. Including the large clumping factor, the number of close encounters agrees roughly with the analytical estimate. Close galactic encounters, which are not included in the present simulations, are shown to contribute a non-negligible fraction of the total tidal heating.

REFERENCES

Bardeen, J. M., Bond, J. R., Kaiser, N., & Szalay, A. S. 1986, ApJ, 304, 15

Binney, J., & Tremaine, S. 1987, Galactic Dynamics (Princeton: Princeton Univ. Press)

Böhringer, H. 1994, in Clusters of Galaxies, ed. F. Durret, A. Mazure, & J. Trân Thanh Vân (Moriond: Editions Frontiers), p. 139

Bryan, G. L., Norman, M. L., Stone, J. M., Cen, R., & Ostriker, J. P. 1995, Comp. Phys. Comm., 89, 149

Carlberg, R. G. 1994, ApJ, 433, 468

Carlberg, R. G., Yee, H. K. C., & Ellingson, E. 1997, ApJ, 478, 462

Carroll, S. M., Press, W. H., & Turner, E. L. 1992, ARA&A, 30, 499

Cen, R. 1992, ApJS, 78, 341

Dressler, A., & Shectman, S. A. 1988, AJ, 95, 985

Eisenstein, D. J., & Hu, W. 1998, ApJ, 496, 605

Eisenstein, D. J., & Hut, P. 1998, ApJ, 498, 137

Eke, V. R., Cole, S., & Frenk, C. S. 1996, MNRAS, 282, 263

Fixsen, D. J., Cheng, E. S., Gales, J. M., Mather, J. C., Shafer, R. A., & Wright, E. L. 1996, ApJ, 473, 576

Frenk, C. S., Evrard, A. E., White, S. D. M., & Summers, F. J. 1996, ApJ, 472, 460

Frenk, C. S., et al. 1998, ApJ, submitted

Gelb, J., & Bertschinger, E. B. 1994, ApJ, 436, 467

Ghigna, S., Moore, B., Governato, F., Lake, G., Quinn, T., & Stadel, J. 1998, MNRAS, 300, 146

Girardi, M., Giuricin, G., Mardirossian, F., Mezzetti, M., & Boschin, W. 1998, ApJ, 505, 74

Gnedin, O. Y., Hernquist, L., & Ostriker J. P. 1999, ApJ, 514, in press; `astro-ph/9709161`

Hernquist, L. 1990, ApJ, 356, 359

Hockney, R. W., & Eastwood, J. W. 1981, Computer Simulations Using Particles (New York: McGraw Hill), p. 212

Hoffman, Y., & Ribak, E. 1991, ApJ, 380, L5

Hu, W., & Sugiyama, N. 1996, ApJ, 471, 542

Huchra, J. P. 1985, in The Virgo Cluster, ed. O.-G. Richter & B. Binggeli (Garching: ESO workshop), p. 181

Kundić, T., Hernquist, L., & Spergel, D. N. 1993, unpublished

Kundić, T. et al. 1997, ApJ, 482, 75

Lahav, O., Lilje, P. B., Primack, J. R., & Rees, M. J. 1991, MNRAS, 251, 128

Merritt, D., & Gebhardt, K. 1994, in Clusters of Galaxies, ed. F. Durret, A. Mazure, & J. Trân Thanh Vân (Moriond: Editions Frontiers), p. 11

Mo, H. J., Mao, S., & White, S. D. M. 1998, MNRAS, 295, 319

Moore, B., Katz, N., & Lake, G. 1996, ApJ, 457, 455

Navarro, J. F., Frenk, C. S., & White, S. D. M. 1997, ApJ, 490, 493

Peebles, P. J. E. 1993, Principles of Physical Cosmology (Princeton: Princeton University Press)

Pen, U.-L. 1998, ApJ, 498, 60

Press, W. H., & Schechter, P. 1974, ApJ, 187, 425

Press, W. H., Teukolsky, S. A., Vetterling, W. T., & Flannery, B. P. 1992, Numerical Recipes (Cambridge: Cambridge University Press)

Summers, F. J., Davis, M., & Evrard, A. E. 1995, ApJ, 454, 1

Tormen, G., Diaferio, A., & Syer, D. 1998, MNRAS, 299, 728

Weinberg, D. H., Hernquist, L., & Katz, N. 1997, ApJ, 477, 8; `http://www-hpcc.astro.washington.edu/tools/SKID/`

Table 1. Cosmological models

Model	Ω_0	Ω_Λ	Ω_B	h	σ_8
I	1	0	0.1	0.65	0.5
II	0.4	0	0.1	0.65	1.0
III	0.4	0.6	0.1	0.65	1.0

Table 2. Parameters of the simulated clusters

Model	$R_{\rm vir}$ (h^{-1} Mpc)	$M_{\rm vir}$ ($M_\odot$)	$\sigma_{\rm los}$ (km s^{-1})	b/a	c/a
I	1.03	3.9×10^{14}	656	0.70	0.58
II	1.47	4.5×10^{14}	664	0.85	0.71
III	1.42	4.1×10^{14}	649	0.85	0.73

Table 3. Resolution test on the parameters of Cluster III

N_{grid}	$R_{\rm vir}$ (h^{-1} Mpc)	$M_{\rm vir}$ ($M_\odot$)	$\sigma_{\rm los}$ (km s^{-1})	b/a	c/a
512	1.42	4.1×10^{14}	649	0.85	0.73
256	1.42	4.1×10^{14}	632	0.84	0.70
128	1.43	4.1×10^{14}	546	0.76	0.61

Table 4. Coefficients of smoothing filters

n	$c_n^{(0)}$	$c_n^{(1)}$	$c_n^{(2)}$
-4	0.034965	0.072391	-0.036713
-3	-0.128205	-0.119529	0.108100
-2	0.069930	-0.162458	0.043998
-1	0.314685	-0.106061	-0.061480
0	0.417249	0.000000	-0.107809
1	0.314685	0.106061	-0.061480
2	0.069930	0.162458	0.043998
3	-0.128205	0.119529	0.108100
4	0.034965	-0.072391	-0.036713

Table 5. Number of close encounters in Cluster III

Δr_i	< 5 kpc	< 10 kpc	< 15 kpc	< 20 kpc
N_{enc}	63	215	398	559
N_{mer}	9	14	25	31
$N_{enc,1}$	1.3	4.3	8.0	11
$N_{mer,1}$	0.09	0.14	0.25	0.31

Table 6. Kinematics of galaxies in Cluster III

Region	$< r$ (h^{-1} Mpc)	$N_g(r)$	$\bar{v}_g$ (km s^{-1})	σ_g (km s^{-1})
1 Δ	0.0625	22	173	226
8 Δ	0.5	22	116	561
R_{vir}	1.4	21	102	895

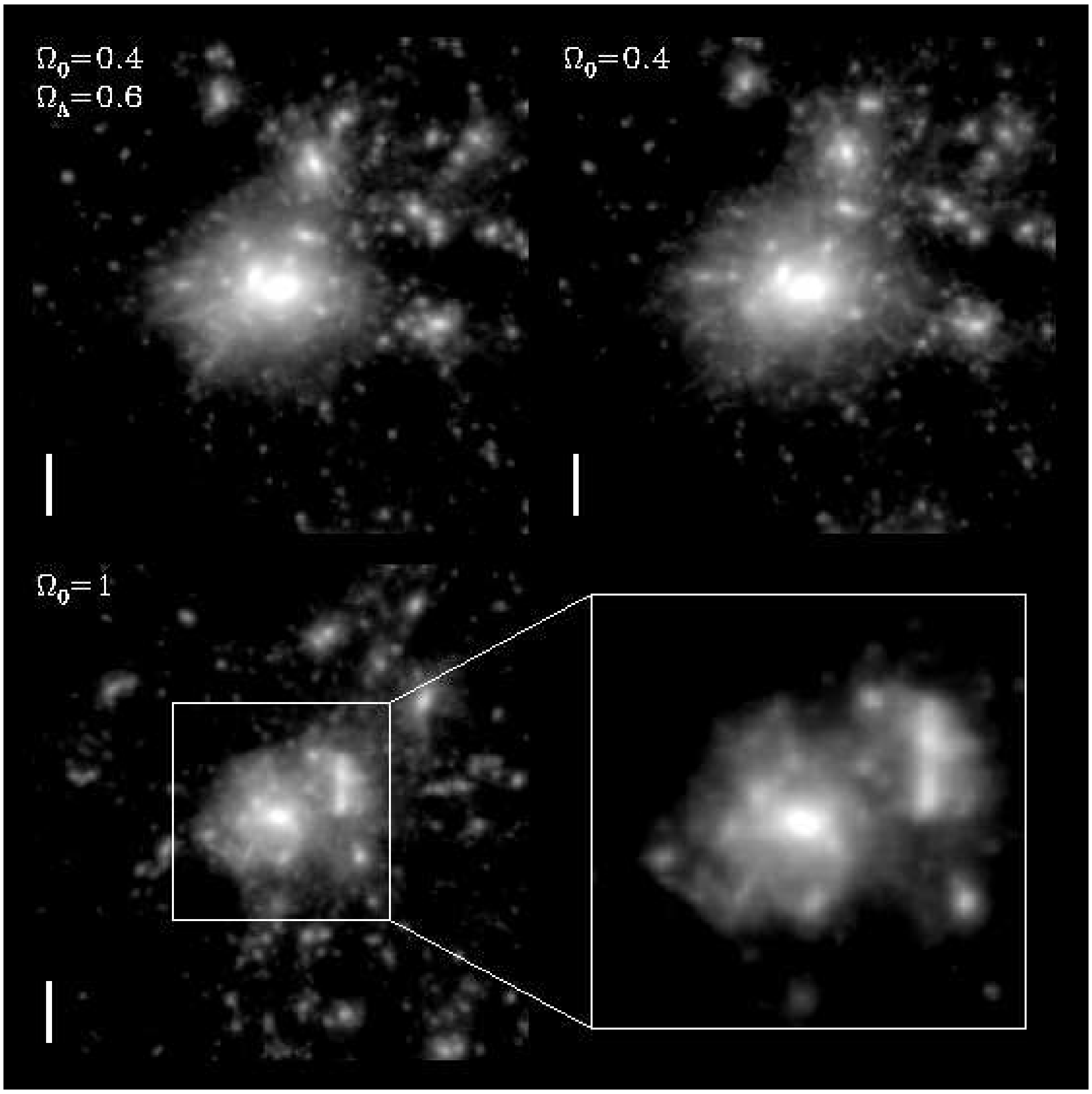

Fig. 2.1.— The surface density map of the three simulated clusters at $z = 0$. The projection is over the X direction. Saturated white regions are denser than 200 times the mean density; regions below the mean density are black. The size of the window is 8 h^{-1} Mpc. The lower right panel shows the enlarged view of the inner region of the $\Omega_0 = 1$ cluster. Thick bars at the lower left corners of each panel indicate 1 h^{-1} Mpc.

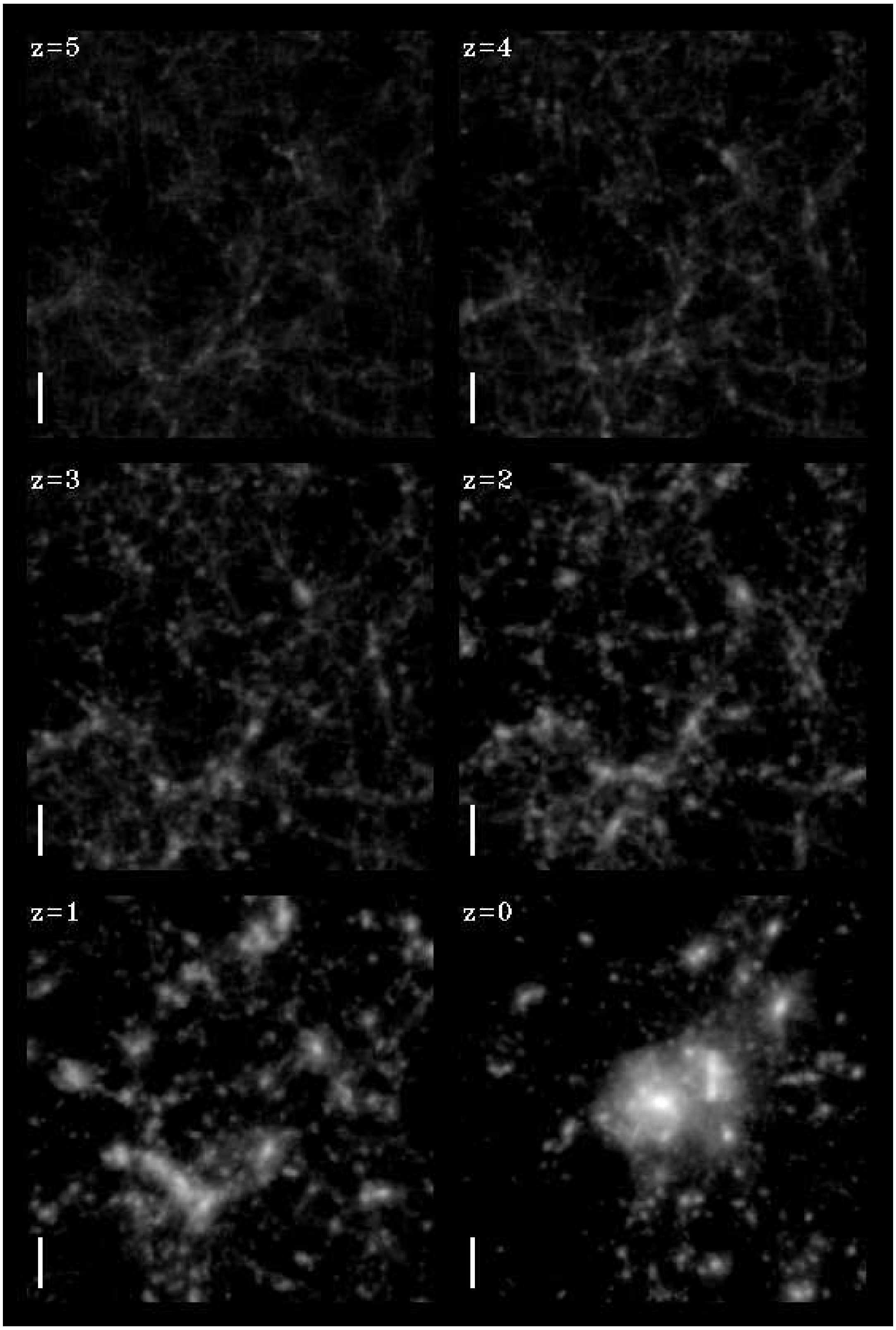

Fig. 2.2.— The projected density maps of the $\Omega_0 = 1$ cluster at six successive redshift slices. Sizes and the brightness stretch as in Figure 2.1.

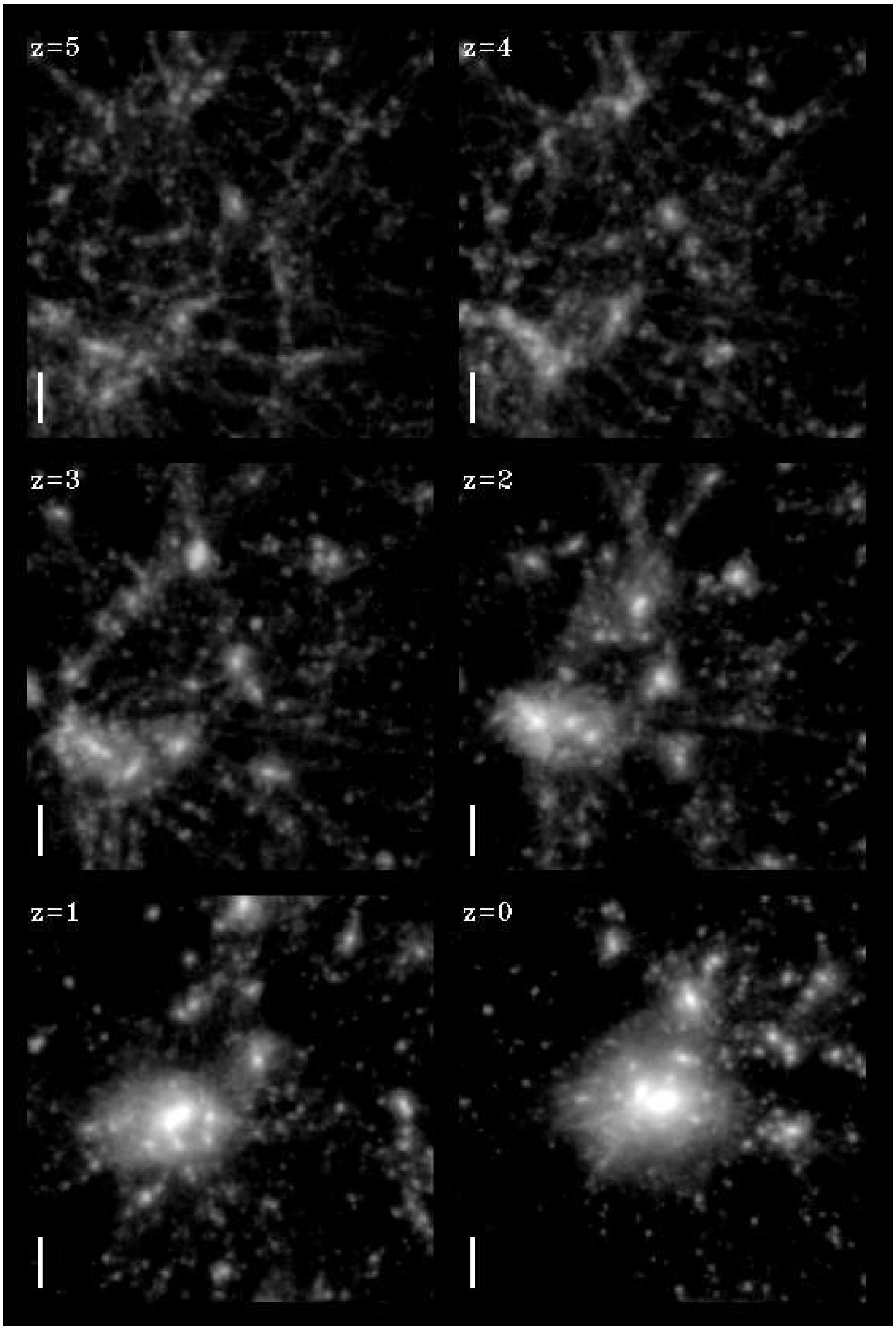

Fig. 2.3.— The projected density maps of the $\Omega_0 = 0.4$ cluster at six successive redshift slices. Sizes and the brightness stretch as in Figure 2.1.

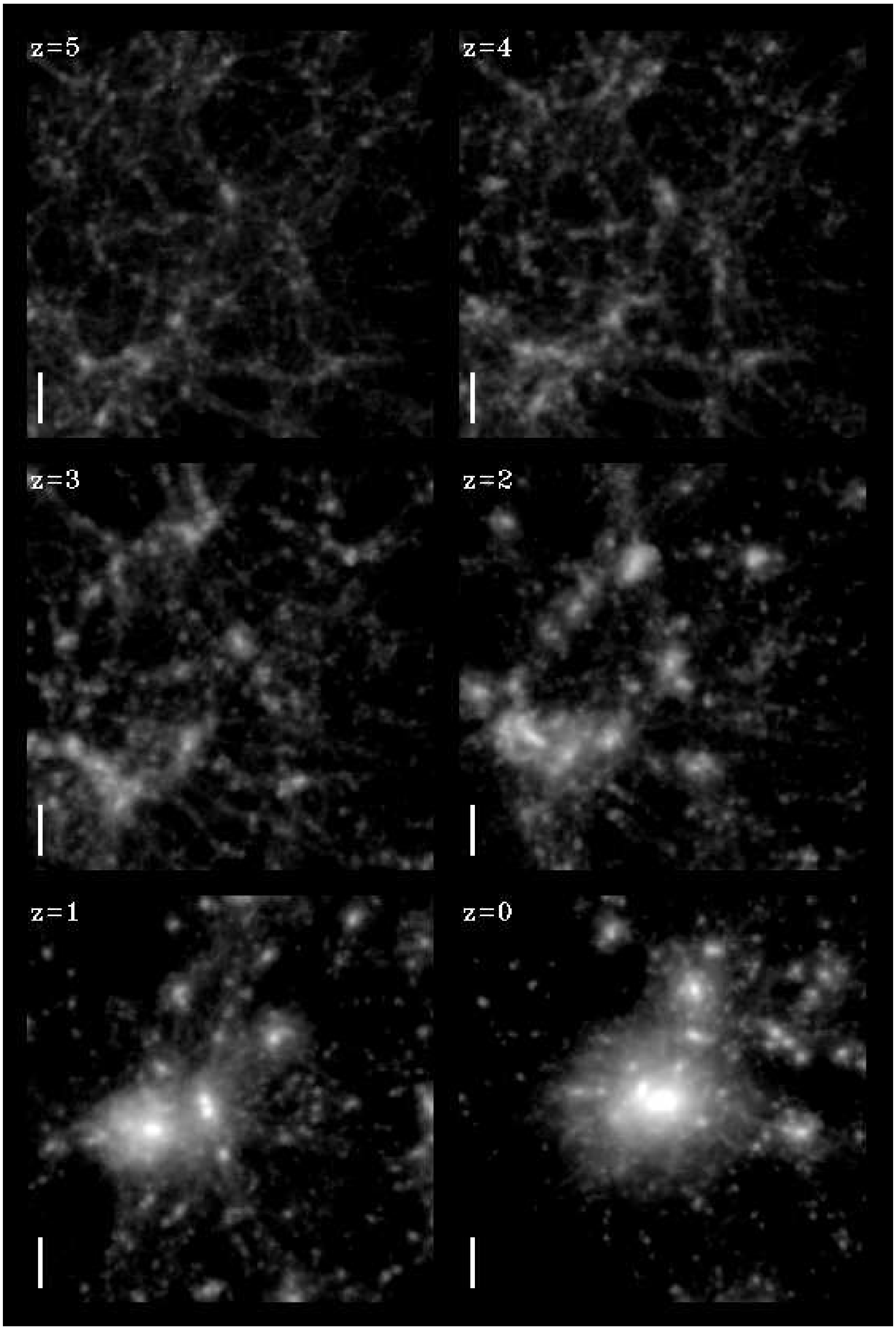

Fig. 2.4.— The projected density maps of the $\Omega_0 = 0.4$, $\Omega_\Lambda = 0.6$ cluster at six successive redshift slices. Sizes and the brightness stretch as in Figure 2.1.

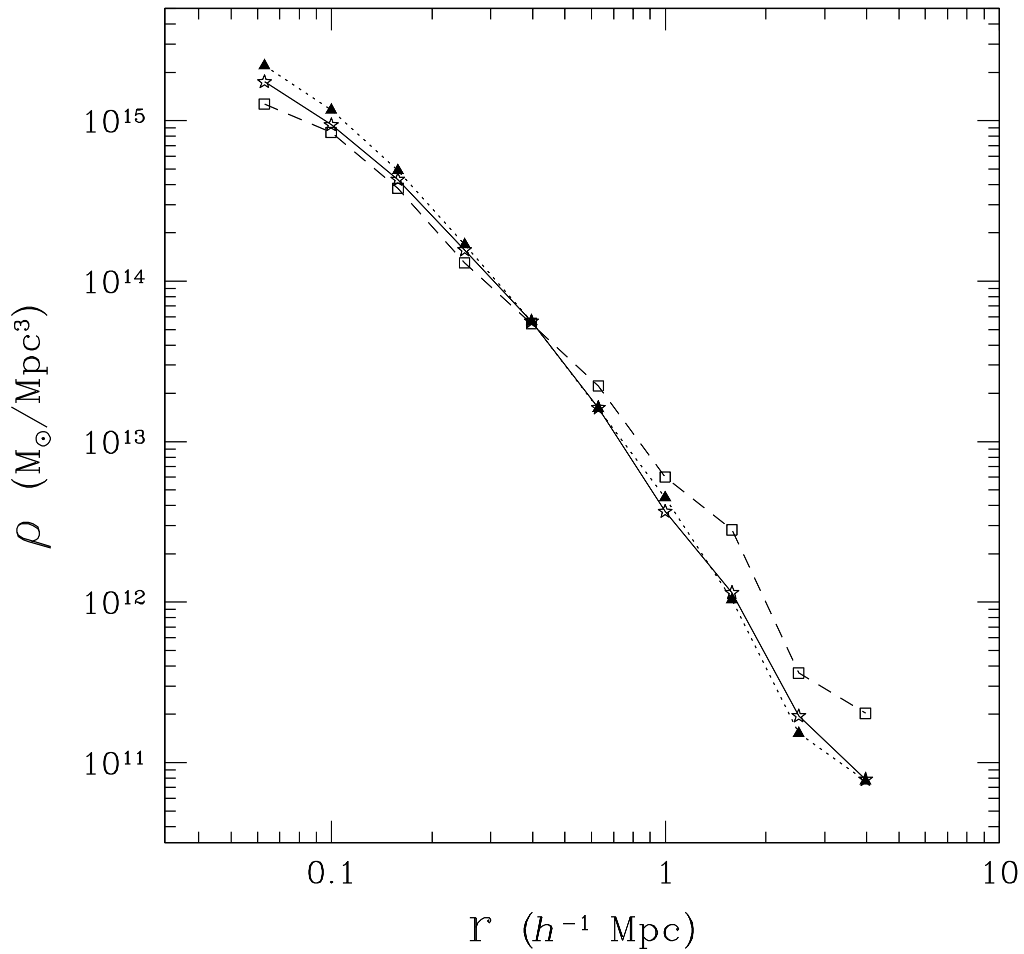

Fig. 2.5.— The density profile of the three clusters. Dashes and open squares are for the $\Omega_0 = 1$ model, dots and filled triangles are for the $\Omega_0 = 0.4$ model, solid line and stars are for the $\Omega_0 = 0.4$, $\Omega_\Lambda = 0.6$ model.

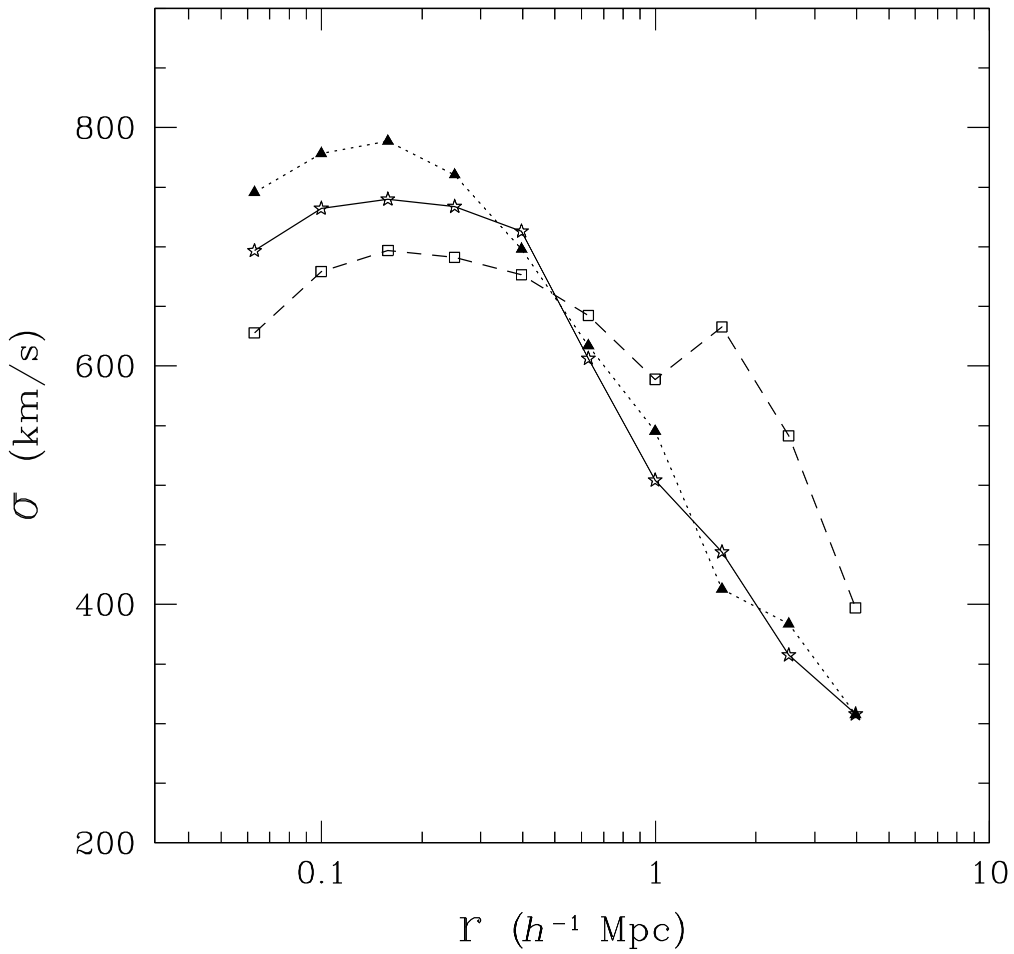

Fig. 2.6.— The velocity dispersion of dark matter in the three clusters. Line notation as in Figure 2.5. Note a rise of the velocity dispersion at 2 h^{-1} Mpc from the center of the $\Omega_0 = 1$ cluster due to the new infalling group of galaxies.

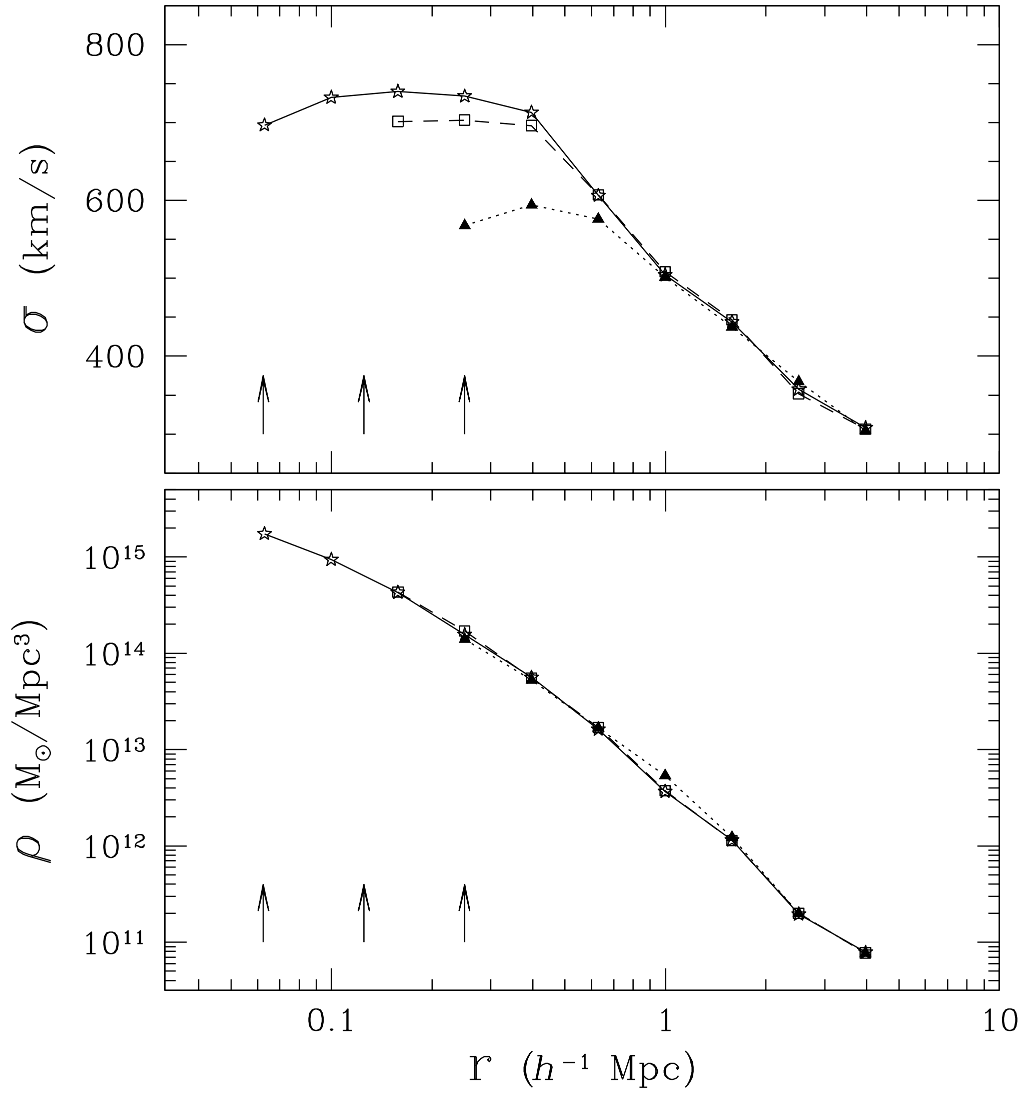

Fig. 2.7.— Resolution effects on the structure of the $\Omega_0 = 0.4$, $\Omega_\Lambda = 0.6$ cluster. Solid line and stars are for the main 512^3 grid cells simulation, dashes and open squares are for 256^3 simulation, and dots and filled triangles are for the 128^3 simulation. Arrows point at the cell size, Δ, for the three simulations, respectively. The nominal PM force resolution is about 2Δ.

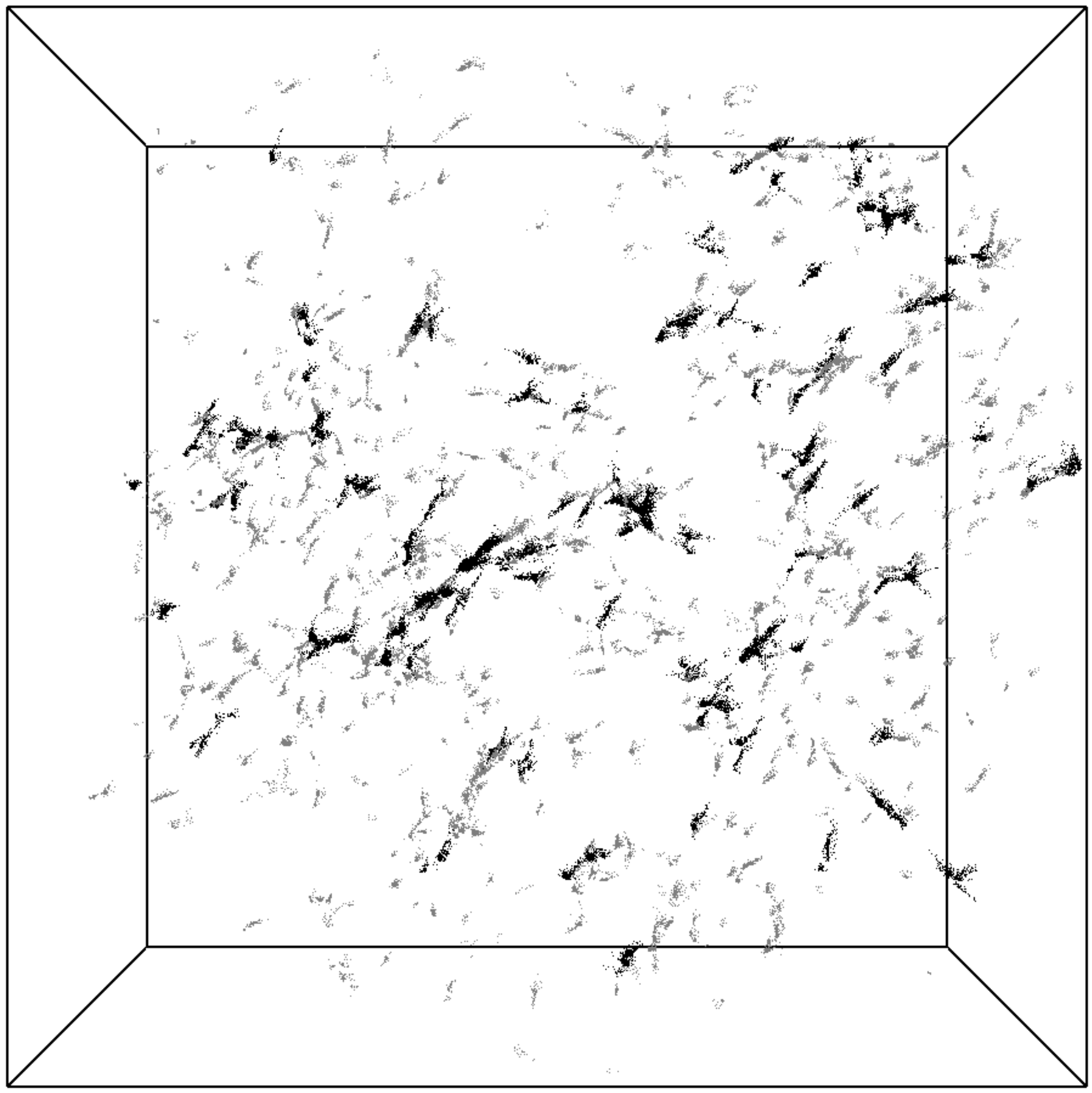

Fig. 2.8.— Particles in the identified galaxies at $z_g = 5$ in the $\Omega_0 = 1$ cluster. The 100 most massive galaxies, whose trajectories are followed in the simulation, are black; others are gray. Boundary size is 16 h^{-1} Mpc comoving.

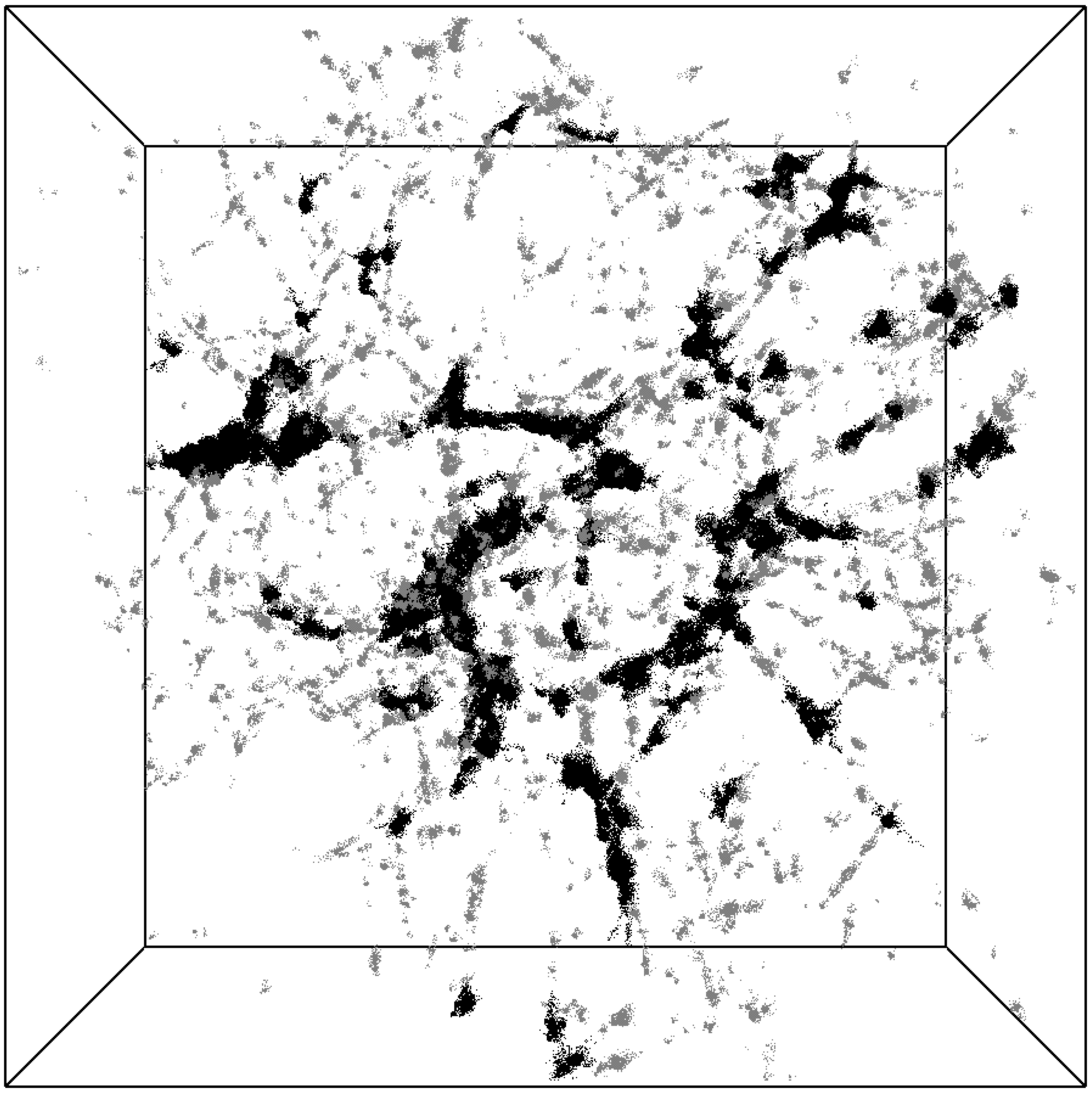

Fig. 2.9.— Particles in the identified galaxies in the $\Omega_0 = 0.4$ cluster.

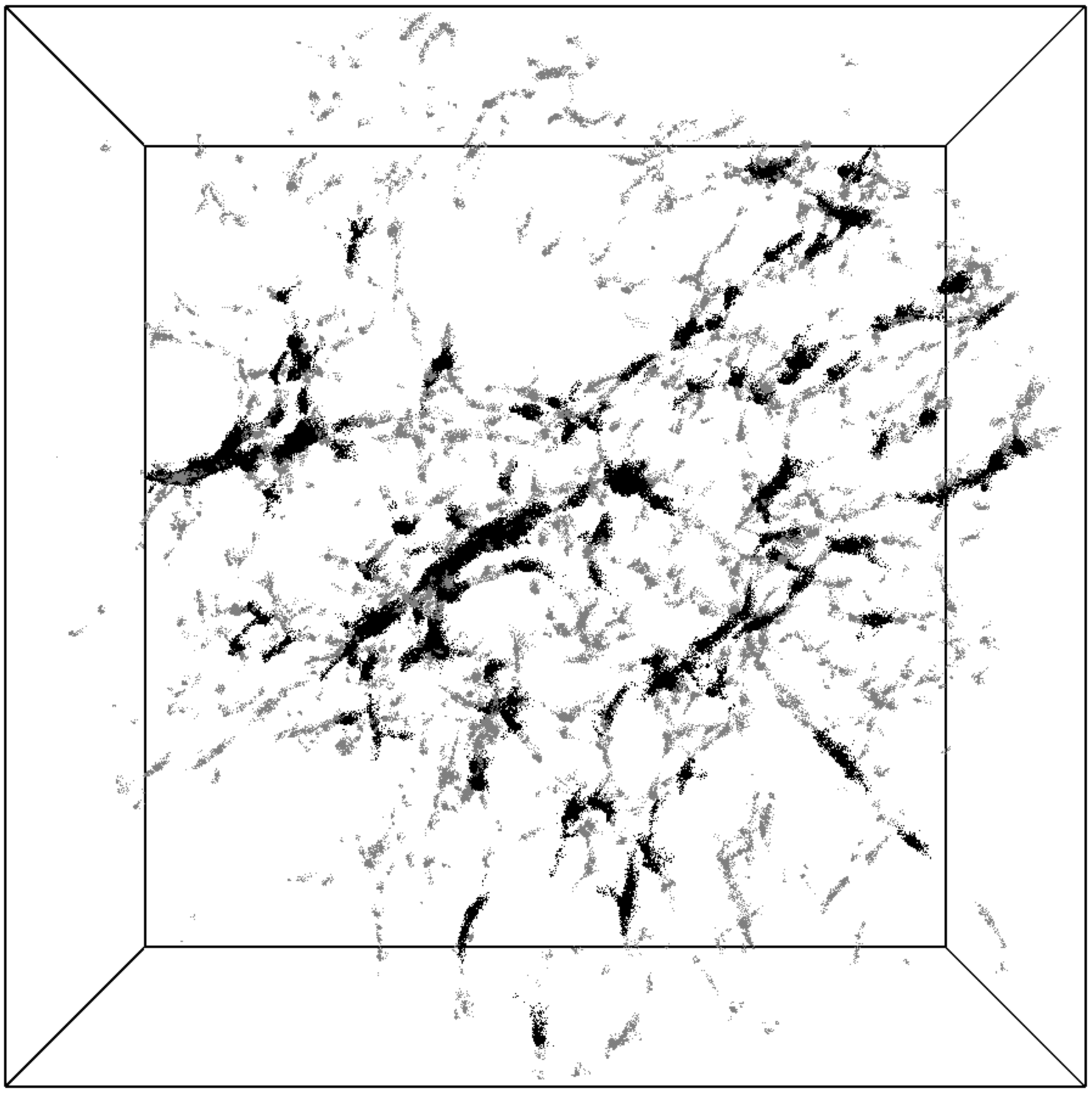

Fig. 2.10.— Particles in the identified galaxies in the $\Omega_0 = 0.4$, $\Omega_\Lambda = 0.6$ cluster.

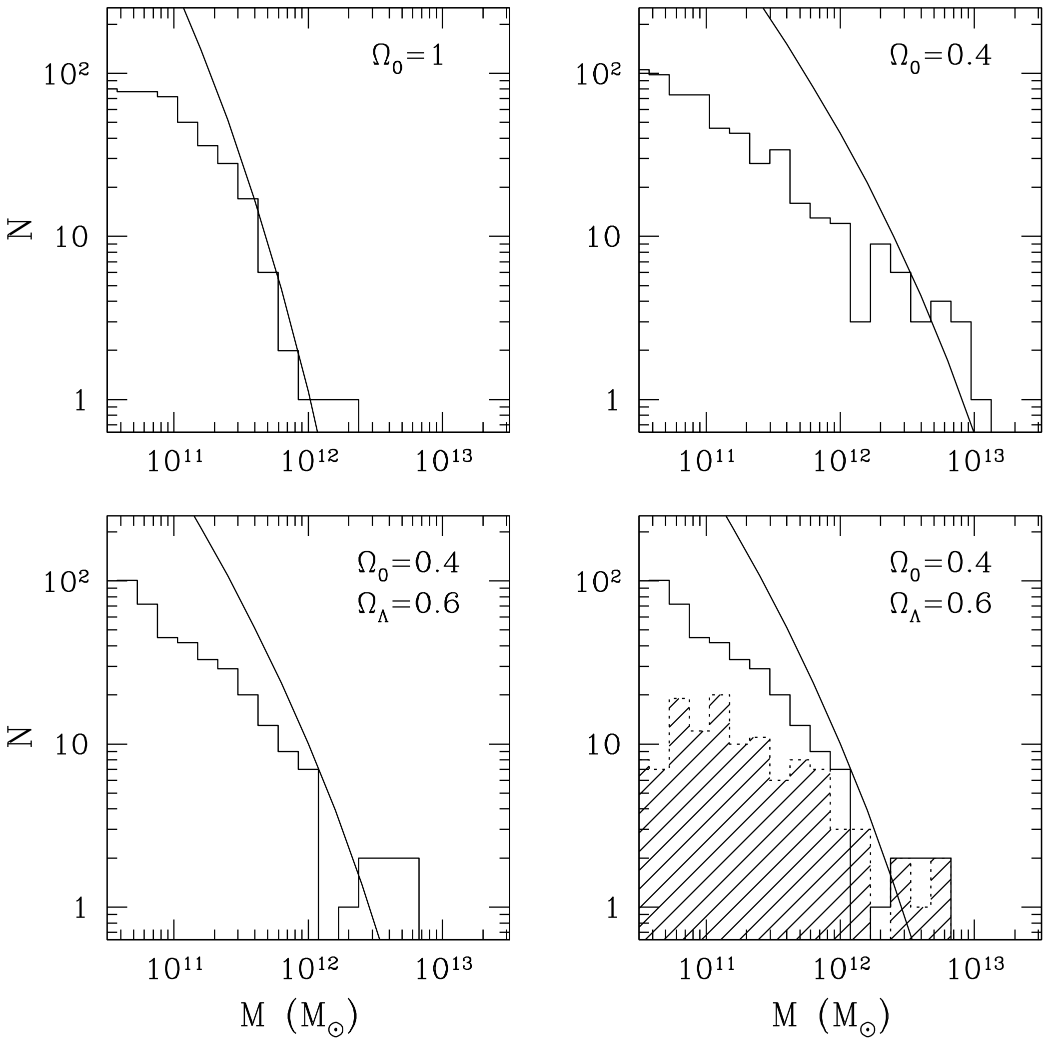

Fig. 2.11.— The mass functions of the identified galaxy halos in the three clusters (histograms). Superimposed are the predictions from the Press-Schechter theory for each of the three power spectra (lines). The lower right panel shows, for comparison, the mass function from the lower resolution, 256^3 simulation for Cluster III (shaded histogram).

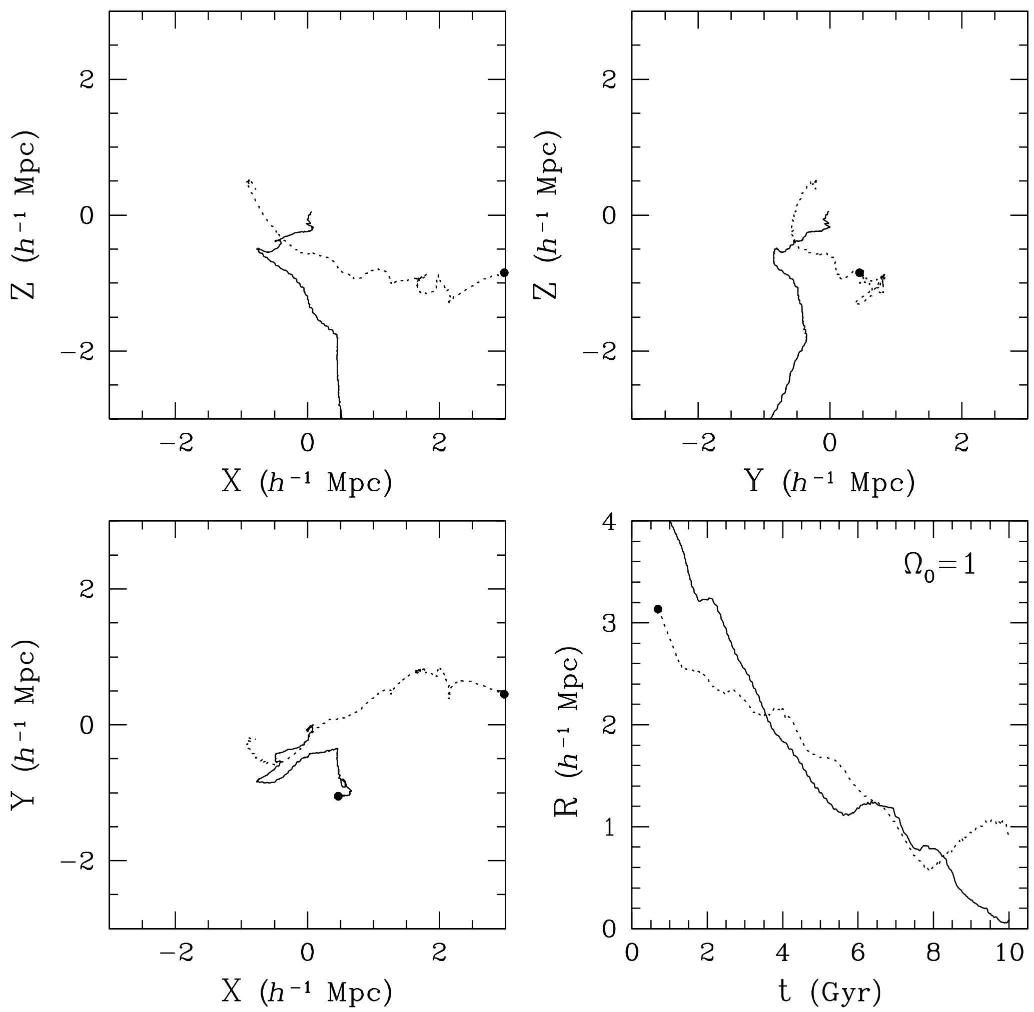

Fig. 2.12.— The three projections of the galaxy trajectories in the $\Omega_0 = 1$ cluster (in comoving coordinates). The lower right panel shows the distance of the galaxies from the final cluster center. Solid line is for the large galaxy used for the SCF simulation, dots are for the dwarf galaxy. Large solid dots mark the initial positions where the galaxies were identified.

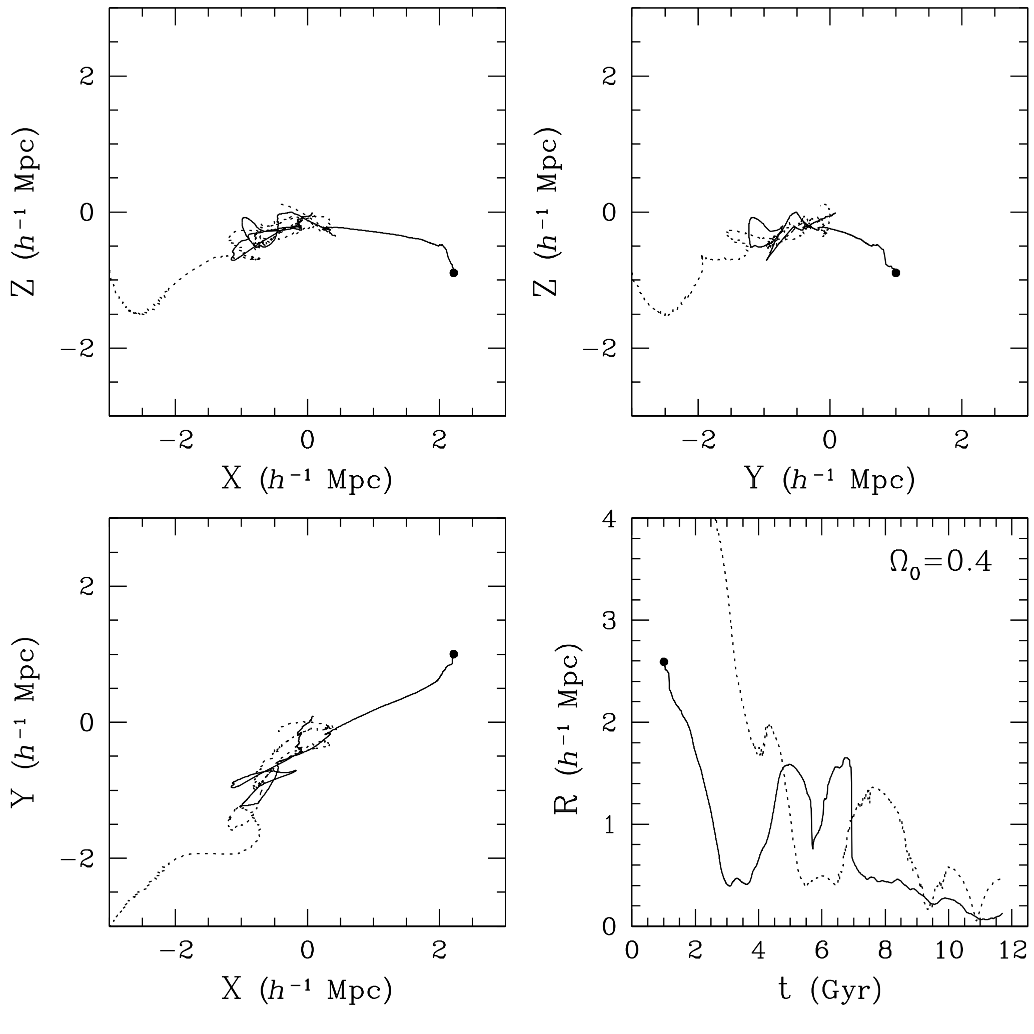

Fig. 2.13.— The three projections of the galaxy trajectories in the $\Omega_0 = 0.4$ cluster. Notation as in Figure 2.12.

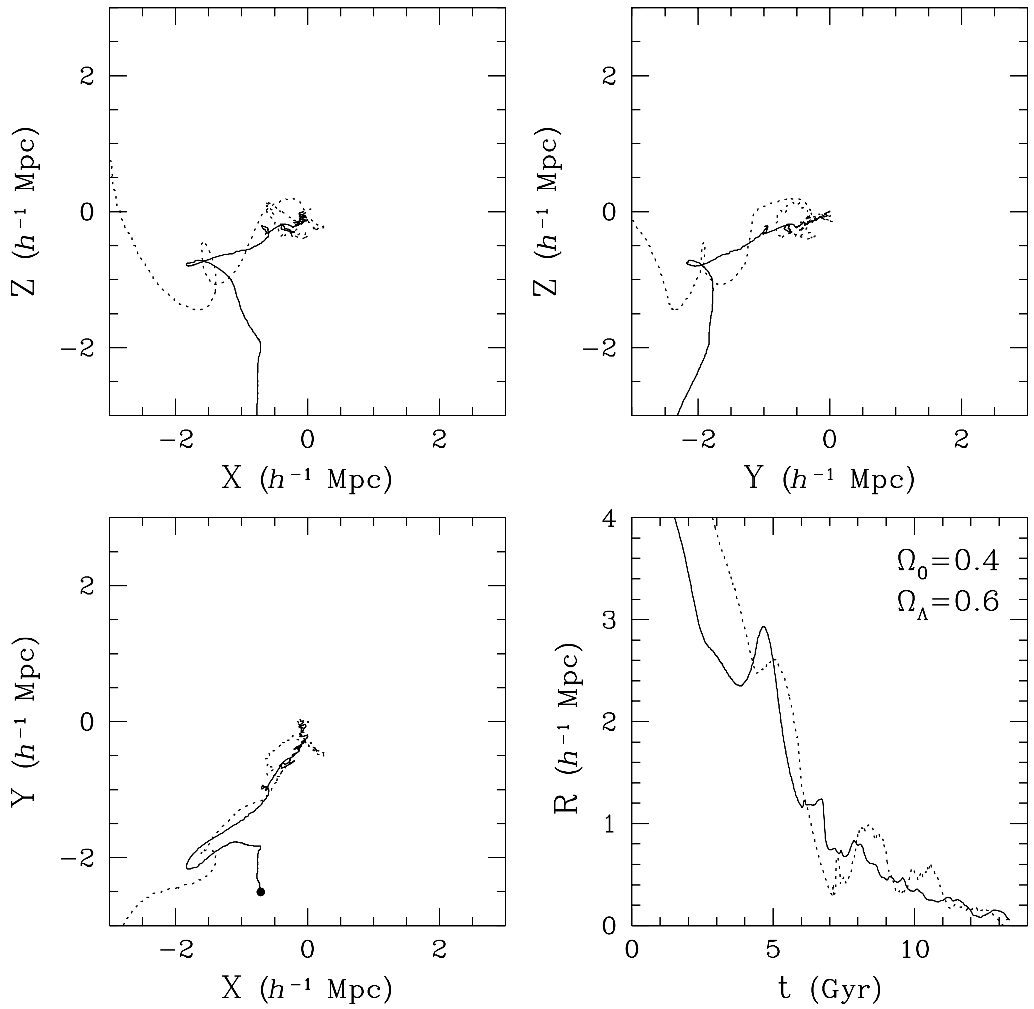

Fig. 2.14.— The three projections of the galaxy trajectories in the $\Omega_0 = 0.4$, $\Omega_\Lambda = 0.6$ cluster. Notation as in Figure 2.12.

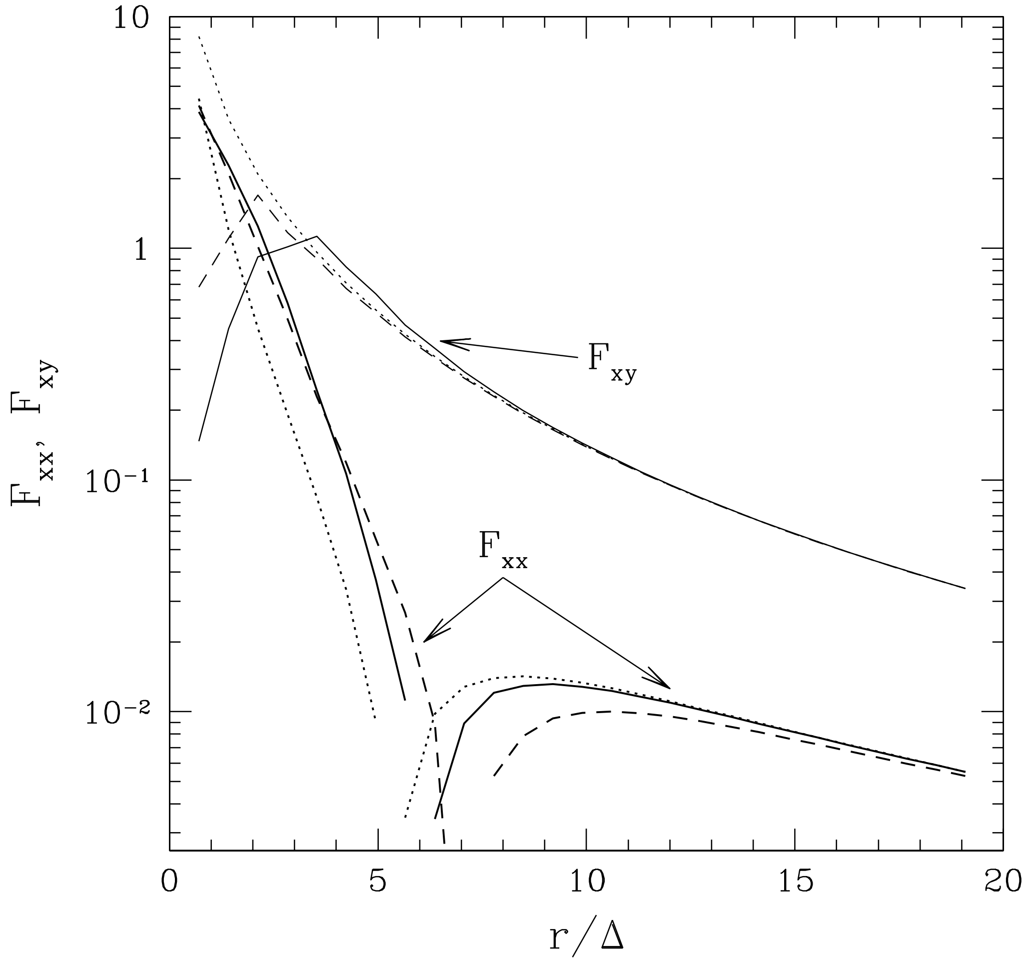

Fig. 2.15.— The tidal components of the NFW model versus radius in units of the cell size. Dashes are obtained with the direct two-point finite difference, solid line with our smoothing filter. Dots show the analytic solution. Notice that the F_{xx} component changes sign at $r \approx 5\,\Delta$; the inner parts show the absolute value of the tidal force. Units are arbitrary.

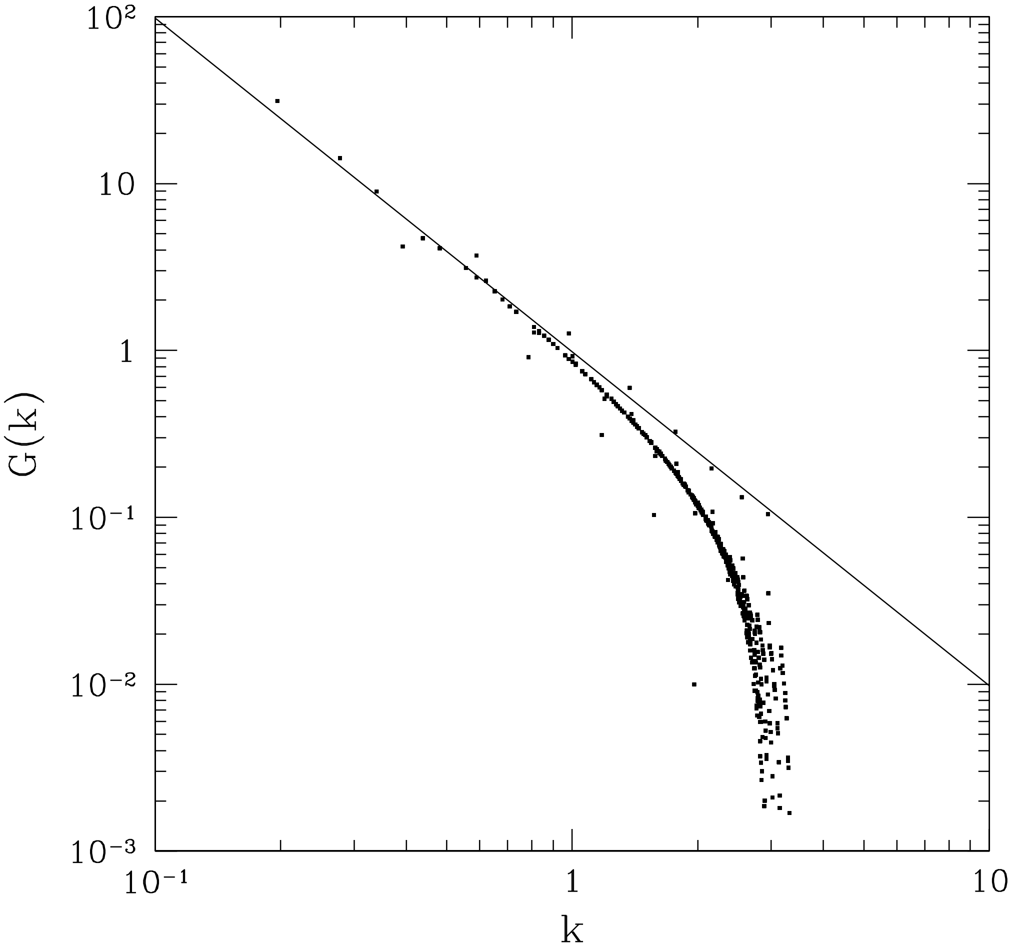

Fig. 2.16.— Green's function for the isolated FFT (dots). Solid line shows the usual Green's function for the periodic FFT, $G(k) = k^{-2}$.

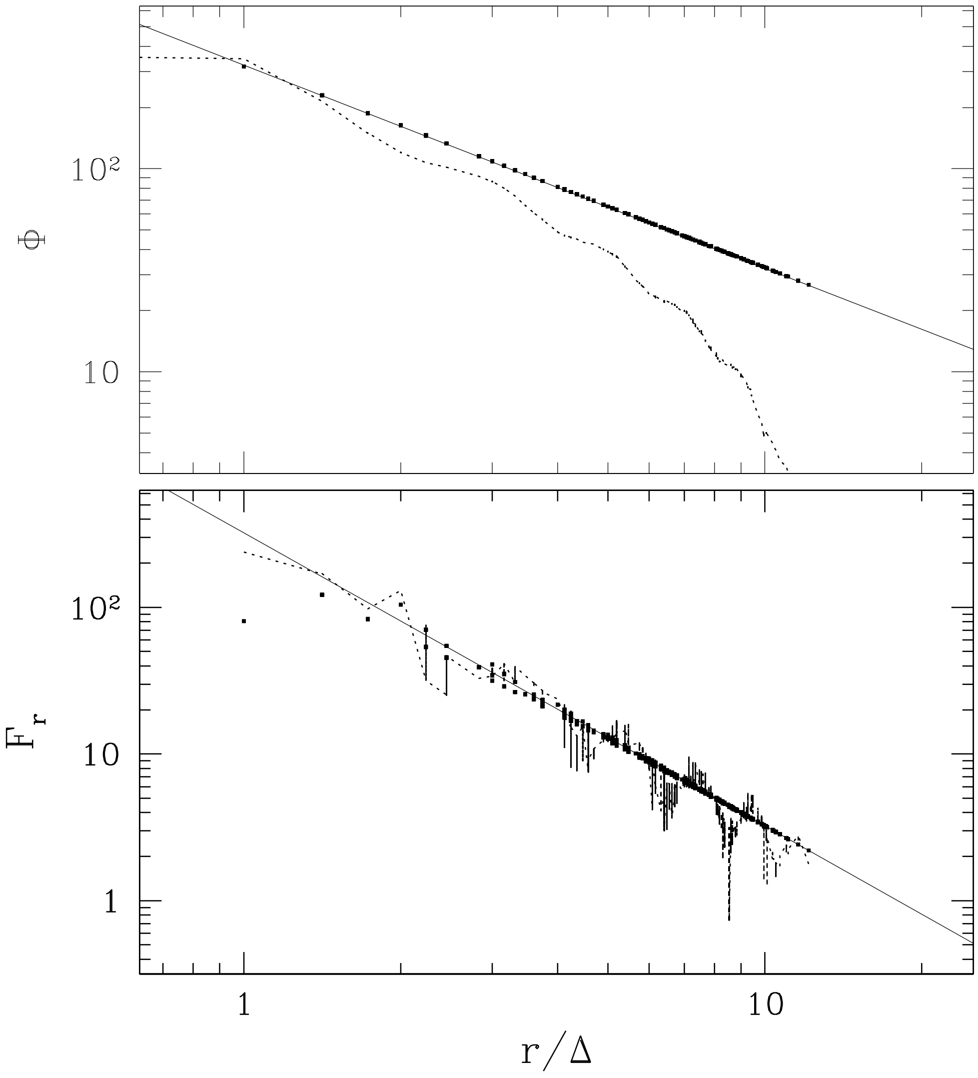

Fig. 2.17.— The potential and force of a point mass using the FFT with the isolated boundary conditions (points) versus the exact values (straight lines). Dotted lines show the result with the usual periodic FFT method.

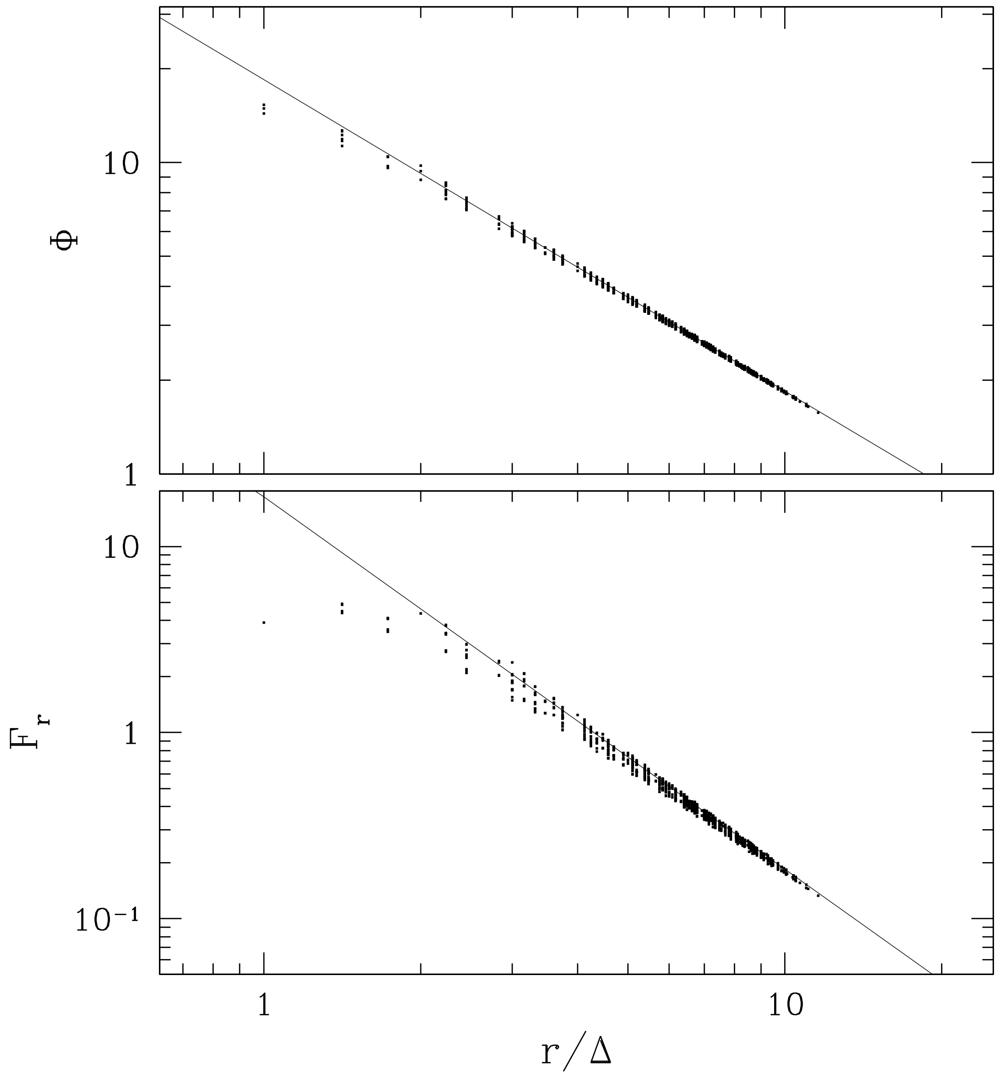

Fig. 2.18.— The potential and force of the particles in a single cell from the real PM simulation.

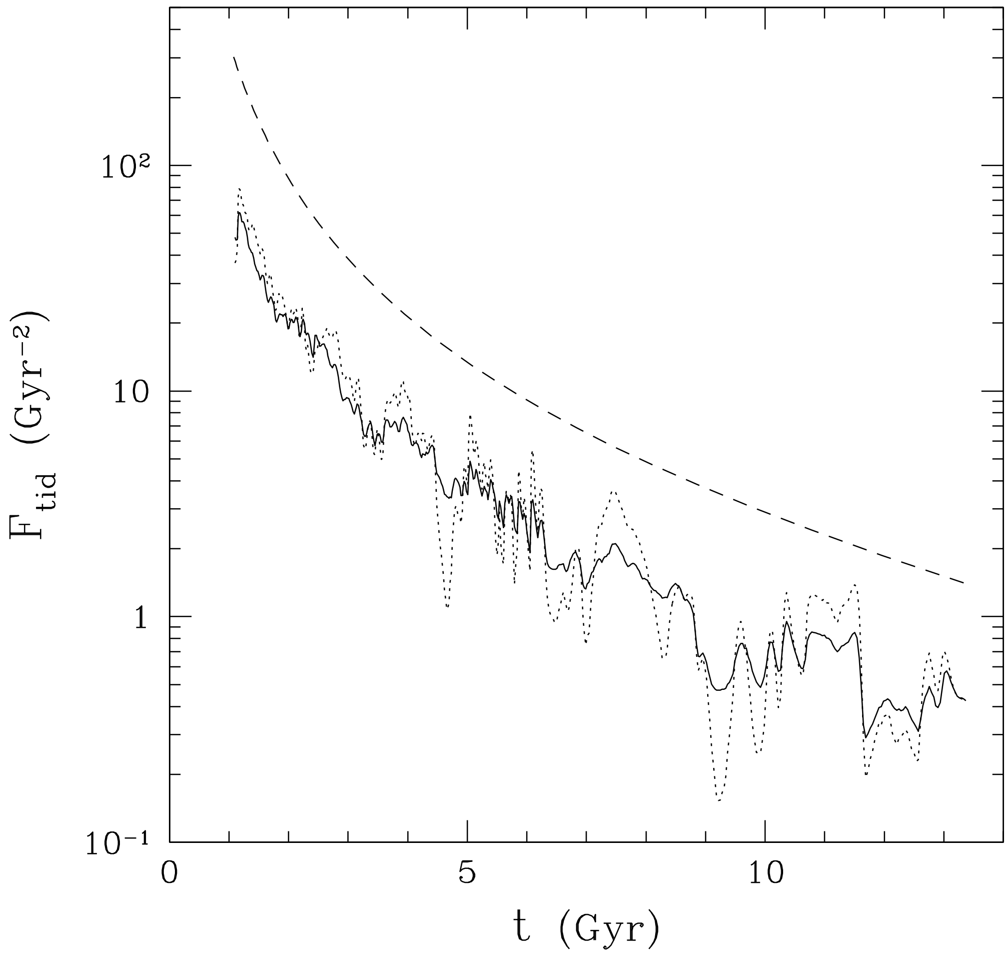

Fig. 2.19.— Galaxy self-contribution to the trace of the tidal tensor (solid line) and the actual density of the galactic particles (dots) of galaxy #4 in the Cluster III simulation. Dashes show the $(1 + z)^3$ scaling of the fixed comoving density.

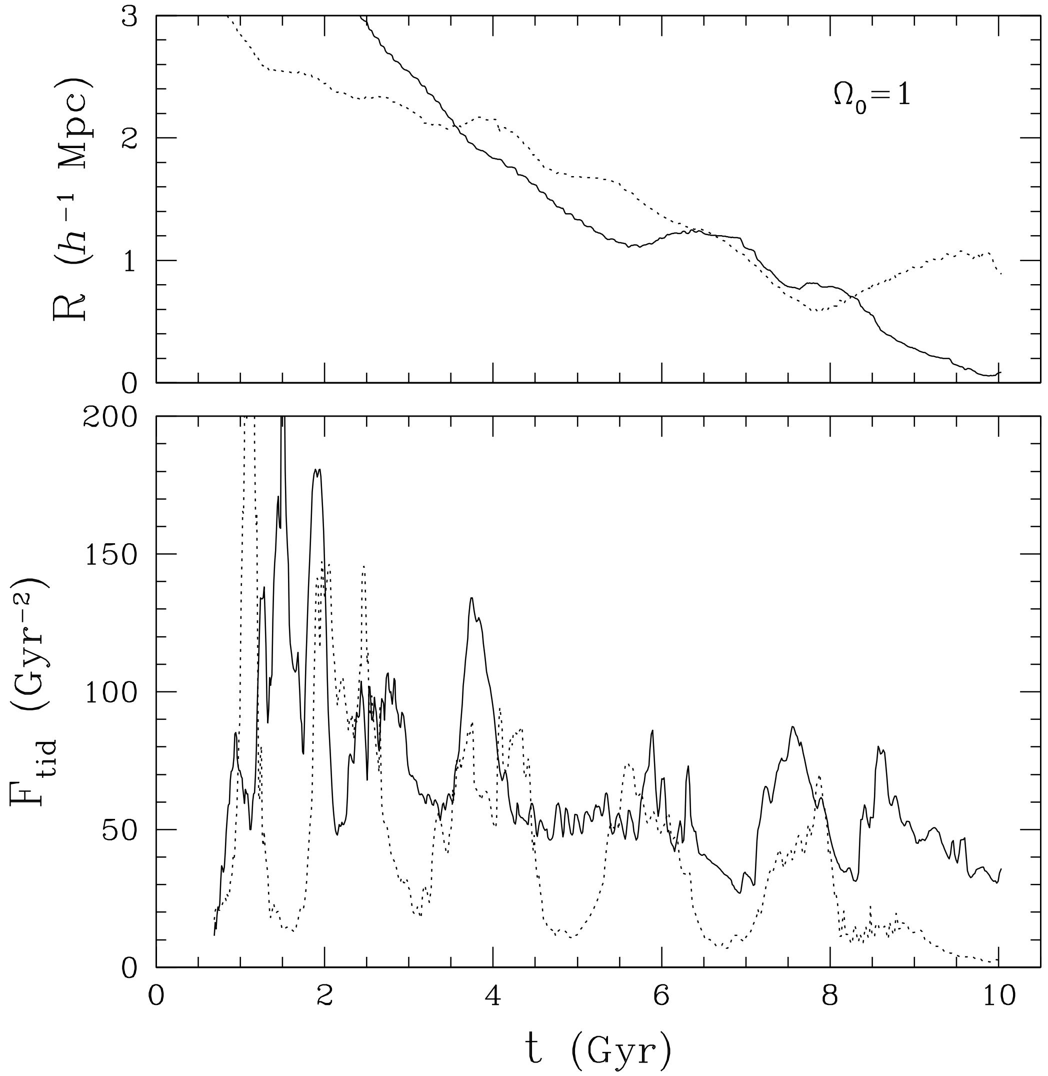

Fig. 2.20.— Tidal field around the large (solid line) and dwarf (dots) galaxies in the $\Omega_0 = 1$ cluster. Upper panel shows the distance from the final center of the cluster.

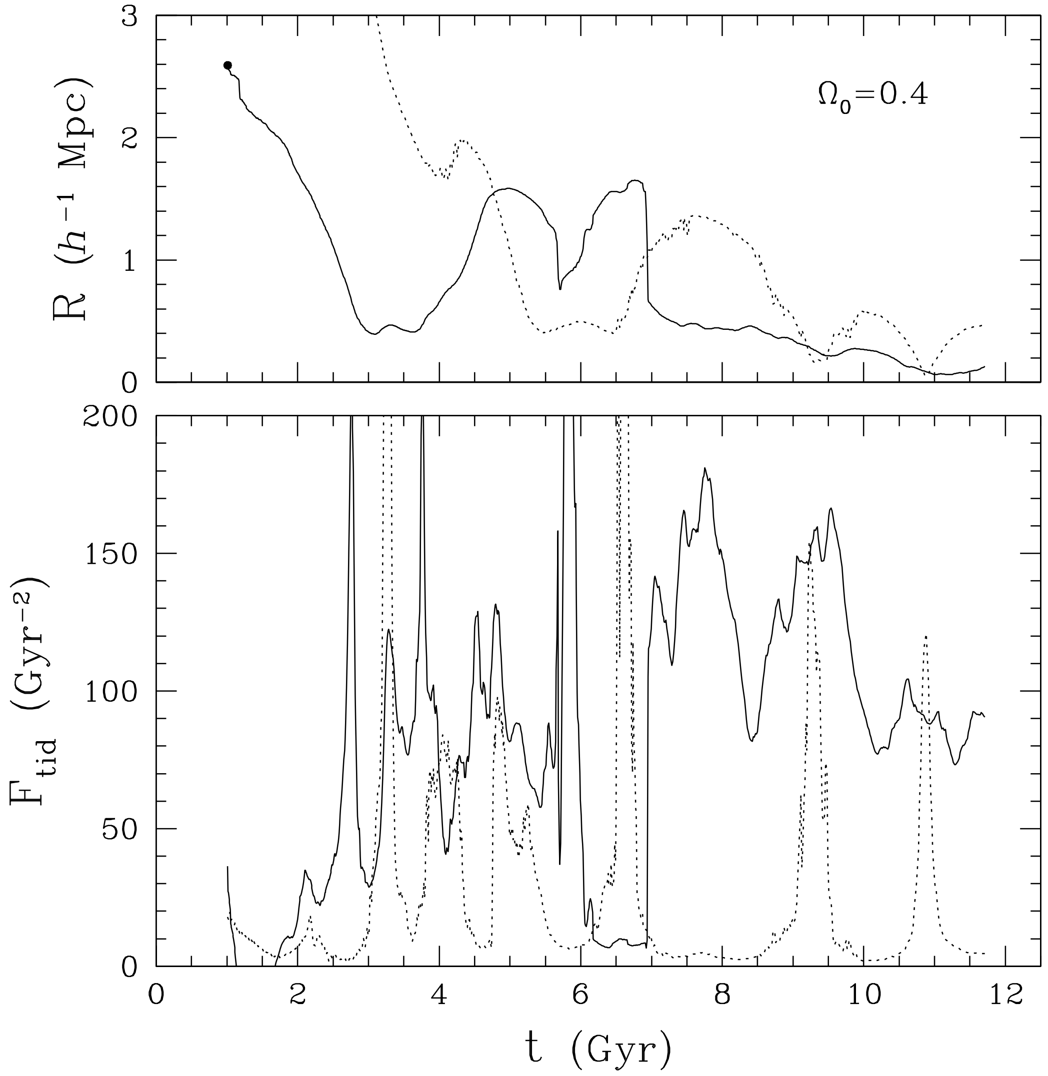

Fig. 2.21.— Tidal field around galaxies in the $\Omega_0 = 0.4$ cluster. Line notation as in Figure 2.20.

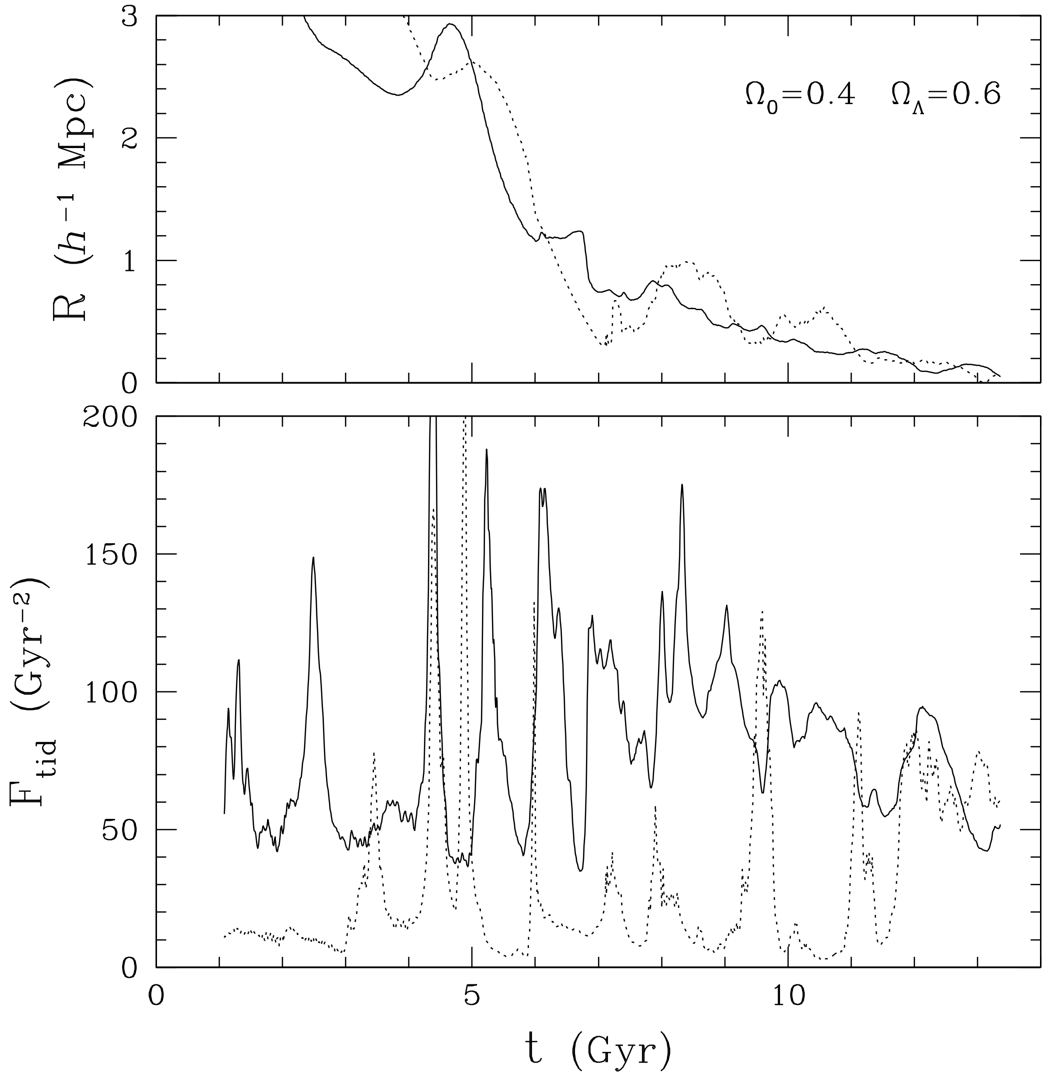

Fig. 2.22.— Tidal field around galaxies in the $\Omega_0 = 0.4$, $\Omega_\Lambda = 0.6$ cluster. Line notation as in Figure 2.20.

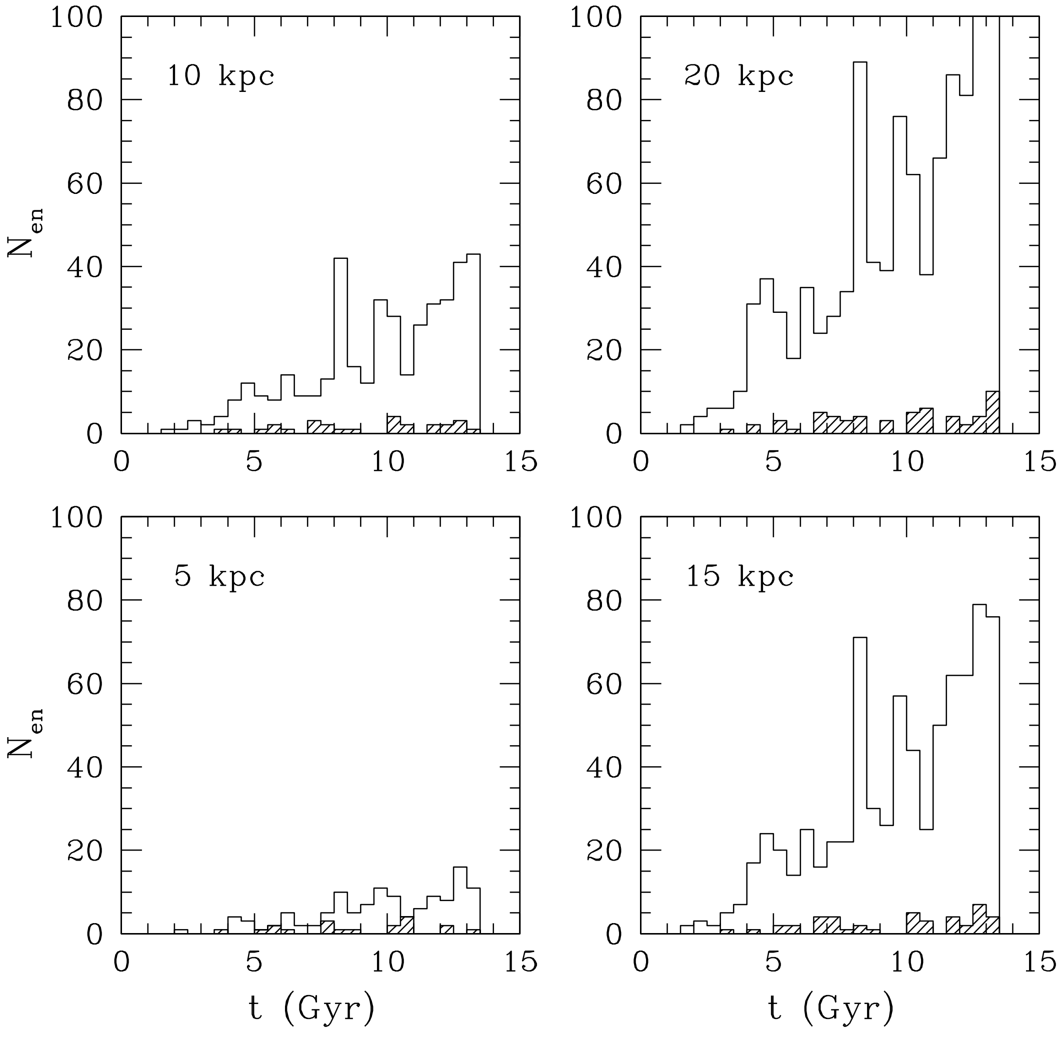

Fig. 2.23.— Distribution of the close encounters of galaxies in the Cluster III simulation for the four values of the impact parameter, Δr_i, indicated on the panels. Shaded histogram shows the number of possible mergers. The distributions are cumulative, including all encounters with the impact parameters from 0 to Δr_i.

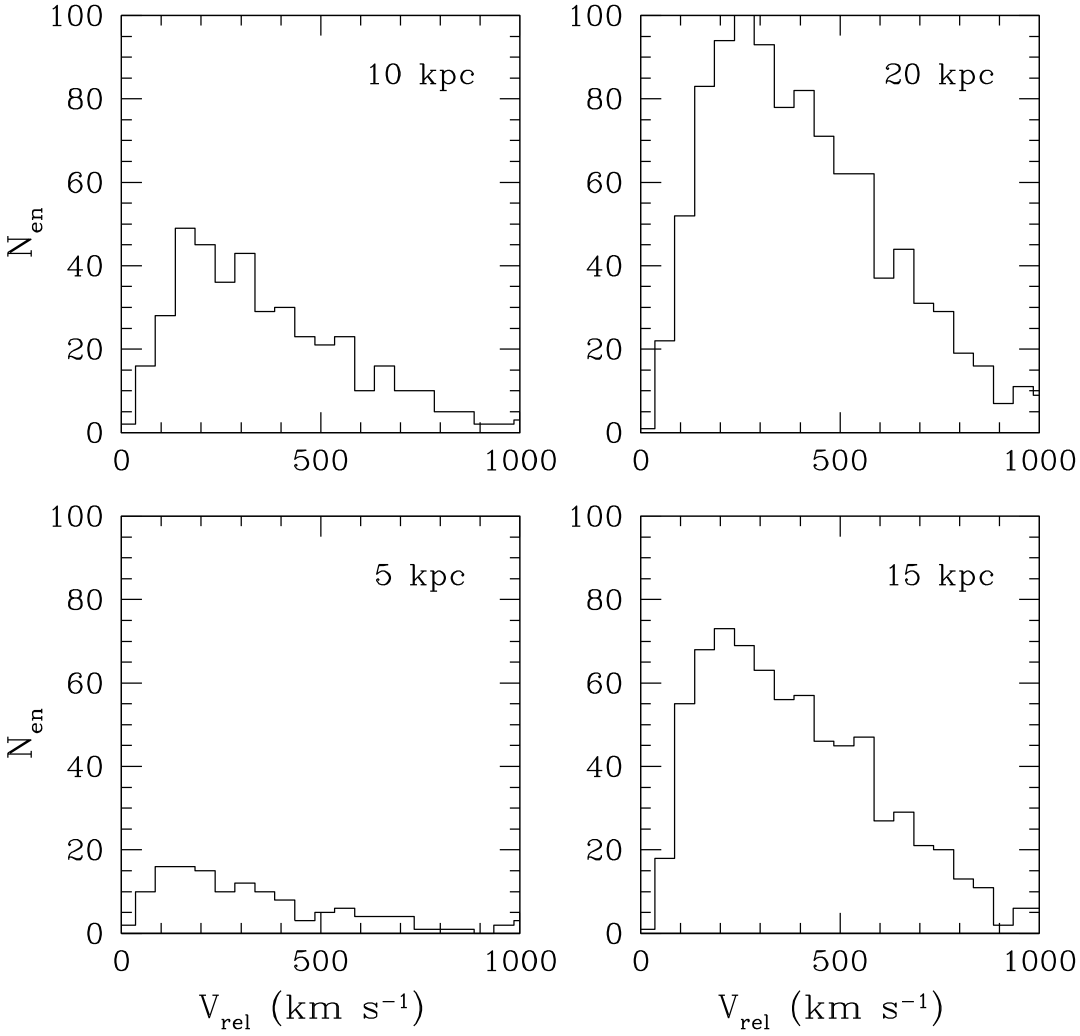

Fig. 2.24.— Distribution of the relative velocities in the close galactic encounters of galaxies in the Cluster III simulation. The values of the impact parameters are as in Figure 2.23.

Chapter 3

Evolution of Galaxies in Clusters

3.1 Abstract

The tidal field calculated from the cosmological cluster simulations in Chapter 2 is applied to investigate the internal dynamics of the galaxies. The galaxy model includes an exponential stellar disk and an isothermal dark matter halo. For large spiral galaxies with the rotation speed of 250 km s^{-1}, tidal interactions (1) truncate the massive halo at a radius of 30 ± 6 kpc, (2) thicken the disk by a factor 2 ± 0.4, increasing Toomre's Q to about 2 and stabilizing the disk against gravitational instabilities, (3) have a negligible effect on the radial scale length. Dwarf galaxies with the rotation speed of 20 km s^{-1} are completely disrupted by the external tidal field. Thus, the likely consequence of tidal shocks is to turn a large fraction of normal spirals into S0 galaxies and to deplete the dwarf population. With regard to cosmological scenario, at a given cluster velocity dispersion the low Ω_0 models agree with observations better. Tidal effects explain both the strong morphological evolution of galaxies in clusters and the present abundances of distorted disk galaxies in nearby clusters.

3.2 Introduction

External tidal perturbations in clusters of galaxies affect the dynamics of disk galaxies in several ways. Firstly, they lead to truncation of the stellar and dark matter distributions at a critical radius of the Roche lobe. Secondly, they increase stellar energy and the amount of random motion of stars in the disk. This tidal heating may be strong enough to completely unbind small galaxies and significantly transform larger ones. Finally, tidal heating is likely to stabilize stellar disks against gravitational instability and suppress subsequent star formation. The result of all these effects would be a morphological transformation of a spiral galaxy to an S0.

I use numerical simulations to investigate the tidal effects on the evolution of galaxies. Assuming that initially all galaxies form as spirals, I study their dynamics from the time of formation until the present. The numerical scheme, described in §3.4 has high enough accuracy and resolution to address all of the above questions adequately. The tidal perturbations are taken from the large-scale cosmological simulation of the representative clusters of galaxies in three different cosmological scenarios.

I take one of the largest galaxies from each of the three cosmological samples. The galaxies are chosen to be located in the vicinity of the cluster center, but no other subjective requirement is applied. All three galaxies rank #4 by mass in their respective lists. They are denoted (L1,L2,L3) for the cluster models (I,II,III), respectively. Also, I take one galaxy from the bottom of each list to represent a dwarf spheroidal. These galaxies are denoted (D1,D2,D3), respectively. Galaxies D1 and D2 rank #93, while D3 ranks #87.

The initial parameters of the galaxies are given in Table 1. The large galaxies are fairly massive spirals, with the peak of the circular velocity of 250 km s^{-1}. The rotation curve is dominated by the dark matter halo. The masses of the dark halos L1-L3 from the cosmological simulations are around $10^{12}\ M_\odot$, in agreement with our fiducial value $8 \times 10^{11}\ M_\odot$. Galaxies D1-D3 are more massive than our fiducial dwarf model, $M = 2 \times 10^9\ M_\odot$. However, these galaxies do not contribute much to the evolution of the cluster potential and therefore follow the same trajectories that their even less massive counterparts would have.

The amplitude of the tidal field relates directly to the critical density of the Roche lobe. If a part of a galaxy has lower density than the critical value, it would be torn apart by tidal forces. A typical value of the peaks of the tidal tensor components from Chapter 2, $F_{\alpha,\beta}$, is 150 Gyr^{-2}. The corresponding tidal density is

$$\rho_{\rm tid} = 3.3 \times 10^{-2} \left(\frac{F_{\alpha,\beta}}{150\ {\rm Gyr}^{-2}} \right) M_\odot\ {\rm pc}^{-3}. \tag{3-1}$$

In the models of the large galaxies L1-L3 (see §3.4.1), the central density of the dark matter halos is $\rho_{h,0} \approx 10^{-1}\, M_\odot\ {\rm pc}^{-3}$, higher than the critical value. Stellar disks are even denser, their central surface density $\Sigma_0 = 700\, M_\odot\ {\rm pc}^{-2}$, which corresponds to a space density of $1.2\, M_\odot\ {\rm pc}^{-3}$. These large galaxies are expected to survive external perturbation, even though they will be affected by tidal heating. On other hand, the dwarf galaxy models are below the critical density. The halo central density is $\rho_{h,0} \approx 6.8 \times 10^{-3}\, M_\odot\ {\rm pc}^{-3}$, the disk density $\rho_{d,0} \approx 7.9 \times 10^{-2}\, M_\odot\ {\rm pc}^{-3}$. The halos of the dwarfs should be destroyed completely, and even the disks should be heated enough to disrupt. These qualitative arguments will be supported by simulations in §§3.5 and 3.6.

3.3 Tidal Heating

The main effect of external tidal forces on a galaxy is the positive energy change of stars and dark matter particles, or *tidal heating.* The amount of tidal heating can be estimated analytically, at least for the spherical component. For a single tidal shock, the energy input is the ensemble average of the velocity change squared, $\frac{1}{2}\langle(\Delta v)^2\rangle$, where Δv is a time integral of the tidal force times a reduction factor, A, which takes into account conservation of adiabatic invariants of stellar orbits (Gnedin, Hernquist & Ostriker 1999). In the simulation, the tidal force presents many peaks of variable duration. In addition, different components of the tidal tensor are not perfectly correlated so that thay may experience maxima and minima at different times. Clearly, this complex behavior cannot be fully described as simply as a single tidal perturbation. Instead, I design a cumulative parameter which gives an approximate amount of heating. This parameter is based on the semi-analytic theory of tidal shocks and provides a scaling relation for tidal heating.

Assume that each peak of the tidal force can be considered as a separate "tidal shock". The total amount of heating is then the sum of the contributions of all peaks. Moreover, since the energy change scales quadratically with the perturbation, all components of the tidal tensor can be treated separately. The resulting expression is

$$\langle \Delta E \rangle = \frac{1}{6} I \, r^2 \, A(E), \tag{3-2}$$

where r is the distance of the particles of energy E from the galactic center, $A(E)$ is the adiabatic correction factor, and I is the tidal heating parameter

$$I \equiv \sum_n \sum_{\alpha,\beta} \left(\int F_{\alpha,\beta} \, dt \right)_n^2 , \tag{3-3}$$

where the sum extends over all peaks n and all components of the tidal tensor, $\alpha, \beta = \{x, y, z\}$. The inner integration is limited to the time intervals between the successive minima of the tidal force. In carrying out the integration, I have linearly interpolated $F_{\alpha,\beta}$ between the output points to the frequency of the time step of the galactic simulation. This provides the most consistent way to compare the estimate I with the simulation results.

Figure 3.1 shows the distribution of the parameter I for the galaxies in the Cluster III simulation. From equation (3-3) it follows that I has the same dimensions as the tidal components, $F_{\alpha,\beta}$. There are more galaxies with low I than with high I; the tidal effects are not the same for different galaxies. The distributions $N(I)$ for the other simulated clusters show similar behavior with a distinct trend: the low Ω_0 clusters have stronger tidal effects than the $\Omega_0 = 1$ cluster. A least-squares fit to the histograms supports this point:

$$N(I) = \begin{cases} 2.0 \times I_4^{-1.40} & \text{(Cluster I)}, \\ 7.7 \times I_4^{-1.24} & \text{(Cluster III)}, \\ 9.6 \times I_4^{-0.93} & \text{(Cluster II)}, \end{cases} \tag{3-4}$$

where $I_4 \equiv I/(10^4 \ \mathrm{Gyr}^{-2})$. The scaling shows that going from the high to low Ω_0, the number of large heating rates increases and the distribution has a shallower tail for high values of I.

The simulations ignore the effect of close encounters by using a spatial smoothing filter. These encounters are estimated to contribute a significant tidal heating, $I_{enc} \approx 1.4 \times 10^4$ Gyr^{-2} (see §2.8). For many galaxies this is an effect of order unity. Thus, the simulations in this Chapter are likely to present a close lower limit of the tidal effects.

3.3.1 Stripping of Dark Matter Halos

The amount of dark matter stripped from the galaxies can be estimated analytically in the spirit of Merritt (1984). Assume that all mass of the cluster is distributed initially in individual galaxies, which obey a Schechter luminosity function

$$N(L) \, dL \propto \left(\frac{L}{L^*} \right)^{-1} e^{-L/L^*} \frac{dL}{L^*}. \tag{3-5}$$

Assume that initially the mass of the galaxies is proportional to their luminosity and the velocity dispersion varies according to the Faber-Jackson (1976) relation, $\sigma_g = \sigma_g^* \, (L/L^*)^{1/4}$.

The characteristic break of the luminosity function, L^*, corresponds to the mass scale $M^* \approx 5 \times 10^{12} h^{-1} M_\odot$ for the Coma cluster. Finally, assume that both the cluster and the galactic density profiles are isothermal with the dispersions σ_{cl} and σ_g, respectively. Then the galactic halos will be truncated at a critical radius

$$R_t \approx \frac{\sigma_g}{\sigma_{cl}} R_p, \tag{3-6}$$

where R_p is the distance of closest approach to the cluster center (pericenter). For many galaxies this distance is of the order the core radius of the cluster, $R_c \approx 100$ kpc. The galactic mass is then greatly reduced to

$$\begin{aligned} M_t &\approx \frac{1}{G} \frac{\sigma_g^3}{\sigma_{cl}} R_p \\ &\approx 3.3 \times 10^{11} \left(\frac{\sigma_g}{250 \text{ km s}^{-1}}\right)^3 \left(\frac{\sigma_{cl}}{1100 \text{ km s}^{-1}}\right)^{-1} \left(\frac{R_p}{100 \text{ kpc}}\right) M_\odot. \end{aligned} \tag{3-7}$$

The corresponding truncation radius is $R_t \approx 23$ kpc. Tidal truncation modifies the mass function of galaxies such that the effective exponential cutoff occurs at M_t instead of M^*.

Merritt (1984) gives the fraction of the mass remaining bound to galaxies as $0.7\ M_t/M^*$, which translates in our case to

$$\frac{M_g}{M_{cl}} \approx 0.04 \left(\frac{\sigma_g}{250 \text{ km s}^{-1}}\right)^3 \left(\frac{\sigma_{cl}}{1100 \text{ km s}^{-1}}\right)^{-1} \left(\frac{R_p}{100 \text{ kpc}}\right). \tag{3-8}$$

For a massive and very smooth cluster CL 0024+1654, Tyson, Kochanski & Dell'Antonio (1998) were able to infer the mass distribution using image reconstruction of the strong gravitational lensing. The potential of the cluster appears to be very smooth, with only about 2% of the mass bound to luminous galaxies. The simulated clusters are certainly less massive and much more irregular, so that a larger fraction of mass in galaxies is expected. Also, Tyson et al. find that galaxies in CL 0024+1654 extend no more than 15 h^{-1} kpc, in agreement with the estimate for R_t. As we will see, both the stars and dark matter are truncated at comparable radii in the simulations.

3.4 Method

The dynamical evolution of galaxies is modeled using the Self-Consistent Field method (Hernquist & Ostriker 1992). In this type of collisionless N-body codes, the potential and density are expanded into a series of biorthogonal basis functions

$$\Phi(\mathbf{r}) = \sum A_{nlm} \Phi_{nlm}(\mathbf{r}), \tag{3-9}$$
$$\rho(\mathbf{r}) = \sum A_{nlm} \rho_{nlm}(\mathbf{r}), \tag{3-10}$$

which satisfy individually Poisson's equation:

$$\nabla^2 \Phi_{nlm}(\mathbf{r}) = 4\pi G \rho_{nlm}(\mathbf{r}). \tag{3-11}$$

This assures that the linear combinations of the basis functions satisfy Poisson's equation automatically. The basis functions employed by Hernquist & Ostriker (1992) use the ultra-spherical polynomials of the radial coordinate r and the spherical harmonics, $Y_{lm}(\theta, \phi)$.

I have attempted to construct a new set of basis functions, more suitable for the thin disk galaxies. An obvious choice is to use cylindrical coordinates and find a set of basis functions satisfying the biorthogonality condition

$$\int \rho_{nlm}(\mathbf{r})\, \Phi^*_{n'l'm'}(\mathbf{r})\, d\mathbf{r} = \delta_{n'n}\, \delta_{l'l}\, \delta_{m'm}. \tag{3-12}$$

Here Φ^* denotes the complex conjugate, and $\delta_{n'n}$ is Kronicker's delta-index. Unfortunately, the only biorthogonal set of functions allowed in the cylindrical coordinates involves the cylindrical Bessel functions, $J_m(R)$, and the trigonometric vertical functions, e^{ikz} (Earn 1996; Robijn & Earn 1996). These functions do not correspond well to the density profiles of real galaxies. Saha (1993) has advocated use of non-biorthogonal basis functions, which are more cumbersome to use but can apply to general underlying density distributions. So far, no successful implementation of such algorithm has been reported. Most recently, Weinberg (1998) has proposed a novel method based on the numerical solution of the Sturm-Liouville equation to which the radial part of Poisson's equation can be reduced. However, I have not succeeded in obtaining a satisfactory Poisson's solver with that method.

Despite the inability to tailor the expansion set to the particular geometry of thin disks, the SCF method can successfully simulate dynamics of the galaxies. Tests of the galaxy evolution in isolation (Section 3.4.3) show that the amount of numerical relaxation is small and well controlled. This relaxation arises because of the graininess of the potential represented by a finite number of particles.

The SCF code has been modified for the current problem by Gnedin & Ostriker (1999) and Gnedin, Hernquist & Ostriker (1999). It has been optimized to run on parallel computers and offers an almost ideal scaling with the number of CPU. The simulations were done on the SGI Origin 2000 supercomputer, using 10^6 particles each in the disk and in the halo. The simulation with 2×10^6 particles takes about 20 hours on 16 SGI R10000 processors.

3.4.1 Galaxy Models

The initial conditions for the disk simulations were generated using the set of routines from Hernquist (1993). The routines were kindly provided by Lars Hernquist. The stellar disk is a double-exponential, with the density profile

$$\rho_d(R, z) = \frac{M_d}{4\pi R_0 z_0}\, e^{-R/R_0}\, e^{-z/z_0}, \tag{3-13}$$

where M_d is the disk mass, R_0 is a radial scale length, and z_0 is a vertical scale height.

The halo is spherically-symmetric and corresponds to the isothermal sphere over some radial interval:

$$\rho_h(r) = \frac{M_h}{2\pi^{3/2}}\, \frac{\alpha}{r_t\,(r^2 + r_c^2)}\, e^{-r^2/r_t^2}, \tag{3-14}$$

where M_h is the halo mass, r_c is a core radius, and r_t is the truncation radius. The normalization constant α is

$$\alpha = \left(1 - \sqrt{\pi}\, q\, e^{q^2}\, [1 - \mathrm{erf}(q)]\right)^{-1}, \tag{3-15}$$

where $q \equiv r_c/r_t$. Halos are effectively truncated at the radius r_t to reduce the computational task of following the orbits of very distant particles. The velocity dispersion of the halo is isotropic.

Figure 3.2 shows the disk and the halo contributions to the circular speed

$$v_c(r) = \left(\frac{G\,M(r)}{r}\right)^{1/2}. \tag{3-16}$$

The disk dominates over the inner scale length, 1 R_0, and the halo dominates at the larger radii.

The figure of the halo is determined using the principal axes of the inertia tensor, I_{jj}. The particle coordinates are transformed into a new frame where the inertia tensor is diagonal. The axis lengths are defined $(a,\, b,\, c)$ as $I_{jj}^{1/2}$, with $c < b < a$.

The orientation of the galactic disk with respect to the coordinate frame of the cluster simulation is arbitrary. In the present runs, I assume the axes of the large galaxies are parallel to the cluster frame and the axes of the dwarf galaxies are tilted by 45°.

3.4.2 Timing of the Simulations

The time step in all simulations is small enough to calculate accurately orbits of stars even in the inner parts of the galaxies. Its value is chosen to be $\Delta t = 0.01\,T_{rot}$, where T_{rot} is the rotational period at the half-mass radius of the disk, $R_{1/2} \approx 1.7\,R_0$ (Table 1).

First, all galaxies are let to run in isolation for one rotational period before switching on the external tidal field. The particles settle into dynamical equilibrium but no appreciable heating is observed. Then the simulations continue for the extent of their tidal histories (Chapter 2). This corresponds to the amount of time elapsing since $z = 5$ until $z = 0$ in their respective cosmologies. The values of the simulation times, T_{sim}, are given in Table 2.

Stellar trajectories are integrated in the internal units of the SCF code, in which $G = M_d = R_0 = 1$. Since the components of the tidal tensor, $F_{\alpha,\beta}$, have the dimensions of Gyr^{-2}, they are converted to the internal units using only one parameter, $t_0 \equiv (R_0/GM_d)^{1/2}$. For the models of large galaxies from Table 1, the conversion factor is $t_0 \approx 0.1\,T_{rot}$. It also follows that the importance of the external tidal force on various galactic models can be measured by the only parameter, t_0.

3.4.3 Tests in Isolation

A number of tests of the galaxy evolution in isolation show that the amount of numerical relaxation rises almost linearly with time, in agreement with theoretical expectation (for example, Weinberg 1996). A constant heating rate arises from pure Poisson's fluctuations due to a finite number of particles.

This relaxation rate is largely due to the interaction of the massive halo particles with the disk particles. Thus, in numerical simulations the halo is effectively composed of $10^6\ M_\odot$ black holes which give a known heating effect on the disk (Lacey & Ostriker 1985).

Without substantial increase in the number of particles used in the simulation, it seems very hard to reduce the rate of numerical relaxation over a long period of time. Instead, I have run the galactic model with the same parameters used in the real simulations for 100 dynamical times (rotational periods T_{rot}), as long as the longest run for galaxy L3 takes. The average energy change at the end of the simulation is relatively small, $\langle \Delta E^2 \rangle / E^2 = 0.0046$. This run in isolation is used as a reference point in the next section, which investigates the effects of real heating by the tidal perturbations.

3.5 Evolution of Large Galaxies

Figure 3.3 shows the particle distribution at the end of the simulation for galaxy L1. The first important conclusion is that the galaxy survives tidal perturbations. It still looks like a disk galaxy of about the same size as initially. Large, coherent spiral arms form in the outer parts of disk. The disk seems to shrink in the radial direction and to flare at the fuzzy edges. But the main difference with the initial configuration is in the substantial vertical heating of the disk. It looks thick and short, if viewed at some surface brightness limit. This galaxy may be identified as an S0.

If we could see dark matter, the galaxy would look different. It has lost about 40% of its halo mass (Table 2). This does not, however, affect much the inner halo. The rotation curve is still flat up to six scale lengths of the disk (cf. Figure 3.4).

The halo density distribution (Figure 3.5) is truncated at large radii but stays almost the same close to the center. The halo is only very mildly triaxial, with the smallest axis ratio $c/a = 0.88$ (Figure 3.6).

The disk of the galaxy is perturbed more significantly. Figure 3.7 shows that the surface density declines in the center, but is larger between the 3 and 4 scale lengths, relative to the initial profile. The surface density exhibits noticeable wiggles, as if a wake of perturbation is superimposed on the otherwise exponential disk.

The vertical heating of the disk is significant: the disk flares (Figure 3.8). The effect in the central parts of the galaxy are corrupted by the numerical noise, but beyond two scale lengths the thickening is clear. The effect increases for larger radii, as expected for tidal perturbations.

A direct evidence of the tidal heating is the increase of the velocity dispersion in all directions (Figure 3.9). Again, the central region is affected by numerical effects but the outer disk shows a dramatic increase of the vertical and radial dispersions with radius. The dispersion increases at the expense of the rotational velocity of the disk, which starts to decline around four scale lengths from the center.

Figure 3.10 shows that the halo velocity dispersion is reduced relative to the initial values. This effect is most likely due to the mass loss, since tidal effects would generally tend to increase the dispersion. In the inner regions, the halo rotates almost as fast as it did in the beginning. The kinematics of both the disk and the halo particles shows that tidal effects are very mild in the central parts of the galaxy.

The analysis of the other two large galaxies shows a lot of similarity (Table 2). As the tidal field is stronger for the low Ω_0 clusters, galaxies L2 and L3 are subject to stronger perturbations than galaxy L1. Galaxy L2 suffers the strongest halo mass loss, about 64%, galaxy L3 provides the intermediate case, about 50%. Both galaxies L2 and L3 have their disks heated more strongly than galaxy L1.

Figure 3.11 shows the halo mass loss with time (the disks retain almost all of their mass). Galaxy L2 leads in terms of the loss rate, but the process is not constant. There are several instants of large losses, associated with the maxima of the tidal perturbation. Examining the particle distribution at successive epochs reveals how the halo is stripped. After a strong tidal shock, a cloud of dark matter particles disperses around the tidal boundary and slowly drifts away from the galaxy in two opposite directions along the same line. That line corresponds to the direction of the strongest component of the tidal tensor at that time. Those unbound particles are later stretched along that line further and further from the galaxy.

Figure 3.12 shows that the radial scale-lengths of the disks do not change by any appreciable amount. On the contrary, the vertical scale heights grow almost monotonically with time. The upper panel of Figure 3.13 demonstrates the amount of numerical "heating", $z_{0,num}$. To account for this artifact, I define the corrected thickness as

$$\bar{z_0} \equiv (z_0^2 - z_{0,num}^2 + z_{0,i}^2)^{1/2}, \tag{3-17}$$

where $z_{0,i}$ is the initial scale height of the model. This equation assumes that the numerical and real effects add in quadrature, true if they are independent. According to this measure $\bar{z_0}/z_{0,i}$, galaxy L2 heats by more than a factor of two, and the others by a slightly smaller amount.

The simulations show similarity but also notable differences in the evolution of the large galaxies in the three cosmological models. The variation in the results may not, however, serve as a clear discriminant among the models. Additional simulations of the two variants of galaxy L3 show a comparable amount of scatter. These simulations, L3a and L3b, employ the same galactic model as L3 but use different input of the tidal force. These two galaxies are chosen to have the maximum values of the tidal heating parameter, I (eq. [3-3]). They represent the extreme cases of the evolution, all other galaxies should be less affected by tidal forces. Galaxy L3a is #13 in the list of galaxies in Cluster III and has $I = 5.3 \times 10^{14}$ Gyr^{-2}; galaxy L3b is #73, with $I = 4.3 \times 10^{14}$ Gyr^{-2}. For comparison, the original galaxy L3 has $I = 3.2 \times 10^{14}$ Gyr^{-2}. Table 2 shows that the final parameters of the galaxies agree with expectations qualitatively but not exactly. Galaxy L3b displays a much stronger heating effect than galaxy L3a despite having a lower value of the parameter I. The difference is due to the temporal structure of the tidal field around the galaxies: the tidal force on galaxy L3b has slightly narrower peaks with higher amplitude. The tidal perturbations are slightly more "impulsive" for L3b, being more "adiabatic" for L3a. Since the parameter I does not include the adiabatic correction factor, it does not completely determine the amount of heating.

When adiabatic corrections are included, the agreement with the simulations is better. Using the adiabatic prescription from Gnedin & Ostriker (1999), the energy change $\langle \Delta E \rangle$ of the halo particles is fitted fairly accurately across the galaxy as a function of the initial energy E. The fit deviates in the outer regions, where the energy change exceeds the initial energy. Those particles become unbound and, obviously, the semi-analytic theory does not apply to them. The tidal radius of the halo, inferred from the energy change, agrees exactly with that inferred from the density profile, Figure 3.5.

To summarize, the vertical thickening of the disks, along with the kinematic heating, results in a strong morphological change of the galaxies. An initially normal spiral galaxy would be now identified as a lenticular disk galaxy, an S0. The next section puts this claim to a thorough observational check.

3.5.1 Comparison with S0 galaxies

The simulated galaxy L1 looks similar to the deep exposures of the galaxy NGC 4762 (Sandage 1961; Burstein 1979). The disk is thick and ends with fuzzy warps. A modest central mass concentration is seen in both the simulation and the real galaxy. Thus, the overall photometric and kinematic properties of the simulated galaxies fall into the general trend of the S0s.

The most detailed data are available for the nearby S0 galaxies in the field (Kent 1985). Recent HST images of lenticulars in distant clusters (Ellis et al. 1997; van Dokkum et al. 1998) usually provide only the integrated light and colors. Typically, the surface brightness profiles of S0s are well fitted by a combination of the exponential disk and the $r^{1/4}$ bulge. The galactic simulations do not include a bulge initially. In fact, one of the goals of this study was to investigate whether a bulge forms as a result of tidal heating. Two competing effects play a role here: stars on average gain energy from the tidal perturbation and move generally outward; on the other hand, the tidally induced dispersion of stellar energies contributes to two-body relaxation and accretion onto the center. Figure 3.7 shows that no appreciable bulge forms from the disk particles, asserting that the relaxation time is still much longer than the age of the galaxy. However, the tidal effects may drive the gas inward and ignite a burst of star formation in the galactic center (see §3.5.2). This effect may assist the formation of a prominent bulge.

The disks of S0s have typically the same scale-lengths as spirals of similar luminosity (Kent 1985). In the present simulations, the scale length of the disk, R_0, is virtually unchanged. Also, the final axis ratios of the simulated disks, 0.15 to 0.25, are consistent with the average observed value of 0.2-0.25 for the "thick disks" (Binney & Merrifield 1998; Burstein 1979). The latter work attempted to decompose the vertical brightness profile of late-type edge-on galaxies into a combination of a thin and a thick disks. The latter dominate in the outer regions of the galaxies and are much more frequent in S0s than in spirals. The thick disks are not as centrally peaked as thin disks and have a shallow radial gradient: they look "diffuse" and "boxy". All this is consistent with having a tidal origin; the flaring of the disk is expected and is detected in the simulations.

The kinematic information is only available for the local sample of galaxies. In a cold axisymmetric disk of spiral galaxies, the vertical velocity dispersion should fall exponentially with radius:

$$\sigma_z^2 = 2\pi\, G\, z_0\, \Sigma_d(R), \tag{3-18}$$

and $\Sigma_d(R) = \Sigma_0 \exp(-R/R_0)$. A sample of 10 S0 galaxies (Seifert & Scorza 1996) shows the flattening of the velocity dispersion at the level about $50 - 100$ km s^{-1}, or even a rise in the outer regions. Similarly, a large study of early type galaxies by Simien & Prugniel (1998, and the previous papers in the series) show a systematic increase of the total velocity dispersion at large radii. The velocity dispersion often exceeds 100 km s^{-1}. The simulations definitely follow the trend, although the data do not yet allow a detailed comparison.

Finally, we note that bars are commonly found in S0 galaxies. Tidal heating isotropizes stellar orbits and stabilizes the disk against bar instability. The actual survival of bars depends on the amount of heating in the inner galaxy. The present simulations, which include a massive dark matter halo, do not show a detectable bar in the large galaxies.

3.5.2 Gas Dynamics and Star Formation

The appearance of galaxies depends sensitively on the amount and distribution of gas. Even though the present simulations do not address gas dynamics directly, it is possible to infer qualitative details of the gas response to tidal heating.

The timescale of the tidal perturbation is of the order 10^8 yr or longer (cf. Figures 2.20-2.22). While the stars would continue to gain energy without dissipation, the gas should cool to its initial temperature fairly quickly. The cooling time is defined as the ratio of the thermal energy to the cooling rate of the gas:

$$t_{cool} = \frac{\frac{3}{2}nkT}{n_e^2\,\Lambda(T)} \approx 7\times 10^3\,\frac{n\,T_4}{n_e^2\,\Lambda_{23}}\ \mathrm{yr}, \tag{3-19}$$

where $\Lambda(T)$ is the cooling function, $\Lambda_{23} \equiv \Lambda/(10^{-23}$ erg cm^3 s$^{-1})$; $T_4 \equiv T/(10^4$ K) is the gas temperature; and n and n_e are the gas and electron number densities, respectively. A typical value of the cooling function in the range of temperatures $10^5 - 10^7$ K is $\Lambda_{23} \sim 1$ (Binney & Tremaine 1987, p. 580). As an extreme case of very fast tidal heating, consider that a 10^4 K and $n \sim 1$ cm^{-3} gas heats up to 8×10^5 K, corresponding to the velocity dispersion of 100 km s^{-1}. Even in this case, the gas would cool back to 10^4 degrees in about 4×10^7 yr. In reality, the gas would be likely to heat less efficiently and therefore cool faster.

However, the thickened stellar disk is now stable against gravitational perturbations and is unlikely to assist the formation of new stars. Figure 3.14 shows Toomre's Q parameter (Toomre 1964) for the final states of the large galaxies. The minimum value, $Q_{min} \approx 2$, is still large enough to suppress any axisymmetric disk instability. It is likely that under such conditions spiral structure and gaseous shocks in the inner regions of the galaxies will not form. Note that the spiral arms prominent in Figure 3.3 extend only in the outer regions, where the gas is likely to be stripped by the intracluster medium or by neighbor galaxies in close collisions.

The stability of the stellar disk is modified in the presence of cold gas. The equivalent low dispersion of the gas amplifies the growth of perturbations and lowers the effective value of Q for pure stellar disk. Jog & Solomon (1984) give a stability criterion for a two-fluid system, stellar plus gaseous disks. From their equation (22), the system is unstable if the modified parameter $Q_{\rm eff}$ is less than unity:

$$Q_{\rm eff} = Q\,\frac{3.36}{2\pi}\left(\frac{x}{x^2+1} + \frac{\beta x}{x^2+c}\right)^{-1} < 1, \tag{3-20}$$

where $\beta \equiv \Sigma_g/\Sigma_s$ is the ratio of the gas to stellar surface densities, $c \equiv \sigma_g/\sigma_s$ is the ratio of the gas thermal velocity to the stellar velocity dispersion, and $x \equiv \kappa\sigma_s^{-1}k^{-1}$ is the ratio of the perturbation wavelength, $2\pi/k$, to the effective scale of stellar motion. Here

$$\kappa = \left(\frac{1}{R}\frac{dV_c^2}{dR} + 2\frac{V_c^2}{R^2}\right)^{1/2} \tag{3-21}$$

is the epicyclic frequency, which includes contributions both from stars and from dark matter. Equation (3-20) allows us to determine the amount of gas, β, required to make the disk unstable. Writing the dispersions of the gas and the stars as $\sigma_g = 11\ T_4^{1/2}$ km s^{-1} and $\sigma_s = 100\ \sigma_{s,100}$ km s^{-1}, I find $c = 0.11\ T_4^{1/2}\,\sigma_{s,100}^{-1}$. The most unstable mode has usually half the maximum allowed wavelength (Binney & Tremaine 1987), which in this case is $x_{max} \approx 1.87(1+\beta)/Q$. With these parameters, equation $Q_{\rm eff} = 1$ can be solved numerically to yield $\beta \approx 0.52$. Thus, disk instability requires about half as much gas as there is stars, a condition rarely satisfied in any spiral or S0 galaxy even in the field.

On the other hand, interaction with the intracluster media (ICM) can remove some of the gas via ram-pressure stripping. The effect for the large galaxies can be estimated as follows. The external pressure (eq. [1-6]) is constant within the galaxy whereas the gravitational force resisting the pressure varies with the position in the galaxy. Equating the two forces gives the critical radius beyond which gas would stripped. I assume that the density of the ICM in the cluster core is of the order 10^{-3} cm^{-3} (Jones & Forman 1984). Since molecular clouds in galaxies are much denser than the diffuse atomic gas, I consider only the stripping of the H I gas. Radio observations in our and other galaxies suggest that the H I surface density is relatively flat with radius and the characteristic value is $\Sigma_s(R) = 4\ M_\odot$ pc^{-2} (Binney & Merrifield 1998). Finally, the surface density of the disk is initially $\Sigma_s(R) = 700\ \exp(-R/R_0)\ M_\odot$ pc^{-2} for the large galaxy models. This results in the critical stripping radius

$$\frac{R_{crit}}{R_0} = 1.3 + \ln\left\{ \left(\frac{n_{\rm ICM}}{10^{-3}\ {\rm cm}^{-3}}\right)^{-1} \left(\frac{v}{10^3\ {\rm km\ s}^{-1}}\right)^{-2} \left(\frac{\Sigma_g}{4\ M_\odot\ {\rm pc}^{-2}}\right) \left(\frac{\Sigma_{s,0}}{700\ M_\odot\ {\rm pc}^{-2}}\right)\right\}. \tag{3-22}$$

The velocities of the galaxies with respect to the ICM vary in the cluster (see discussion in §2.8). I adopt the two typical values, 400 km s^{-1} and 800 km s^{-1}, which correspond to the stripping radii $R_{crit} = 5$ kpc and 9 kpc, respectively. Thus, a significant fraction, but not all of the gas would be stripped by the ram-pressure of the ambient media.

Another process may lead to the stripping of gas from the galaxies: their interpenetrating encounters. While stars are likely to be unaffected by the high-speed collision, the gas would shock and dissipate. Most importantly, it would decelerate in the center of mass of the system and leave both galaxies. The same analysis as above can be applied for the direct collision of the two gas disks, substituting for the ICM density the density of the H I gas, $n_g \approx 0.3$ cm^{-3}. For the velocities of encounter greater than 100 km s^{-1}, at no position would gas remain bound to the galaxies. Thus, direct collisions completely remove the gas from the regions in which the two galaxies overlap. However, in order to surpass the effect of ram-pressure stripping, the collisions must occur closer than within 5 kpc. As Table 5 in Chapter 2 shows, such encounters may happen for a significant fraction of all massive galaxies.

Numerical simulations of the ram-pressure stripping of gas from an elliptical galaxy on a radial orbit in the cluster (Takeda, Nulsen & Fabian 1984) show that continuous stripping can be as important as the sudden stripping of Gunn & Gott (1972). The former process operates on the gas shed by the stars after the initial gas abundance has been removed by the sudden stripping. In either case, the gas leaves the galaxy in a form of blobs which can persist for $\sim 10^8$ yr and provide enhancements of the X-ray emission (Takeda, Nulsen & Fabian 1984).

Current theories of star formation in normal spiral galaxies often rely on the continuous infall of fresh gas (Edvardsson et al. 1993; Dalcanton, Spergel & Summers 1997). This infall supplies material for new stars and also helps to sustain marginal dynamical instability of the disk. Tidal forces would halt a late infall of gas after the galaxy enters the cluster. Thus, it is possible that even retaining its old gas, the galaxy would be unable to convert it to new stars.

The observed situation is quite complex. A comparison of the Hα emission in spirals in the eight nearby Abell clusters with those in the field (Moss & Whittle 1993) shows an approximately 40% lower Hα detection rate among Sb and Sc galaxies in the clusters. This can be explained by the ram-pressure stripping of gas in the core of the cluster. On the other hand, earlier type Sa galaxies in the clusters show a 50% higher detection rate than in the field. This indicates an enhanced star formation (Kennicutt 1998), which could be caused by the starbursts triggered by tides. The latter explanation is supported by the observation that the galaxies with distorted profiles are more likely to be detected in Hα than undistorted spirals.

From the survey of 17 bright spirals in the Virgo cluster, Cayatte et al. (1994) were able to point to different gas removal mechanisms for different groups of galaxies. One group has a typical surface density of H I ($\sim 4\ M_\odot\ \mathrm{pc}^{-2}$) in the inner regions, but a steeply falling one beyond the half of the optical radii of the galaxies. These galaxies are likely to be affected by the ram-pressure stripping. Another group of galaxies has lower central densities of the gas but it extends much larger, often beyond the optical radius. In other words, those galaxies are modestly deficient of H I at all radii, independently of the local gravitational force. Cayatte et al. (1994) suggest that other mechanisms may play a role here, such as viscous and turbulent stripping, and evaporation of gas. These processes transport energy from the intracluster to the galactic gas via either turbulent mixing or heat conduction. This leads to the removal of gas from the galaxy (see Sarazin 1988 for more details). Even though the transport processes can sometimes be faster than the ram-pressure stripping, they may be significantly reduced if the viscous stresses and the conductivity saturate (for example, when the electrons cannot diffuse faster than their thermal speed). Finally, Cayatte et al. (1994) point out that ram-pressure may compress some of the H I into molecular clouds.

The gas-removal processes discussed above do not strongly affect the molecular gas which is located in dense and compact molecular clouds (Kritsuk 1983). If the molecular clouds maintain their identity, they may provide a source of ongoing star formation. However, direct interpenetrating collisions between galaxies would likely remove the clouds as well as the atomic gas. The final distribution of gas in the galaxies would therefore depend on the exact tidal and collision history in the cluster.

Finally, note that numerical simulations of tidal interactions between galaxies (Hernquist & Mihos 1995; Barnes & Hernquist 1996) often show a dramatic loss of angular momentum of the gas, drawing it to the center and resulting in a single powerful starburst. Such starburst may heat and blow out the remaining gas from the galaxies, if the gravitational potential corresponds to a velocity dispersion lower than about 100 km s^{-1} (Dekel & Silk 1986). The large galaxies in the present simulations maintain circular velocity exceeding this critical value and should be able to retain most of their gas. However, the effect may be important to lower mass galaxies.

3.6 Disruption of Dwarf Spheroidal Galaxies

Dwarf galaxies are abundant in the Universe (Ferguson & Binggeli 1994; Gallagher & Wyse 1994). They are the most numerous galaxy type in the Local Group and are likely to dominate number counts both in the field and in clusters. While in the field they are usually found around large luminous galaxies, their distribution in clusters is dramatically different. There are many fewer dwarfs in the centers of clusters than on the periphery (Phillipps et al. 1998). Less massive clusters are also likely to have more dwarf galaxies than the large virialized clusters. Driver, Couch & Phillipps (1998) find strong anti-correlation of the ratio of dwarf to giant galaxies with the local projected density of galaxies. Also, in the Coma cluster dwarfs tend to lie in groups of five or more galaxies (Conselice & Gallagher 1998).

Dwarf galaxies are usually divided into two distinct classes, dwarf ellipticals (dE) and dwarf spheroidals (dSph). The difference between the two is very clear: dE have higher central surface brightness than either spirals or ellipticals, while dSph have very low surface brightness and correspondingly low density (Kormendy 1985). Observational evidence suggests that dwarf spheroidal galaxies are subject to strong selection effects in clusters. The observed trend is consistent with the dynamical origin: low-density dwarfs are very sensitive to tidal effects. It is therefore an important issue if simulations confirm the destruction of dwarfs in clusters.

The question whether dwarf spheroidals contain dark matter is still open (see Burkert 1997 and Kroupa 1997 for various points of view). I have assumed that the dSph galaxies are dominated by dark matter and form initially a stellar disk. The surface brightness profiles of many spheroidals are fairly good exponentials (Ferguson & Binggeli 1994), which supports the disk origin. Typical dwarfs have the disk scale-length of about 1 kpc (Kormendy 1985; Ferguson & Binggeli 1994), comparable to that of dwarf irregulars: the scale-length of the LMC is estimated to be $R_0 \approx 1.2$ kpc (from de Vaucouleurs & Freeman 1972).

The velocity dispersions of the dSph are very low, about 10 km s^{-1} (Kormendy 1985), with the maximum of 20 km s^{-1}. I have assumed the latter extreme value to investigate if any of the dwarfs would survive in clusters. The model still has a low central density of the halo, $\rho_{h,0} \approx 6.8 \times 10^{-3}\, M_\odot$ pc^{-3}, below the critical tidal density (eq. [3-1]). Tidal perturbations should easily dissolve such galaxies.

The dwarf galaxy models, D1-D3 (Table 1), represent dwarf spheroidals for each of the three clusters. None of them survives until the end of the simulation. The galaxies lose all of their halos and most of the disks in 6, 4.5, and 5 Gyr, respectively. Again, galaxy D2 has experienced the strongest tidal force, while D1 has the weakest. The final state of the dwarf galaxies is very peculiar. They are squeezed into a single line stretching for several hundred of kiloparsecs. The shape of the structure is truly one-dimensional, the axis ratios are smaller than a few percent. The orientation must be in the direction of the strongest component of the tidal field. Such a very long line is possible only in the tidal approximation. In a real cluster, the former galactic particles would be bent and stretched beyond a few tens of kpc.

3.7 Comparison with Previous Work

A detailed, high-resolution study of galactic dynamics in clusters has not been possible until very recently. Moore et al. (1996) and Moore, Lake & Katz (1998a) have conducted a similar investigation of the tidal effects on galactic evolution. The authors assumed a fixed isothermal cluster populated by a number of tidally-truncated galaxies. The parameters were appropriate for a rich, Coma-size cluster in the $\Omega_0 = 1$ cosmology. Both the test galaxies and the cluster itself exerted tides on the galaxy simulated with higher resolution. Medium size spirals (with the circular velocity 160 km s^{-1}) were largely destroyed and transformed into dwarf spheroidals. The predicted evolution was much stronger than follows from my simulations.

The galactic model employed by Moore, Lake & Katz (1998a) is similar to the large galaxies, L1-L3. Therefore, the results of both studies can be compared through the characteristic density parameter, or the half-mass rotational period. For their models, $T_{rot} = 2.0 \times 10^8$ yr, slightly larger than the values in the present simulations. This would amplify tidal effects. However, most importantly, the differences in the results must be attributed to the different tidal history of the galaxies, namely to the size and time evolution of the clusters.

The authors assumed a singular isothermal potential of the cluster, which places a large number of galaxies very close to the center. As a result, the number of close encounters and the heating rate are strongly overestimated. On the other hand, my simulations do not include very close encounters. This may account for some of the difference, though unlikely all of it, since the additional contribution of close encounters is relatively small (see §2.8).

At the time of writing, I have learned that new calculations of Moore et al. (1998b), incorporating the self-consistent evolution of the cluster, indicate more moderate tidal effects and less evolution. Thus, these authors reach conclusions similar to the present study.

Dubinski (1998) has combined the self-consistent cluster evolution with the galactic simulation in a single parallel tree-code run. The goal was to study the formation of a giant cD galaxy in the cluster center through a sequence of mergers of smaller galaxies. However, his study did not have enough resolution to follow the dynamics of the galactic disks in as much detail as is done here. Since Dubinski (1998) does not report the results on individual galaxies, except for the central galaxy, it is not possible to compare our results directly.

3.8 Discussion and Future Work

The main conclusion of this work is that tidal effects provide a natural and quantitative way of transforming normal spiral galaxies into S0s. These effects are the strongest for the galaxies having spent more time in the dense cluster environment. Thus, one of the testable predictions of the tidally-driven evolution is the preferential abundance of S0 galaxies in the centers of large clusters at the expense of spirals. This prediction is confirmed by observations.

New HST images provide $B-V$ colors for S0s and ellipticals in the cluster CL 1358+62 (van Dokkum et al. 1998). They are similar in the inner parts of the cluster but differ significantly in the outer regions. The outer S0s are systematically bluer with large color gradients. The data and modeling by these authors suggest that the S0 galaxies in the outer parts of the cluster have formed stars more recently than the S0s in the inner parts. Some of the galaxies in the sample have blue disks and some have blue bulges. Interestingly, the brightest blue galaxies are bulge dominated. The predicted tidal evolution, with a possible massive starburst in the galaxy center at the epoch of cluster formation, is consistent with the observed color distribution.

Close encounters and mergers of galaxies play an important role in the evolution of galaxies. They are effective at removing gas from the galaxies, although an interpenetrating collision is required. That galaxy interactions are important for the history of star formation is indicated by such objects as the "E+A" galaxies (Gunn 1989; Zabludoff 1998). These galaxies are found both in clusters and in the field and are the result of close and violent tidal interactions.

Also, S0 galaxies are systematically less luminous than both ellipticals and spirals, and have prominent bulges (van den Bergh 1998). This is expected if star formation has ceased after the galaxies entered the cluster. Left without gas and dust, disks may dim by up to 2 mag, whereas both disks and bulges would brighten due to the reduced extinction. This, however, may not be enough to account for the prominence of the bulges relative to the disks (Kent 1985), even including a possible starburst. It seems likely that a large part of the bulges of disk galaxies has accumulated at the time of formation of the galaxies.

The most significant limitation of the present simulations is the absence of gas dynamics. Future work should include self-consistent treatment of the gas, both in the cluster and the galaxy simulations. Parallel Tree-SPH codes should be able to address this issue, although the amount of computations is very large. If the present trend of advance in the speed and capacity of modern supercomputers continues, such a gas simulation may be possible by the time this work appears in publication.

Also, high resolution simulations should help to resolve the close galactic encounters. A nested grid method is necessary here, since the dynamical range should be extended by at least a factor of 10, from 63 h^{-1} kpc to 5 h^{-1} kpc or less. Adaptive mesh codes, such as AMR (Bryan et al. 1995), could reach the desired level but the computational expense is again not currently possible.

Another interesting side of the tidal truncation of large galaxies and disruption of dwarfs is the amount of diffuse light in clusters. The fuzzy extended envelopes around the centers of many clusters may contribute 10% to 50% of the total light in places where they are found (Vilchez-Gomez 1998). A study of the distribution of unbound stars should shed light on the origin of the diffuse light.

Finally, the observational picture will soon be improved by the recently commissioned Sloan Digital Sky Survey (SDSS 1997). The Survey will allow a detailed and systematic comparison of galaxies at various stages of their evolution in clusters. The models of tidal evolution will be put to a direct test, which will no doubt lead to further modification and sophistication of the theory and a better understanding of galaxy evolution.

3.9 Conclusions

Tidal effects from the cluster potential and neighboring galaxies are capable of inducing a strong dynamical and morphological evolution of galaxies. The disks of large spiral galaxies thicken by a factor of two or larger, while their velocity dispersion in the outer regions rises to 100 km s^{-1}. Toomre's Q parameter increases to 2 or larger, and even a large amount of cold gas is unable to make the disk gravitationally unstable. The gas in the outer regions of the disk can be stripped by the ram-pressure of the ambient media, while close interpenetrating collisions with neighbor galaxies could remove all of the gas. Even when galaxies retain some of their gas, they are unlikely to form new stars. A significant amount of the dark matter halo is stripped, truncating it to about 30 kpc, as indicated by the density profile. Note, that the truncation radius is independent of the initial size, so that the large galaxies may lose most of their mass. On the other hand, the stellar disks still look like disks and their radial scale lengths are essentially constant. The effect of all these tidal transformations is the conversion of normal spirals, abundant in high redshift clusters, into S0 galaxies. Many of the galaxies would show distorted profiles, in agreement with observations of nearby clusters.

Dwarf spheroidal galaxies have too low central density to survive strong tidal shocks. In all three simulations, the dwarfs are disrupted and their material stretches in a very long thin filament. The unbound stars would contribute to the diffuse cluster light, while the stripped dark matter would add to the global cluster potential.

The present simulations cannot differentiate conclusively between the cosmological models. In all three models considered, the large galaxies experience significant tidal heating and the dwarf galaxies disrupt. The variation in the results is as large as the scatter among the galaxies in the same cosmological model but with different tidal histories. Nevertheless, the number of tidal peaks, the distribution of the tidal heating parameter I, and the axis ratios of the disks indicate that on average the low Ω_0 models have a larger degree of tidal modification of galaxies and may be in better agreement with observations than is the $\Omega_0 = 1$ model.

REFERENCES

Barnes, J. E., & Hernquist, L. 1996, ApJ, 471, 115

Binney, J., & Merrifield, M. 1998, Galactic Astronomy (Princeton: Princeton University Press)

Binney, J., & Tremaine, S. 1987, Galactic Dynamics (Princeton: Princeton Univ. Press)

Bryan, G. L., Norman, M. L., Stone, J. M., Cen, R., & Ostriker, J. P. 1995, Comp. Phys. Comm., 89, 149

Burkert, A. 1997, ApJ, 474, L99

Burstein, D. 1979, ApJ, 234, 829

Cayatte, V., Kotanyi, C., Balkowski, C., & van Gorkom, J. H. 1994, AJ, 107, 1003

Conselice, C. J., & Gallagher, J. S. III 1998, AJ, submitted; `astro-ph/9809390`

Dalcanton, J. J., Spergel, D. N., & Summers, F. J. 1997, ApJ, 482, 659

Dekel, A., & Silk, J. 1986, ApJ, 303, 39

de Vaucouleurs, G., & Freeman, K. C. 1972, Vistas in Astronomy, 14, 163

Driver, S. P., Couch, W. J., & Phillipps, S. 1998, `astro-ph/9809206`

Dubinski, J. 1998, ApJ, 502, 141

Earn, D. J. D. 1996, ApJ, 465, 91

Edvardsson, B., Andersen, J., Gustafsson, B., Lambert, D.L., Nissen, P.E., & Tomkin, J. 1993, A&A, 275, 101

Ellis, R. S., Smail, I., Dressler, A., Couch, W. J., Oemler, A., Butcher, H., & Sharples, R. 1997, ApJ, 483, 582

Faber, S. M., & Jackson, R. E. 1976, ApJ, 204, 668

Ferguson, H. C., & Binggeli, B. 1994, A&A Rev., 6, 67

Gallagher, J. S. III, & Wyse, R. F. G. 1994, PASP, 106, 1225

Gnedin, O. Y., Hernquist, L., & Ostriker J. P. 1999, ApJ, 514, in press; `astro-ph/9709161`

Gnedin, O. Y., & Ostriker, J. P. 1999, ApJ, 513, in press

Gunn, J. E. 1989, in The Epoch of Galaxy Formation, eds. C. S. Frenk et al. (Dordrecht: Kluwer)

Gunn, J. E., & Gott, J. R. III 1972, ApJ, 176, 1

Hernquist, L. 1993, ApJS, 86, 389

Hernquist, L., & Mihos, J. C. 1995, ApJ, 448, 41

Hernquist, L., & Ostriker, J. P. 1992, ApJ, 386, 375

Jog, C. J., & Solomon, P. M. 1984, ApJ, 276, 114

Jones, C., & Forman, W. 1984, ApJ, 276, 38

Kennicutt, R. C. 1998, ARA&A, 36, 189

Kent, S. M. 1985, ApJS, 59, 115

Kormendy, J. 1985, ApJ, 295, 73

Kritsuk, A. G. 1983, Astrophysics, 19, 263

Kroupa, P. 1997, New Astronomy, 2, 139

Lacey, C. G., & Ostriker, J. P. 1985, ApJ, 299, 633

Merritt, D. 1984, ApJ, 276, 26

Moore, B., Katz, N., Lake, G., Dressler, A., & Oemler, A. 1996, Nature, 379, 613

Moore, B., Lake, G., & Katz, N. 1998a, ApJ, 495, 139

Moore, B., Lake, G., Quinn, T., & Stadel, J. 1998b, MNRAS, in press; `astro-ph/9811127`

Moss, C., & Whittle, M. 1993, ApJ, 407, L17

Phillipps, S., Driver, S. P., Couch, W. J., & Smith, R. M. 1998, ApJ, 498, L119

Robijn, F. H. A., & Earn, D. J. D. 1996, MNRAS, 282, 1129

Saha, P. 1993, MNRAS, 262, 1062

Sandage, A. 1961, The Hubble Atlas of Galaxies (Washington,DC: Carnegie Institution of Washington)

Sarazin, C. L. 1988, X-ray emission from clusters of galaxies (Cambridge: Cambridge University Press), p. 216

Seifert, W., & Scorza, C. 1996, A&A, 310, 75

Simien, F., & Prugniel, Ph. 1998, A&AS, 131, 287

The Sloan Digital Sky Survey collaboration 1997, `http://astro.princeton.edu/BBOOK/`

Takeda, H., Nulsen, P. E. J., & Fabian, A. C. 1984, MNRAS, 208, 261

Toomre, A. 1964, ApJ, 139, 1217

Tyson, J. A., Kochanski, G. P., & Dell'Antonio, I. P. 1998, ApJ, 498, L107

van den Bergh, S. 1998, Galaxy Morphology and Classification (Cambridge: Cambridge University Press)

van Dokkum, P. G., Franx, M., Kelson, D. D., Illingworth, G. D., Fisher, D., & Fabricant, D. 1998, ApJ, 500, 714

Vilchez-Gomez, R. 1998, astro-ph/9810292

Weinberg, M. D. 1996, ApJ, 470, 715

Weinberg, M. D. 1998, astro-ph/9805357

Zabludoff, A. I. 1998, in Galaxy Interactions al Low and High Redshift, ed. D. B. Sanders (Dordrecht: Kluwer), astro-ph/9712036

Table 1. Initial parameters of the simulated galaxies

Model	M_h ($M_\odot$)	M_d ($M_\odot$)	V_c (km s^{-1})	R_0 (kpc)	z_0 (kpc)	T_{rot} (yr)
L1,L2,L3	8×10^{11}	4×10^{10}	250	3	0.3	1.3×10^8
D1,D2,D3	2×10^9	10^8	20	1	0.1	5.0×10^8

Table 2. Final parameters of the large galaxies

Model	T_{sim} (Gyr)	$M_h/M_{h,i}$	$M_d/M_{d,i}$	$V_c/V_{c,i}$	$R_0/R_{0,i}$	$\bar{z}_0/z_{0,i}$	b/a	c/a
L1	9.35	0.63	1.00	0.97	1.02	1.61	0.93	0.88
L2	10.71	0.36	1.00	0.92	1.04	2.35	0.96	0.88
L3	12.28	0.48	1.00	0.94	1.03	1.79	0.90	0.85
L3a	12.28	0.55	1.00	0.97	1.01	1.42	0.89	0.87
L3b	12.28	0.39	1.00	0.91	1.02	2.48	0.94	0.88

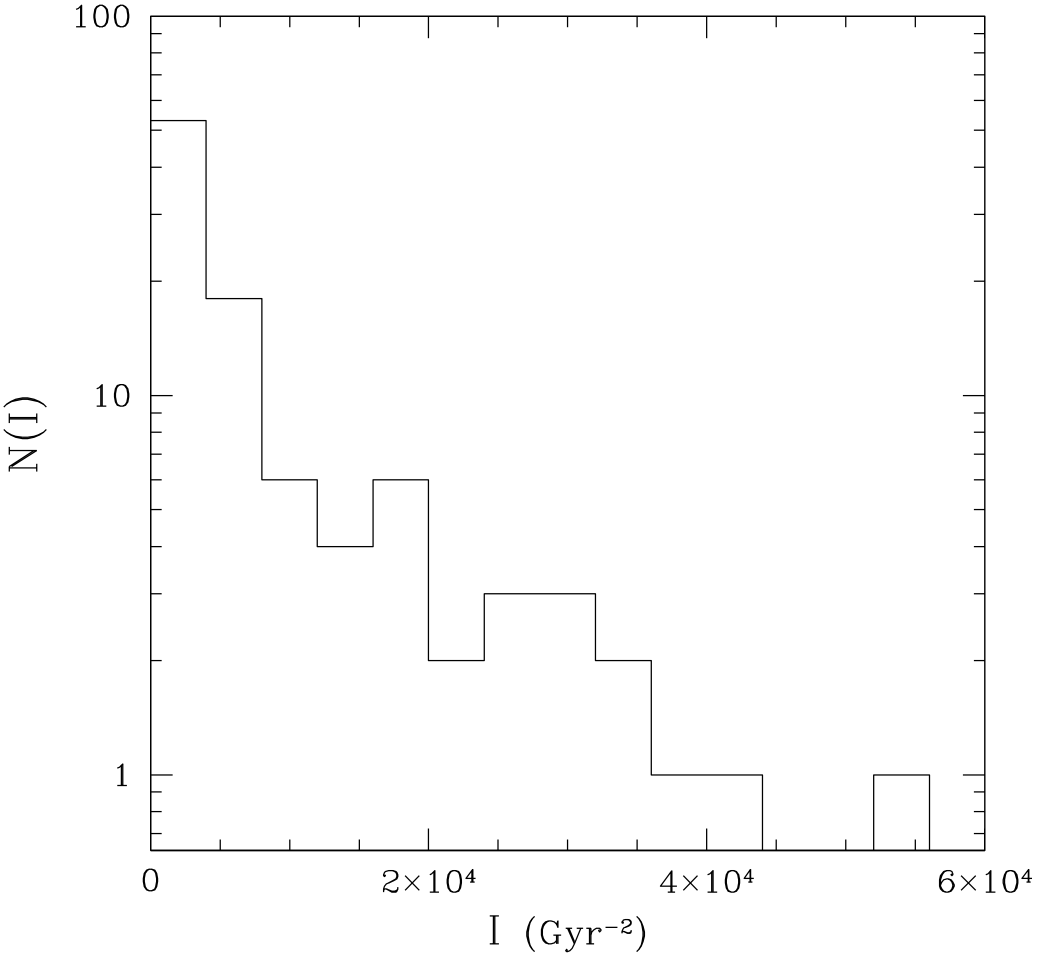

Fig. 3.1.— The distribution of the tidal heating parameter, I (eq. [3-3]), for the galaxies in Cluster III.

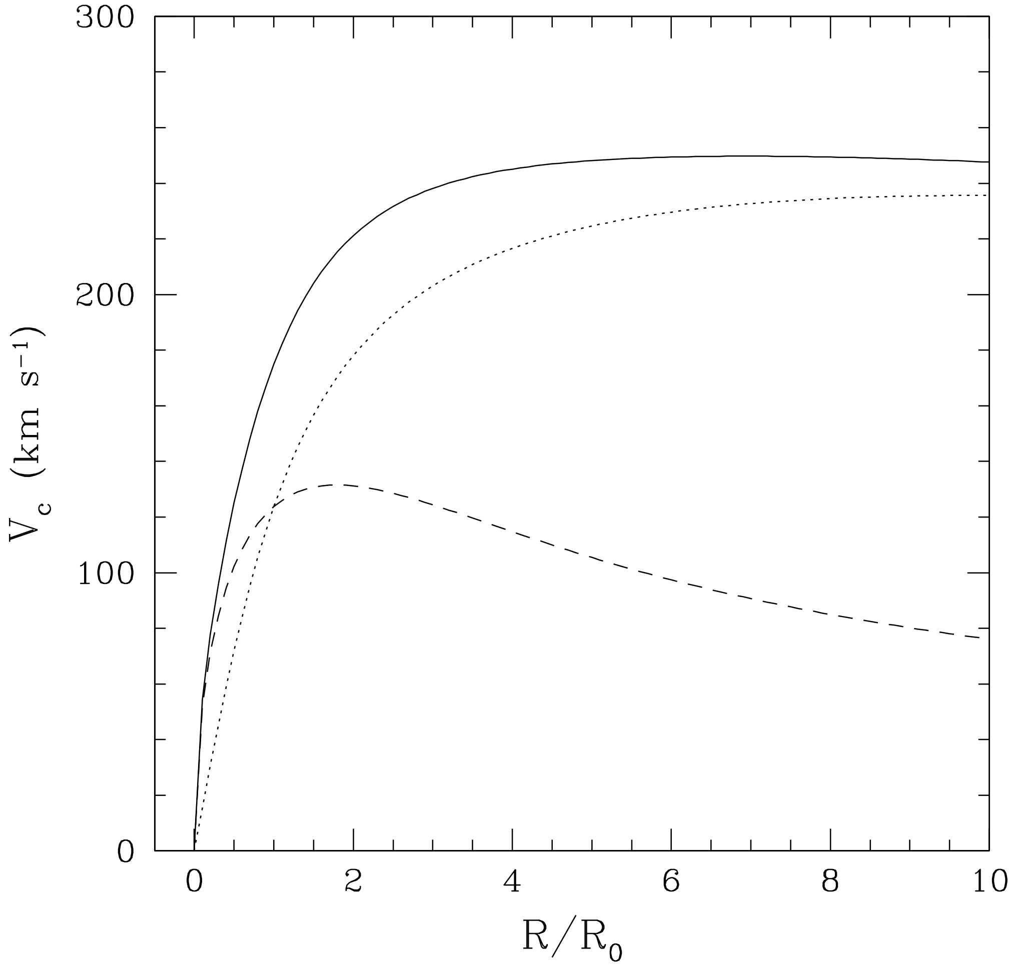

Fig. 3.2.— Rotation curve of the large disk galaxy (solid line) and the individual contributions from the exponential disk (dashes) and isothermal halo (dots). Cylindrical radius is in units of the disk scale length, R_0.

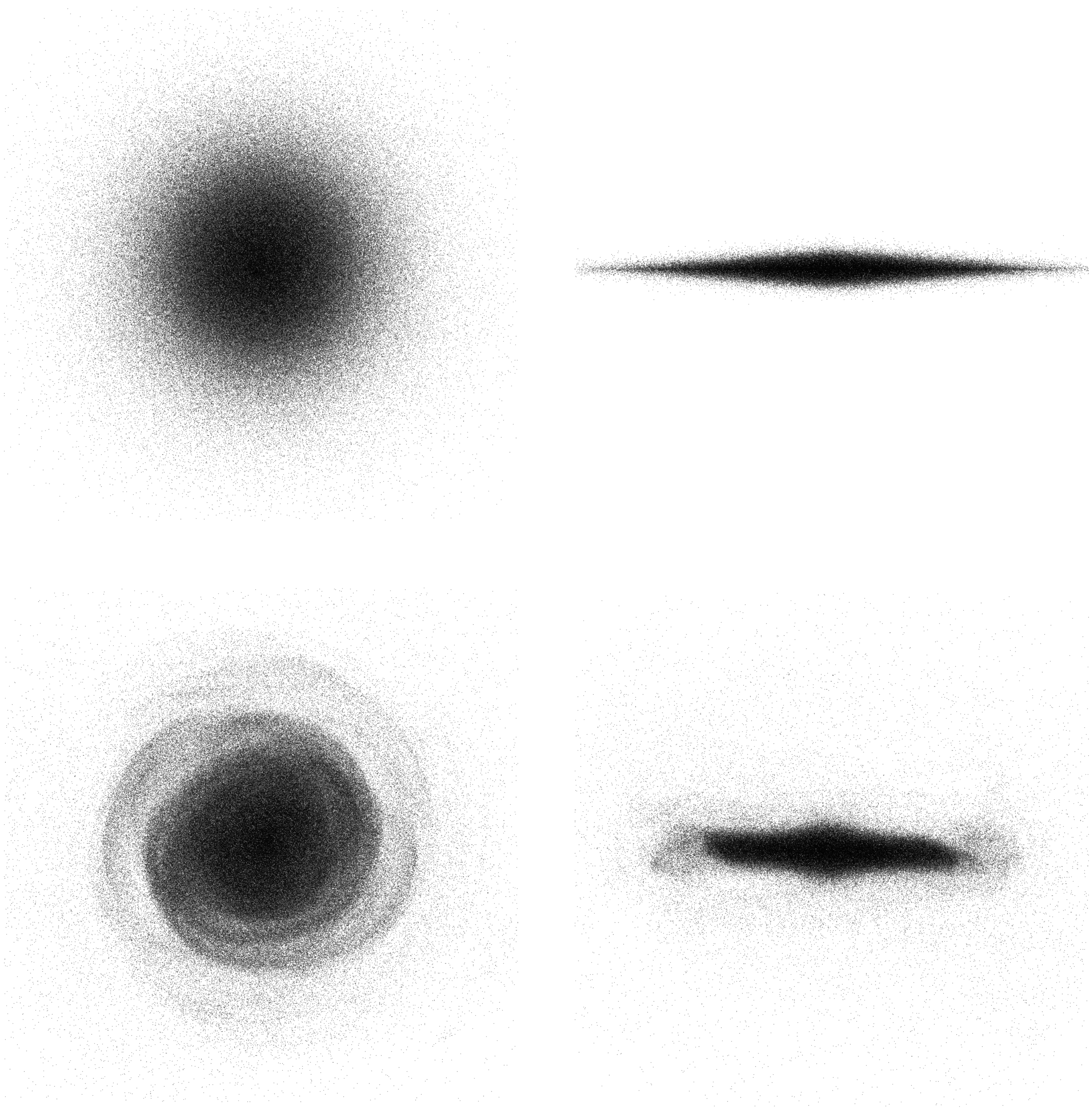

Fig. 3.3.— Upper panels: Initial conditions for the large galaxy, face-on and edge-on views. Lower panel: Final configuration of the galaxy L1. Only star particles are shown.

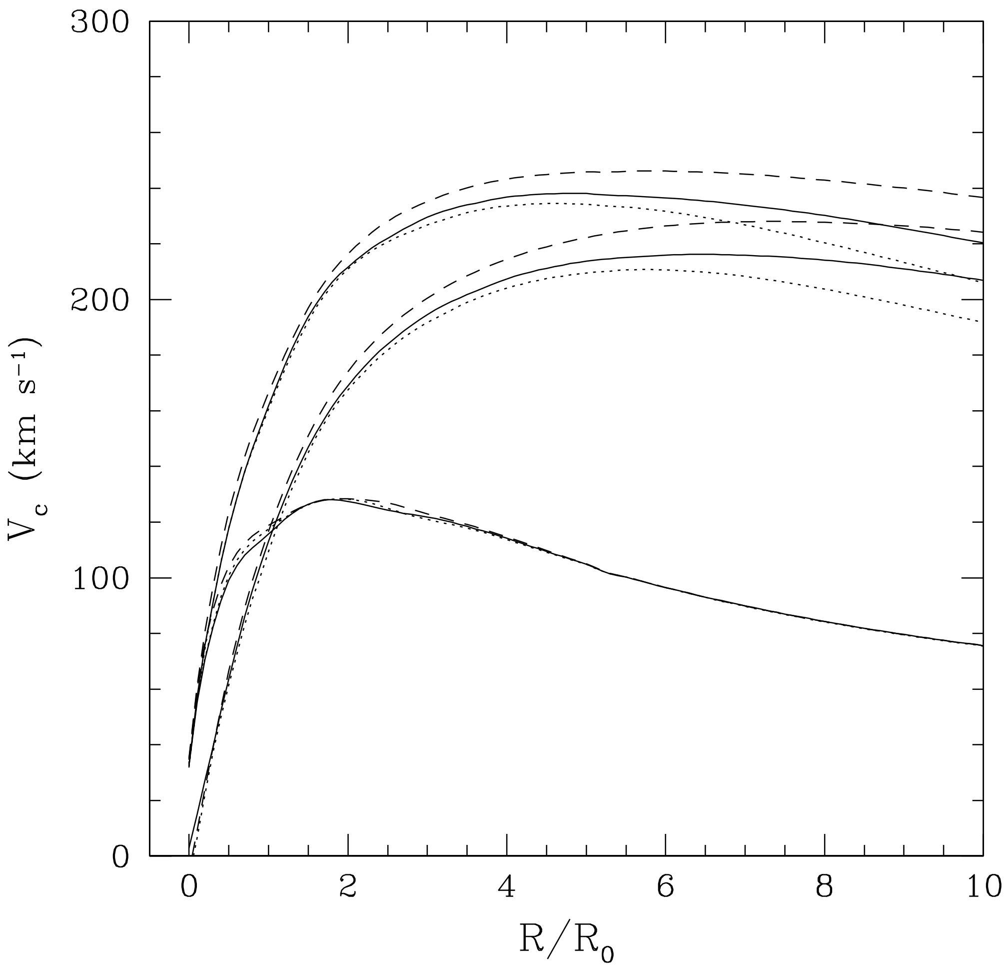

Fig. 3.4.— Rotation curve of the large galaxies and the disk and halo contributions for the large galaxies, L1 (dashes), L2 (dots), and L3 (solid lines) at the end of each simulation.

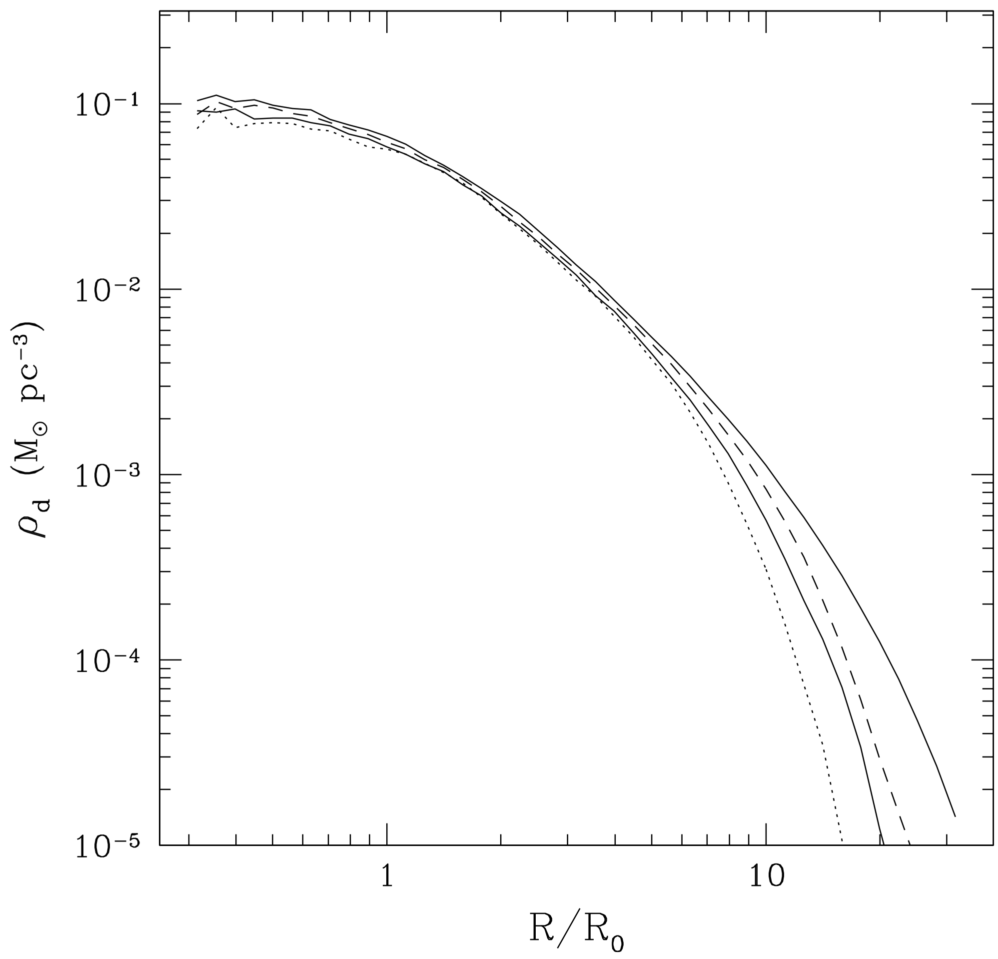

Fig. 3.5.— Density profile of the halos of large galaxies, L1 (dashes), L2 (dots), and L3 (solid line), at the end of each simulation. The outer solid line shows the initial density distribution.

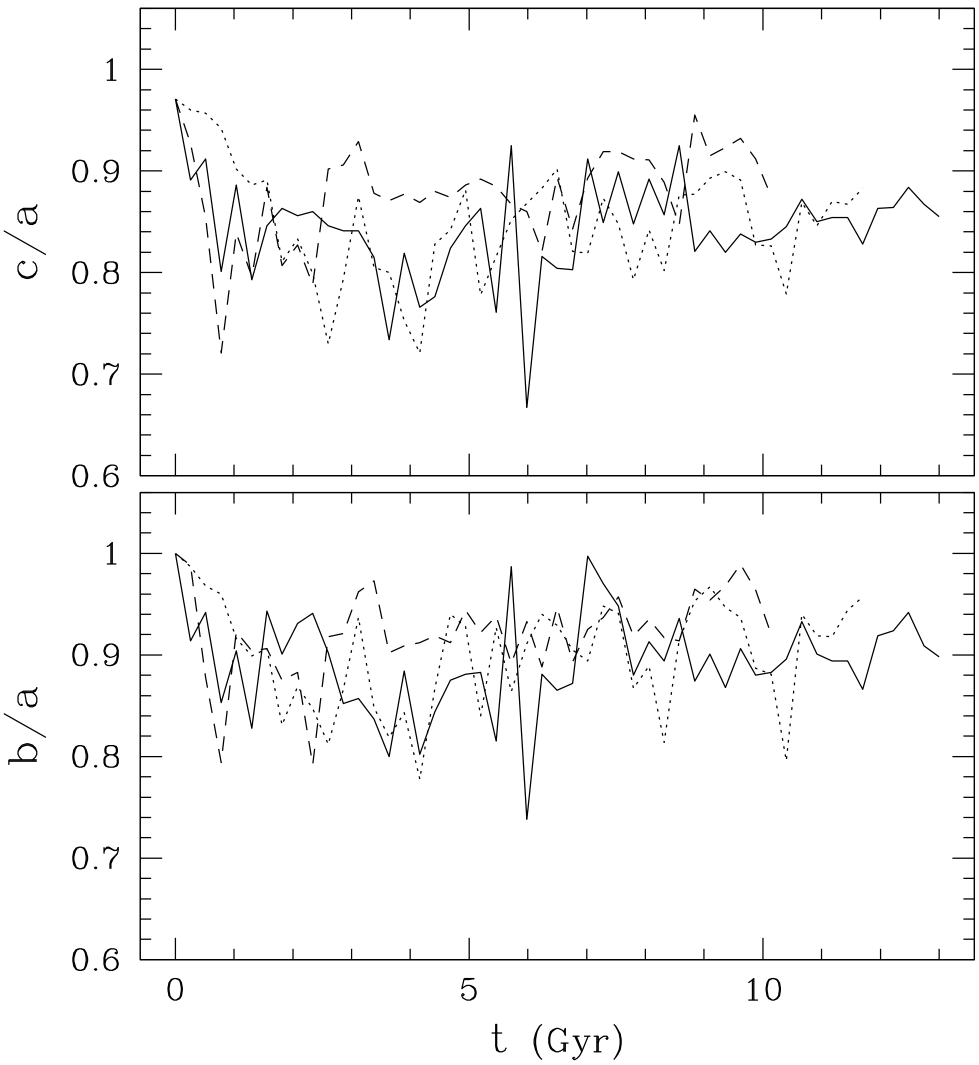

Fig. 3.6.— Axis ratios of the halos of large galaxies, L1 (dashes), L2 (dots), and L3 (solid line), at the end of each simulation.

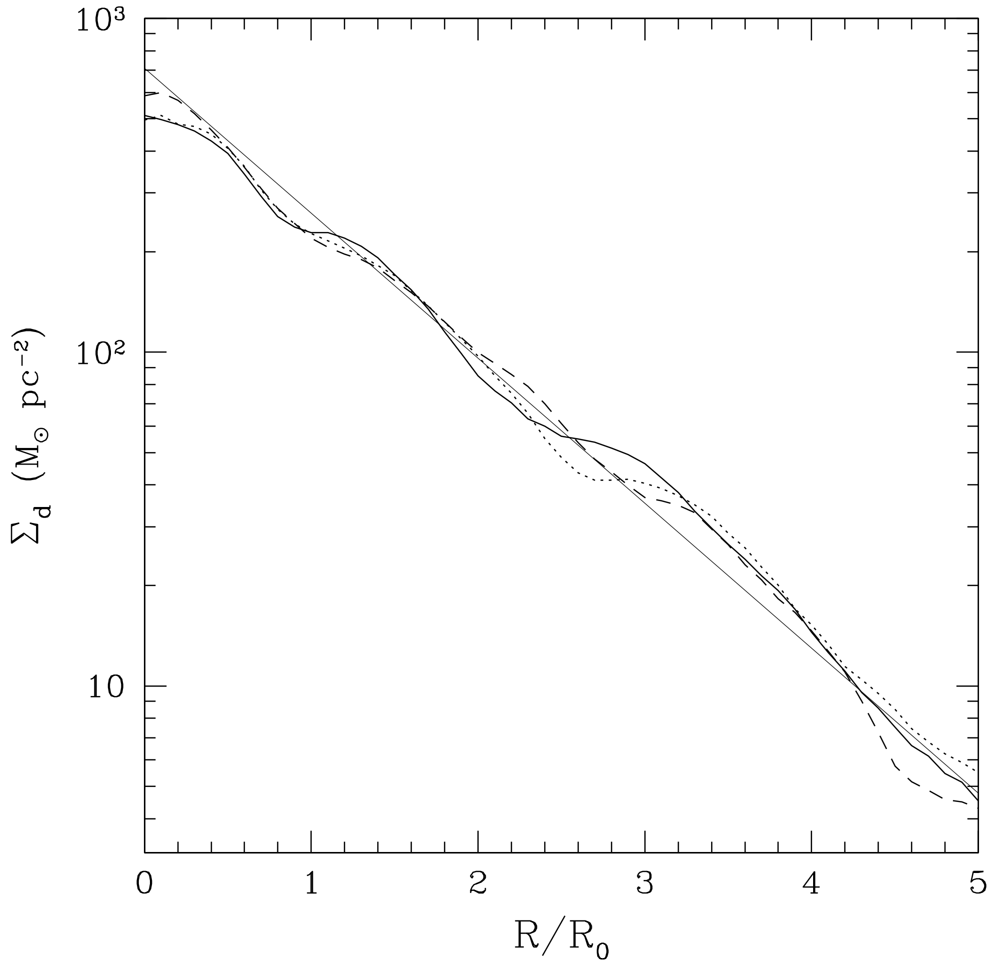

Fig. 3.7.— Surface density of the disk of large galaxies, L1 (dashes), L2 (dots), and L3 (solid line), at the end of each simulation. Straight solid line shows the initial exponential profile.

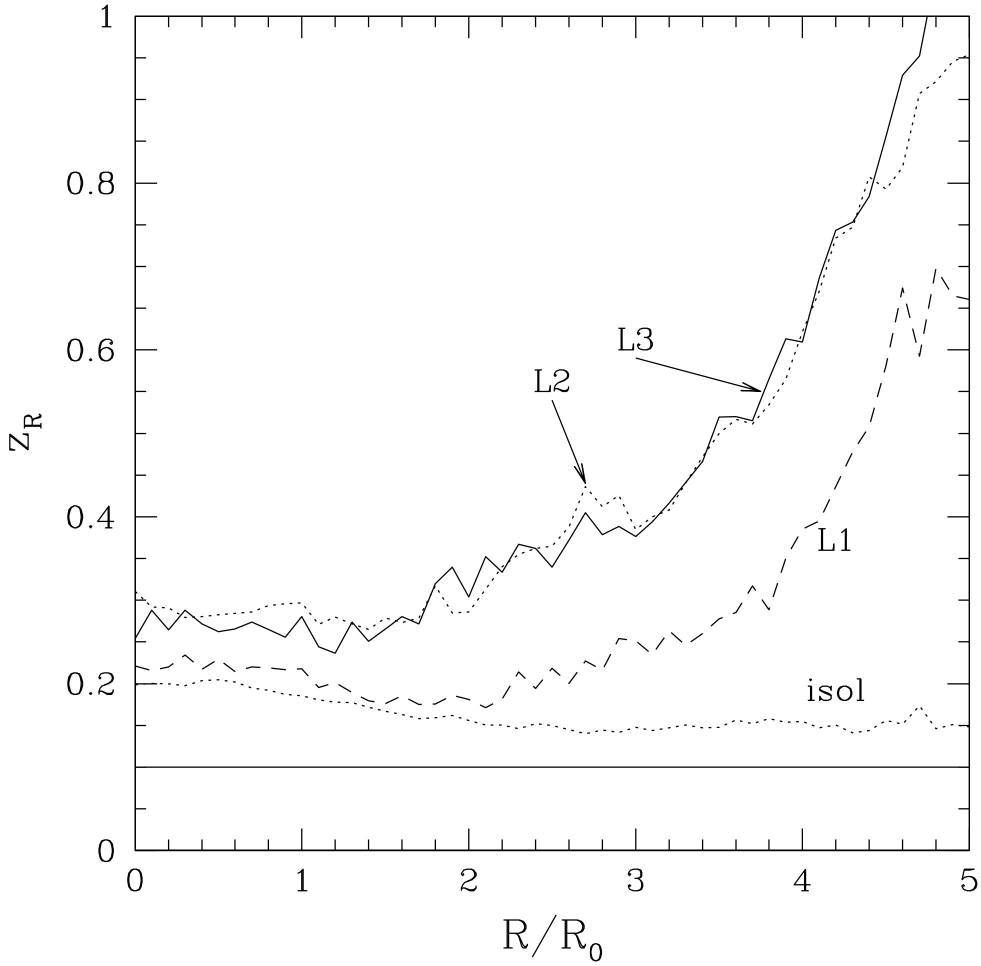

Fig. 3.8.— Disk scale height as a function of radius, z_R, for the large galaxies, L1 (dashes), L2 (dots), and L3 (solid line), at the end of each simulation. The declining dotted line shows the respective heating in the isolated run. The solid horizontal line is the initial scale height.

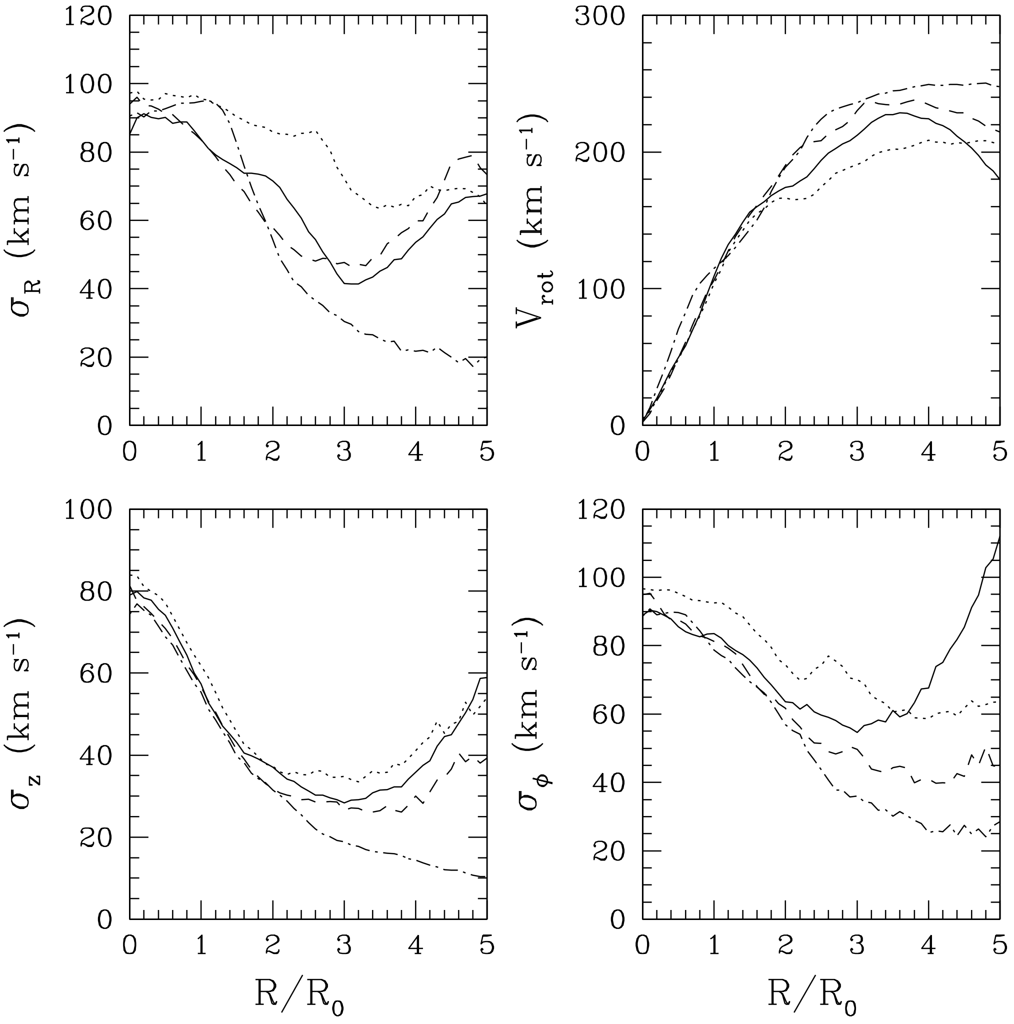

Fig. 3.9.— Velocity dispersions σ_R, σ_ϕ, σ_z and the rotational velocity V_{rot} of the disks of large galaxies, L1 (dashes), L2 (dots), and L3 (solid line), at the end of each simulation. The dash-dotted line is for the isolated run.

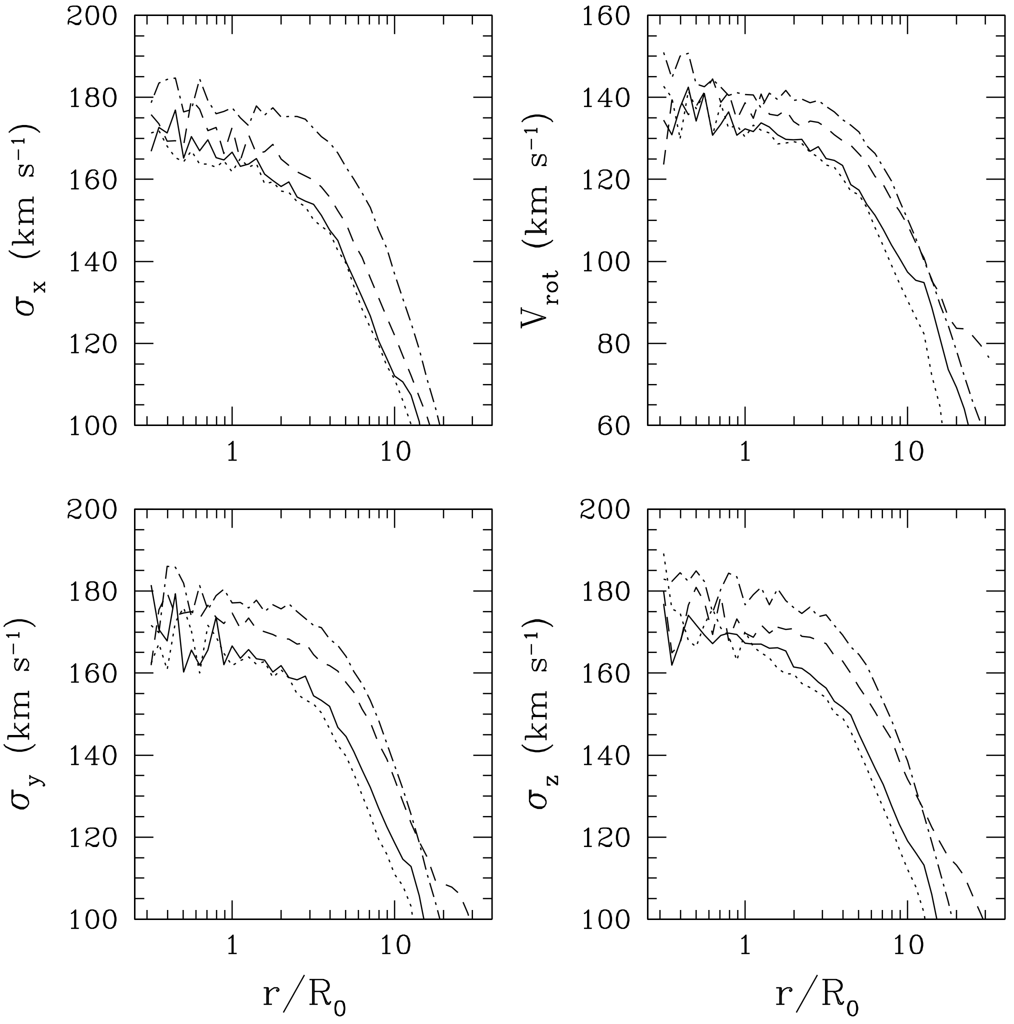

Fig. 3.10.— Velocity dispersions σ_x, σ_y, σ_z and the rotational velocity V_{rot} of the halos of large galaxies, L1 (dashes), L2 (dots), and L3 (solid line), at the end of each simulation. The dash-dotted line is for the isolated run.

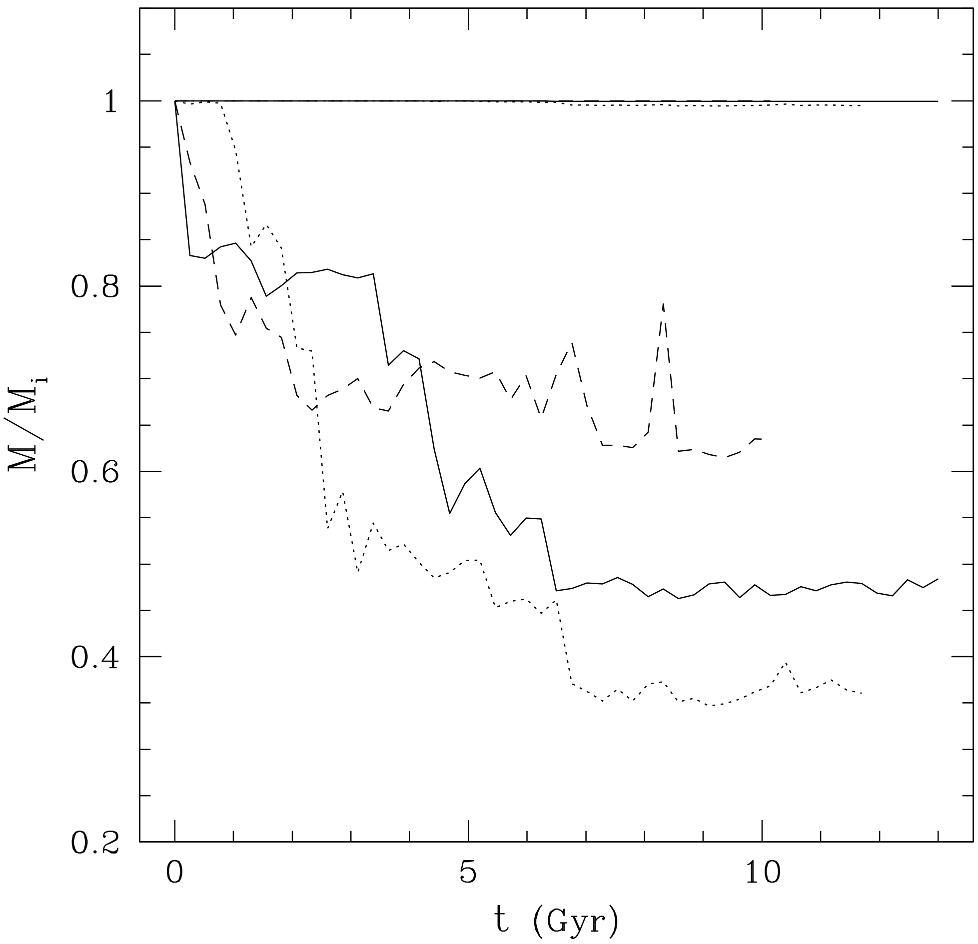

Fig. 3.11.— The disk and halo masses of large galaxies, L1 (dashes), L2 (dots), and L3 (solid line), versus time. Note that the individual simulation times differ for each galaxy. The disk masses essentially do not change (horizontal lines). The declining lines show the halo masses.

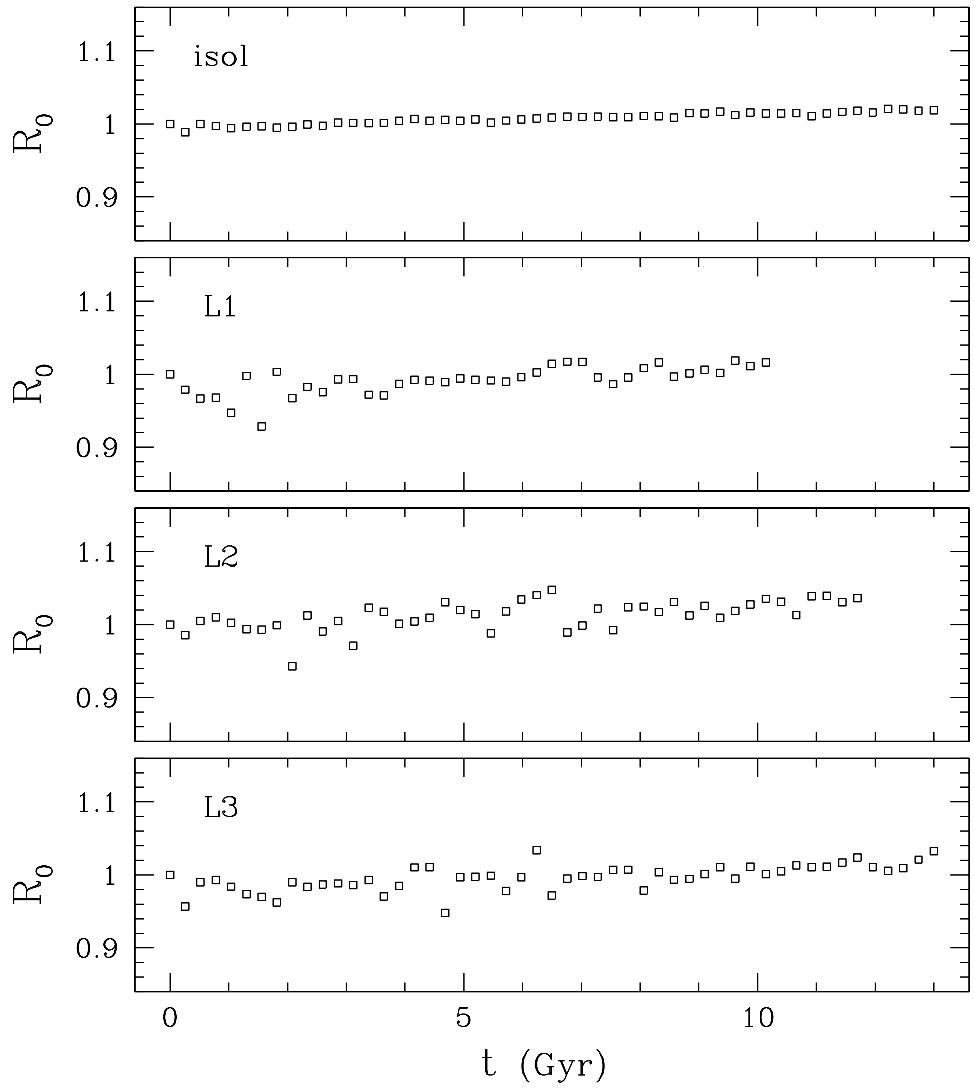

Fig. 3.12.— Variation of the disk scale length, R_0, with time for the large galaxies, L1, L2, L3, and for the isolated run.

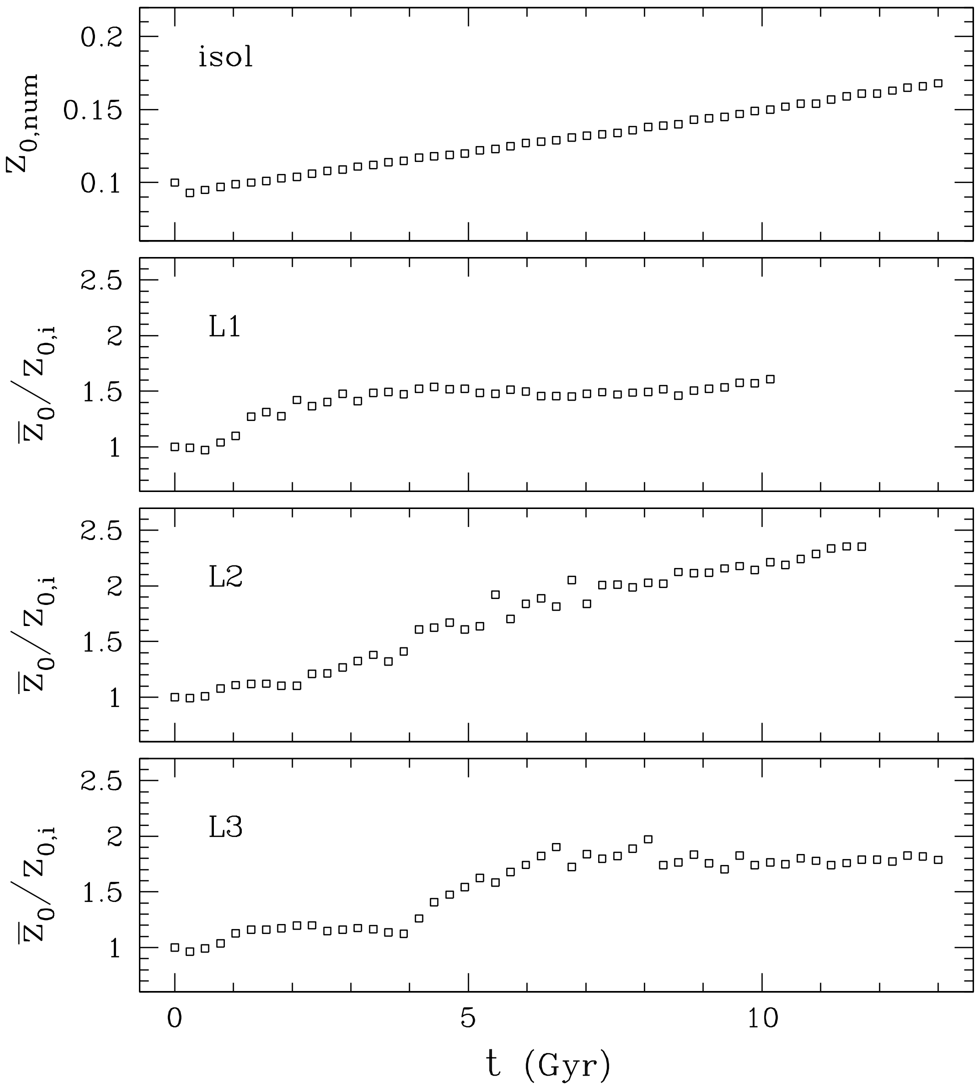

Fig. 3.13.— Variation of the disk scale height, z_0, with time for the large galaxies, L1, L2, L3, and for the isolated run.

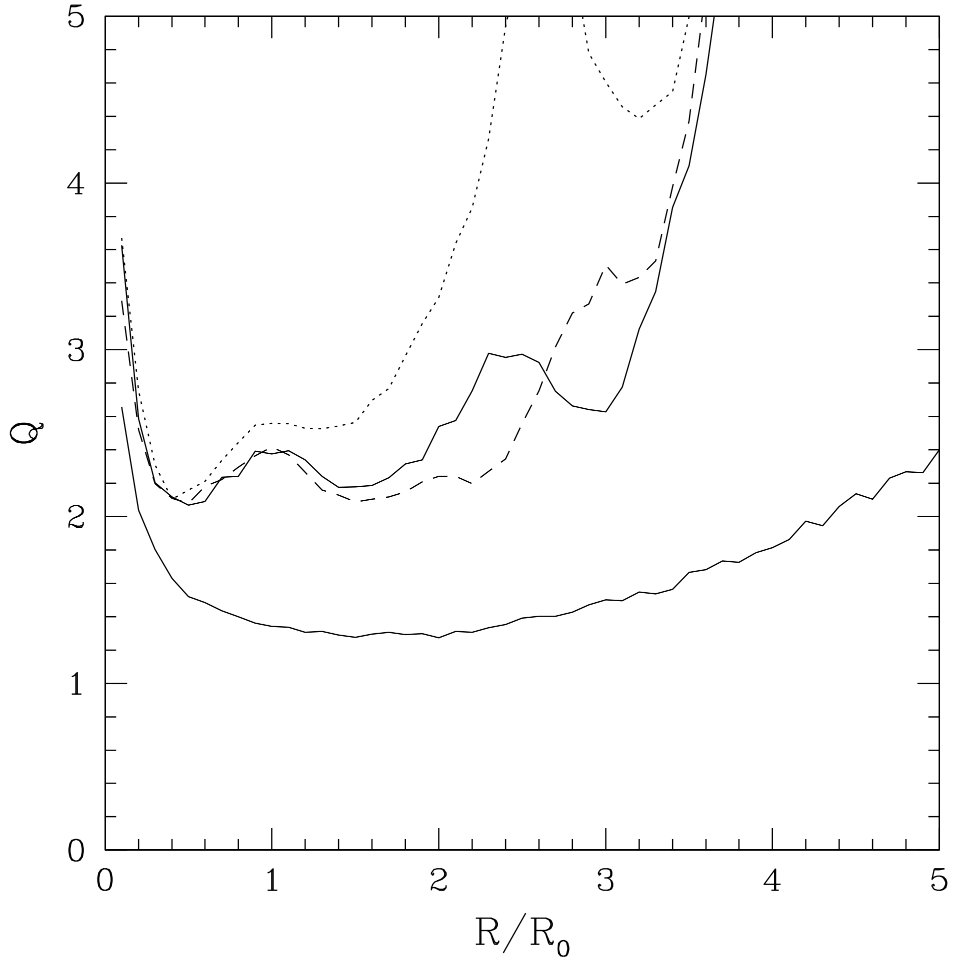

Fig. 3.14.— Toomre's Q parameter for the large galaxies, L1 (dashes), L2 (dots), L3 (solid line). The lower solid line shows the initial values of Q.